

**STRUCTURE-PROPERTY RELATIONSHIPS IN CARBON NANOTUBE-
POLYMER SYSTEMS: INFLUENCE OF NONCOVALENT STABILIZATION
TECHNIQUES**

A Dissertation

by

LEI LIU

Submitted to the Office of Graduate Studies of
Texas A&M University
in partial fulfillment of the requirements for the degree of
DOCTOR OF PHILOSOPHY

May 2009

Major Subject: Materials Science and Engineering

**STRUCTURE-PROPERTY RELATIONSHIPS IN CARBON NANOTUBE-
POLYMER SYSTEMS: INFLUENCE OF NONCOVALENT STABILIZATION
TECHNIQUES**

A Dissertation

by

LEI LIU

Submitted to the Office of Graduate Studies of
Texas A&M University
in partial fulfillment of the requirements for the degree of

DOCTOR OF PHILOSOPHY

Approved by:

Chair of Committee,
Committee Members,

Intercollegiate Faculty Chair,

Jaime C. Grunlan
Zoubeida Ounaies
Choongho Yu
Zhengdong Cheng
Tahir Cagin

May 2009

Major Subject: Materials Science and Engineering

ABSTRACT

Structure-Property Relationships in Carbon Nanotube-Polymer Systems: Influence of
Noncovalent Stabilization Techniques. (May 2009)

Lei Liu, B.E., Beijing University of Aeronautics and Astronautics;

M.S., National University of Singapore

Chair of Advisory Committee: Dr. Jaime C. Grunlan

A variety of experiments were carried out to study the dispersion and microstructure of carbon nanotubes in aqueous suspensions and polymer composites with the goal to improve the electrical conductivity of the composites containing nanotubes. Epoxy composites containing covalently and noncovalently functionalized nanotubes were compared in terms of electrical and mechanical behavior. Covalent functionalization of nanotubes is based on chemical attachments of polyethylenimine (PEI) whereas noncovalent functionalization takes place through physical mixing of nanotubes and PEI. The electrical conductivity is reduced in composites containing covalently functionalized nanotubes due to damage of the tube's conjugated surface that reduces intrinsic conductivity. Conversely, the mechanical properties are always better for epoxy composites containing covalently functionalized nanotubes.

Clay particles were used as a rigid dispersing aid for nanotubes in aqueous suspensions and epoxy composites. When both nanotubes and clay were introduced into water by sonication, the suspension is stable for weeks, whereas the nanotubes

precipitate almost instantly for the suspension without clay. In epoxy composites, nanotubes form separated clusters of aggregation, whereas a continuous three-dimensional nanotube network is achieved when clay is introduced. Electrical conductivity of the epoxy composite is shown to significantly improve with a small addition of clay and the percolation threshold is simultaneously decreased (from 0.05 wt% nanotubes, when there is no clay, to 0.01 wt% when 2 wt% clay is introduced). The addition of clay can also improve the mechanical properties of the composites, especially at higher clay concentration.

Weak polyelectrolytes (i.e., pH-responsive polymers) were also studied for their interaction with nanotubes and the electrical properties of the dried composite films. When dispersed by sonication, Nanotubes show pH-dependent dispersion and stability in poly(acrylic acid) water solution, as evidenced by changes in suspension viscosity and cryo-TEM images. The nanotube suspensions were then dried under ambient conditions and the composite films exhibit tailorable nanotube dispersion as a function of pH. The percolation threshold and maximum electrical conductivity are reduced when the pH is changed from low to high. Some other pH-responsive polymers were also studied, but their pH-dependent viscosity and conductivity were not as large or reversible as poly(acrylic acid).

ACKNOWLEDGEMENTS

I would like to express my sincere gratitude to my academic advisor, Dr. Jaime C. Grunlan, for his advice, encouragement, inspiration and financial aid. I also thank my committee members, Dr. Zoubeida Ounaies, Dr. Choongho Yu, and Dr. Zhengdong Cheng for their help. Special thanks are given to Dr. David E. Bergbreiter and his Ph.D. student Kang-Shyang Liao (Chemistry Department, TAMU), who helped with the covalent functionalization of multi-walled carbon nanotubes by using polyethylenimine. Dr. Hung-Jue Sue is acknowledged for his help for epoxy composites processing. I also want to thank Mr. Tom Stephens, Mr. Michael Pendleton, and Dr. Christos Savva at Microscopy & Imaging Center for their assistance of SEM and TEM. My former and current colleagues: Krishna C. Etika, Woosik Jang, Yeon Seok Kim, Thomas Dawidczyk, Sethu Miriyala, Jason Jan, Charlene Dvoracek, Andrea D. Ilg, Yu-Chin Li, Yong Tae Park, Morgan Priolo, Galina Sukhonosova, Lance A. Hess, Jia Liu, Han Jiang, Dazhi Sun, Luyi Sun, Bobby Browning, Sumanth Banda, Sanjay Kalidindi, and Andrew J. Stephenson are also acknowledged. Finally, I deeply appreciate the support from my family and this dissertation would have been impossible without my family.

TABLE OF CONTENTS

		Page
ABSTRACT		iii
ACKNOWLEDGEMENTS		v
TABLE OF CONTENTS.....		vi
LIST OF FIGURES		ix
CHAPTER		
I	INTRODUCTION.....	1
	1.1 Background and Objectives	1
	1.2 Dissertation Outline.....	3
II	LITERATURE REVIEW	5
	2.1 Carbon Nanotubes	5
	2.2 Nanotube Functionalization	9
	2.2.1 Covalent Functionalization of Carbon Nanotubes.....	10
	2.2.2 Noncovalent Functionalization of Carbon Nanotubes	14
	2.3 Nanotube-Filled Polymer Composites.....	17
	2.3.1 Electrical Properties of Polymer-Nanotube Composites.....	18
	2.3.2 Mechanical Properties of Polymer-Nanotube Composites ...	23
	2.3.3 Other Properties and Applications for Polymer-Nanotube Composites	27
III	COMPARISON OF NONCOVALENTLY AND COVALENTLY FUNCTIONALIZED CARBON NANOUTBES IN EPOXY	29
	3.1 Introduction.....	29
	3.2 Experimental	31
	3.2.1 Materials.....	31
	3.2.2 Sample Preparation	32
	3.2.3 Characterization.....	33
	3.3 Results and Discussion	33

CHAPTER	Page
3.3.1 MWNT Functionalization	33
3.3.2 Epoxy Composites Containing Low Conductivity MWNTs.....	36
3.3.3 Epoxy Composites Containing High Conductivity MWNTs.....	42
3.4 Conclusions.....	48
 IV CLAY-ASSISTED DISPERSION OF CARBON NANOTUBES.....	 50
4.1 Introduction.....	50
4.2 Experimental	53
4.2.1 Materials.....	53
4.2.2 Preparation of Nanotube Suspension and Nanocomposites ..	53
4.2.3 Liquid Suspension and Nanocomposite Characterization.....	54
4.3 Results and Discussion	56
4.3.1 Clay-Nanotube Interaction in Water.....	56
4.3.2 Electrical Conductivity of Epoxy Containing SWNT and Clay	61
4.3.3 Nanotube Dispersion in Epoxy Containing Nanotubes and Clay.....	64
4.3.4 Mechanical Properties.....	72
4.4 Conclusions.....	74
 V MICROSTRUCTURE TAILORING OF CARBON NANOTUBES BY PH-RESPONSIVE POLYMERS.....	 76
5.1 Introduction.....	76
5.2 Experimental	78
5.2.1 Materials.....	78
5.2.2 Sample Preparation and Characterization	78
5.3 Results and Discussion	79
5.3.1 Reversible Microstructure Tailoring of Nanotubes with Poly(acrylic acid).....	79
5.3.2 Microstructure Tailoring of Nanotubes with Poly(allylamine hydrochloride)	91
5.3.3 Microstructure Tailoring of Nanotubes with Other pH- Responsive Polymers	99
5.4 Conclusions.....	101

CHAPTER	Page
VI CONCLUSIONS AND FUTURE RESEARCH PLAN	103
6.1 Conclusions	104
6.1.1 Comparison of Noncovalent and Covalent Functionalization (Chapter III).....	104
6.1.2 Clay Assisted Dispersion of Single-Walled Carbon Nanotube (Chapter IV).....	105
6.1.3 Weak Polyelectrolyte Control of Nanotube Dispersion (Chapter V)	106
6.2 Future Work	107
6.2.1 Covalently Functionalized Nanotubes with Intrinsically Conductive Polymers	107
6.2.2 Nanotube Interaction with Stimuli-Responsive Polymers	108
REFERENCES.....	110
VITA.....	129

LIST OF FIGURES

FIGURE	Page
2.1 Atomic structure of SWNT with different helicity: armchair (5, 5) (a), zigzag (9, 0) (b), helicity (10, 5) (c), and atomic structure of MWNT (d) (from Ref. 37)	6
2.2 Schematic diagram of rolling a graphene sheet into a carbon nanotube (from Ref. 38)	7
2.3 Transmission electron microscope (TEM) images for a SWNT rope (a) (from Ref. 40) and exfoliated MWNT (b) (from Ref. 37)	8
2.4 (A) Covalent binding of proteins to nanotubes via a diimide-activated amidation. (B) TEM image of ferritin-attached MWNTs. (C,D) AFM images of BSA-functionalized MWNTs (from Ref. 56).....	12
2.5 Some possible addition reactions for functionalization of carbon nanotubes (from Ref. 36).....	13
2.6 Schematic illustration of noncovalent nanotube functionalization through: (a) surfactant adsorption, (b) polymer wrapping, (c) endohedral storage of guest molecules (from Ref. 79), and (d) π - π stacking (from Ref. 89).....	16
2.7 Electrical conductivity as a function of SWNT concentration in PVAc emulsion matrix (a), Schematic illustration of drying process for SWNT-filled emulsion (b): from uniform suspension containing both SWNTs and latex particle (upper left) to close-packed configuration when most of the water has evaporated (upper right) and eventually polymer particles coalesce to lock the SWNT dispersion and form a consistent film (lower center) (from Re. 131)	21
2.8 Cryo-TEM image of 1 wt% SWNT in an aqueous suspension containing 1 wt% Gum Arabic and 5 wt% of polystyrene latex. Scale bar: 100 nm (from Ref. 132)	22
2.9 Electrical conductivity as a function of SWNT loading for SWNTs/PC composites. Dashed lines represent the approximate conductivity lower bound required for specific electrical applications (from Ref. 141)	23

FIGURE	Page
2.10 Fracture surface SEM images for epoxy composites reinforced by 1wt% pristine SWNT (a) and 1wt% functionalized SWNT (b) (from Ref. 145)	24
2.11 Top: Scheme of the preparation of SWNT/PA-6 composites via ring-opening polymerization of caprolactam. Bottom: Scheme of the spinneret setup (a); photograph of the setup (b); photograph of the composite fiber (c); SEM image of the cross-sectional fracture of the composite fiber (d) (from Ref. 155)	26
3.1 Reaction scheme for covalent functionalization of MWNT with PEI	34
3.2 Weight loss as a function of temperature for pristine MWNTs, PEI, and the PEI-functionalized MWNTs (shown for low conductivity MWNTs).....	35
3.3 SEM images of freeze-fractured cross sections of epoxy composites containing 1 wt% MWNT (a, b), 1 wt% N-MWNT-PEI (c, d), and 1 wt% C-MWNT-PEI (e, f). These composites contain the MWNT that is stabilized by 8 wt% PEI. Arrows indicate points of MWNT pullout.....	37
3.4 Electrical conductivity as a function of nanotube concentration for composites containing MWNT, C-MWNT-PEI, and N-MWNT-PEI, for low conductivity MWNTs with 8 wt% PEI attachment	39
3.5 Storage modulus as a function of temperature for composites containing 1 wt% nanotubes.....	40
3.6 Thermal expansion of epoxy composites containing 1 wt% nanotubes.....	42
3.7 SEM images for epoxy composites containing 0.47 wt% MWNTs ((a) and (b)) and 0.94 wt% MWNTs ((c) and (d)). Image (a) and (c) are for N-MWNT-PEI while (b) and (d) are for C-MWNT-PEI	43
3.8 Electrical conductivity for the composites containing 0.47 wt% and 0.94 wt% MWNTs	45
3.9 DMA for epoxy composites containing pristine MWNTs, N-MWNT-PEI, and C-MWNT-PEI at nanotube concentration of 0.94 wt% (a) and 0.47 wt% (b).....	47

FIGURE	Page
4.1 Schematic illustration of the three types of clay-polymer composites: conventional composite (a), intercalated nanocomposite (b), and exfoliated nanocomposite (c) (From Ref. 198).....	51
4.2 Digital images of SWNT suspensions in water with a 10:1 weight ratio of clay to SWNTs (left) and without any clay (right). Images were taken right after sonication (a), one day after sonication (b), and one week after sonication (c)	57
4.3 Cryo-TEM image of an aqueous suspension containing both nanotubes and clay	59
4.4 Raman spectra of aqueous suspensions of SWNT, with and without clay	61
4.5 Electrical conductivity as a function of single-walled carbon nanotube loading for epoxy nanocomposites, with and without 2 wt% clay (Cloisite [®] Na ⁺).....	62
4.6 Electrical conductivity as a function of clay concentration for epoxy nanocomposites containing 0.05 wt% SWNT	64
4.7 Optical microscopy images of epoxy composites containing: 0.05 wt% SWNT (a), 0.05 wt% SWNT and 2 wt% clay (c), and 2 wt% clay (e) under bright field light condition. Images (b), (d), and (f) are the same respective positions, but under cross-polarized light condition.....	66
4.8 Cross-sectional SEM images of epoxy nanocomposites containing 0.1 wt% SWNTs (a) and both 0.1 wt% SWNTs and 2 wt% clay (b)	68
4.9 TEM image of the epoxy composite containing 0.1 wt% SWNT and 2 wt% clay.....	69
4.10 Optical microscope image of an epoxy composite containing 0.05 wt% SWNT and 2 wt% clay under partially polarized light (a) and schematic of clay-assisted dispersion of SWNT (b)	71
4.11 Storage modulus as a function of temperature for clay/SWNT/epoxy composites (a) and as a function of clay concentration for composites containing 0.05 wt% SWNT (b).....	73

FIGURE	Page
5.1 Influence of pH on conformation of poly(acrylic acid) (PAA) (from Ref. 230)	77
5.2 Viscosity as a function of shear rate for suspensions containing 0.11 wt% SWNT and 1 wt% PAA as pH is progressively increased (a) and then decreased (b) to demonstrate reversibility	81
5.3 Viscosity as a function of pH for suspensions containing 0.11 wt% SWNT and 1 wt% PAA.....	82
5.4 Viscosity as a function of shear rate for 1 wt% neat PAA aqueous solution	82
5.5 Cryo-TEM imaging of aqueous suspensions containing 0.11 wt% SWNT and 1 wt% PAA at pH (a) 2.9 and (b) 9.2, and respective schematic representations of the SWNT (black) and the polymer (red) (c, d). This figure is from Ref. 230	84
5.6 Digital image of nanotube suspensions, containing 0.011 wt% SWNTs and 0.1 wt% PAA at different pH after centrifugation	85
5.7 Freeze-fractured cross sections of dried suspensions, having 10 wt% SWNT in PAA, as pH is increased from 2.9 to 9.2 and then decreased back to 2.9. This figure is from Ref. 222	88
5.8 Freeze-fractured cross sections of PAA containing 1 wt% SWNT. Composites were prepared from aqueous mixtures with a pH of 2.9 (a) and 9.2 (b). These images are from Ref. 222.....	89
5.9 Electrical conductivity as a function of nanotube concentration for PAA composites prepared from aqueous suspensions at a pH of 2.9 and 9.2. The results are fitted using the percolation power law (Eq. 1), resulting in the parameters shown for each data set. The R^2 values for the curve fit are 0.9999 and 0.9978 for pH of 2.9 and 9.2 films, respectively	91
5.10 Influence of pH on conformation of poly(allylamine hydrochloride) (PAH) (from Ref. 230).....	93
5.11 Viscosity as a function of shear rate for suspensions containing 0.11 wt% SWNT and 1 wt% PAH as pH is progressively increased (a) and then decreased (b).....	93

FIGURE	Page
5.12 Viscosity as a function of pH for suspensions containing 0.11 wt% SWNT and 1 wt% PAH.....	95
5.13 Freeze-fractured cross-sectional micrographs for PAH films containing 10 wt% SWNT that are dried from suspensions at a pH of 3.8 (a, c) and 10.2 (b, d).....	97
5.14 Electrical conductivity as a function of pH for dried PAH films containing 10 wt% SWNTs.....	98
5.15 Cryo-TEM images for PMAA suspensions containing 0.11 wt% SWNTs at pH 3 (a) and pH 9 (b).....	100
5.16 Cryo-TEM images for BPEI suspensions containing 0.11 wt% SWNTs at pH 4 (a) and pH 10 (b).....	100
6.1 Schematic illustration of single stranded DNA functionalized SWNTs that subsequently attached with poly(aniline boronic acid) (PABA) (from Ref. 233).....	108
6.2 Chemical structures for PNIPAAm (a) and PAEKA (b). (from Ref. 236 and 237, respectively).....	109

CHAPTER I

INTRODUCTION

1.1. Background and Objectives

Polymer composites containing nanofillers is among the most promising research fields for advanced materials.^[1-3] The main advantages that these materials have include low density, ease of processing, and property tailoring.^[4,5] A filler is normally called nano if it is less than 100 nm in at least one dimension.^[6,7] In general, there are three types of nanomaterials: zero-dimensional (e.g., nanoparticles and nanocrystals), one-dimensional (e.g., nanotubes and nanowires), and two-dimensional (e.g., clay platelet).^[8] All of these nanomaterials have been introduced into polymers to make polymer nanocomposites, however, dispersion of these nanomaterials is a key challenge.^[9,10] Nanoparticle dispersion controls the composite performance, with better dispersion indicating better nanomaterial/polymer interaction and hence helps to transfer the filler properties to the final composites.^[11,12]

Although some nanoparticles-filled composites have been used for more than a century, little attention was paid to their structure-property relationships until the last two decades.^[13] Perhaps the most famous nanofiller studied is clay (two-dimensional nanomaterial), which has been well-studied in terms of its exfoliation and reinforcement in polymer matrices.^[14-16] These clay/polymer composites show good mechanical improvement, barrier properties and flame retardancy.^[17,18]

This dissertation follows the style of *Advanced Functional Materials*.

The first commercial application of clay nanocomposite was the use of clay/nylon-6 as timing belt covers in Toyota cars in 1991.^[19] Later on General Motors developed clay/polyolefin nanocomposites for the GMC Safari as a step-assist component.^[20]

Carbon nanotubes are the most widely studied one-dimensional nanoparticles, but solvent insolubility and a chemically inert surface hindered their successful dispersion in composites early on.^[21,22] Nanotube synthesis is also limited to small batches with a considerable amount of impurities, which makes them very expensive.^[23] More recently, high purity carbon nanotubes have become commercially available through reliable companies at higher yields and lower prices. Moreover, a series of approaches have been developed to chemically or physically modify nanotube surfaces to make them readily dispersible in many solvents.^[24-26] All of these advances make carbon nanotube/polymer composites an exciting research area and a wide variety of applications are now possible, ranging from gas sensors to hydrogen storage.^[27,28] Some improvements, such as reduced nanotube cost, are still desired but the most important issue in nanotube/polymer composites is nanotube exfoliation.^[29] Covalent and noncovalent functionalization of nanotubes can be employed to control nanotube microstructure in a polymer matrix.

This dissertation focuses on the structure-property relationships of nanotubes in polymers, with an emphasis on noncovalent stabilization and electrical conductivity. The key objectives are:

1. To directly compare the electrical and mechanical behavior of composites containing covalently and noncovalently functionalized carbon nanotubes.
2. To understand the ability and effectiveness of clay as a rigid surfactant for nanotubes in water and epoxy composites.
3. To examine and understand the tailorable microstructural control of carbon nanotubes using pH-responsive polymers.

1.2. Dissertation Outline

Chapter II is a literature review that discusses carbon nanotubes and their composites. Detailed information regarding nanotube synthesis, chemical structure, intrinsic properties, and functionalization (physical and chemical) is provided. It also provides a brief review of polymer composites containing nanotubes and their influence on electrical, mechanical, and other properties.

Chapter III compares the electrical conductivity and mechanical reinforcement of epoxy containing covalently and noncovalently functionalized carbon nanotubes. Polyethylenimine (PEI) is either chemically attached on the surface of nanotubes or physically mixed with nanotubes before introducing into epoxy. This results in epoxy composites containing same amount of PEI and nanotubes, but different bonding conditions (covalent vs. noncovalent). Two kinds of multi-walled carbon nanotubes with different lengths were used and TGA was conducted to determine the weight percentage of PEI attachment after covalent functionalization. DMA and TMA testing for the

composites were carried out to study the interaction between functionalized nanotubes and epoxy matrix.

Chapter IV examines the use clay to disperse nanotubes in water and the synergetic effects of clay addition to epoxy composites containing SWNT. Aqueous suspensions containing just nanotubes and nanotube/clay mixture were imaged and studied by Raman and cryo-TEM. Electrical conductivity and dynamic mechanical properties of the composites were tested for the samples containing just nanotubes and nanotube/clay mixture. Dispersion of nanotubes and clay were studied by optical microscopy under different light conditions. A variety of clay concentrations were looked for their effectiveness in improving electrical and mechanical properties and a clay-nanotube affinity mechanism was proposed.

Chapter V studies the tailorable interaction between nanotubes and pH-responsive polymers in both liquid suspensions and solid composite films. Four weak (pH-responsive) polyelectrolytes were used to disperse nanotubes in water and their interaction with nanotubes at different pH were examined by suspension viscosity and cryo-TEM. Solid composite films were prepared by drying nanotube/polymer suspensions at a given pH and the pH effect on nanotube dispersion was studied by SEM. Electrical conductivity for the films dried at different pH was examined and the nanotube-polymer interaction was studied.

Chapter VI provides the concluding remarks to summarize the findings of this dissertation and the future research plans.

CHAPTER II

LITERATURE REVIEW

2.1. Carbon Nanotubes

Carbon nanotubes were first discovered by Endo in 1976^[30] and more famously rediscovered reported by Iijima in 1991.^[21] Since the early '90s, nanotubes have been extensively studied due to their combination of superior electrical,^[31,32] thermal,^[33,34] and mechanical properties.^[26,35] These properties result from the unique atomic structure of nanotubes. A nanotube is a long cylinder made of a hexagonal honeycomb lattice of carbon atoms that are connected by two pieces of semi-fullerenes at the ends. The diameter of the tube will depend on the size of the semi-fullerene at its end. This novel architecture is entirely based on sp^2 bonding of carbon, which is similar to graphite. The sp^2 bonding has each carbon atom strongly attached to three neighboring carbon atoms that contribute to the excellent mechanical properties. Furthermore, the valence electron that is not covalently shared by other carbon atoms is able to be delocalized and play an important role in electrical properties of nanotubes.^[36]

There are two basic categories of nanotubes: single-walled carbon nanotube (SWNT) and multi-walled carbon nanotube (MWNT). A SWNT can be thought of as rolling a single graphene sheet (single layer of graphite) into a seamless cylinder, while MWNT is composed of coaxial graphene cylinders arranged around a central hollow core with interlayer separation of ~ 0.34 nm, which is close to the interlayer distance of graphite (see Figure 2.1).^[37] Helicity is involved with this graphene rolling because

different rolling processes can still satisfy the criterion that the dangling bonds present at both ends are matched by a corresponding semi-fullerene. The circumferential vector $C_h = na_1 + ma_2$, where the integers (n, m) are the number of steps along the unit lattice vector $(a_1$ and $a_2)$, can be seen from the graphene mapping in Figure 2.2.^[38] The definition of nanotubes by (n, m) is very important because it clearly demonstrates the chemical structure, nanotube diameter, and helicity. The $(n, 0)$ and (n, n) nanotubes are termed zigzag (Fig. 2.1(b)) and armchair (Fig. 2.1(c)), respectively. Different nanotube helicity has a strong impact on its transport properties, particularly electrical properties. All armchair SWNTs are metallic with a band gap of 0 eV. SWNT with $n - m = 3i$ (i is integer and $\neq 0$) are semi-metallic with a band gap of a few meV, while SWNT with $n - m \neq 3i$ are semiconductors with band gap of about 0.5-1 eV. MWNT contains different tube helicity, which makes the electrical properties more complicated.^[39]

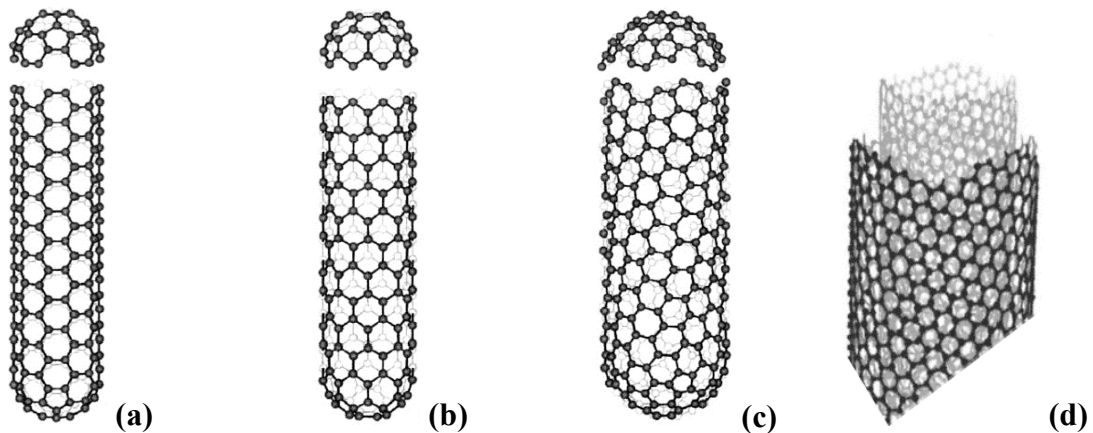


Figure 2.1. Atomic structure of SWNT with different helicity: armchair (5, 5) (a), zigzag (9, 0) (b), helicity (10, 5) (c), and atomic structure of MWNT (d) (from Ref. 37).

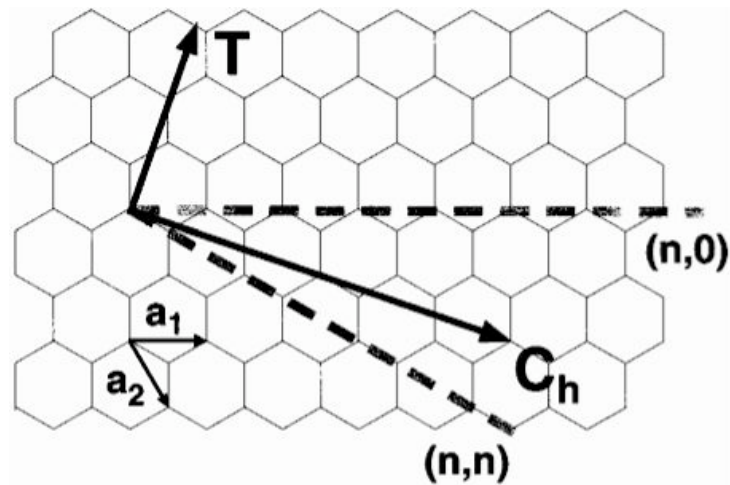


Figure 2.2. Schematic diagram of rolling a graphene sheet into a carbon nanotube (from Ref. 38).

SWNT has a typical diameter of 1.2-1.4 nm, while that of MWNT is 2-100 nm, depending on the number of tubes. They have very large aspect ratios with lengths being in the micrometer range, as shown by transmission electron microscope images in Figure 2.3.^[37,40] Nanotubes with lengths in the centimeter range are possible.^[41] Carbon nanotubes' elastic moduli and strength can be ~ 1 TPa (1000 GPa) and tens of GPa, respectively. Additionally, nanotube has low density (~ 1.3 g/cm³ for single-walled carbon nanotubes)^[42] with superb flexibility, which is evidenced by 25 nm radii of curvature for MWNT. Nanotubes also possess a large photon mean free path length that results in high thermal conductivity. Molecular dynamics simulations indicate the theoretical value of thermal conductivity for an isolated SWNT is larger than 6000 W/(m

K). The experimentally determined room temperature thermal conductivity value for individual MWNT and metallic SWNT are >3000 W/(m K) and 3500 W/(m K), respectively.^[29]

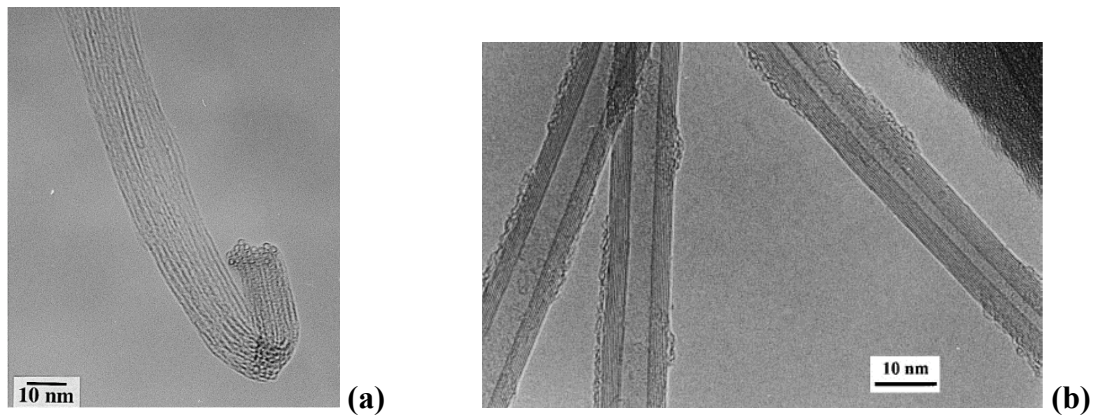


Figure 2.3. Transmission electron microscope (TEM) images for a SWNT rope (a) (from Ref. 40) and exfoliated MWNT (b) (from Ref. 37).

Three methods (arc discharge, laser ablation, and gas-phase techniques) are commonly used to synthesize carbon nanotubes. Arc discharge evaporation was discovered by Iijima in 1991 when he was using it for fullerene synthesis.^[21] One year later, larger scale synthesis was achieved in gram quantities by the same method.^[23] Arc discharge requires high temperature to generate carbon atoms between two graphite rods. The generated carbon atoms can form nanotubes at one of the graphite rods. Laser ablation was first discovered in 1995 by a research group lead by R. E. Smalley.^[43] In this method, a mixture of carbon and transition metals were vaporized by shining a laser

on a metal-graphite composite target. Laser ablation can produce higher quality nanotubes than arc discharge method, but is more costly. Gas-phase techniques,^[44] such as chemical vapor deposition (CVD), utilize hydrocarbon gases as the source for carbon atoms and metal catalyst particles are heated at relatively low temperature (500-1000°C) to act as “seeds” for nanotube growth in the tube reactor. This method is useful for large scale production of carbon nanotubes, but the defect density is higher than the nanotubes made by the other two methods. A successful utilization of gas-phase nanotube growth was achieved by Smalley’s group,^[45] which enabled mass production of SWNT with remarkable purity. This so-called HiPco (high-pressure conversion of carbon monoxide) nanotube has been commercialized by Carbon Nanotechnologies Inc (Houston, TX) for large-scale production of SWNT with high purity. All the methods to prepare carbon nanotubes give mixtures of nanotube chiralities, diameter, and lengths with different amount of impurities and structural defects.

2.2. Nanotube Functionalization

Due to their inert surface composed of only sp^2 carbon, carbon nanotubes are insoluble in most organic solvents or water, thus making composite processing rather difficult. Moreover, nanotubes naturally form bundles because of strong intertubular van der Waals interactions, which is the main hurdle for their widespread utilization. In terms of polymer nanotube composites, properties are largely affected by the exfoliation and interfacial characteristics of the nanotubes, so the expected performance will be compromised if adequate dispersion is not achieved. As a result, there have been

extensive investigations on the development of both chemical and physical functionalization techniques that result in better nanotube dispersion with easier processing.^[46]

2.2.1. Covalent Functionalization of Carbon Nanotubes

Chemical (covalent) functionalization of carbon nanotubes relies on the transformation of sp^2 to sp^3 hybridized of carbon atoms, which is associated with a change from trigonal-planar local bonding geometry to a tetrahedral geometry.^[25] This reaction is more favorable at the nanotube caps due to the two dimensional curvature. Similarly, the curvature on the sidewall of nanotubes makes them more reactive than a planar graphene sheet. On the contrary, the inner surface of nanotubes shows very low reactivity that is ideal for the storage of chemicals (such as gas atoms).^[47] End cap and sidewall functionalization are the two commonly used approaches for chemical manipulation of nanotubes.^[48] Covalent functionalization of nanotubes can significantly improve their solubility in different solvents, which makes them easier to handle. The functionalized nanotubes can undergo chemical reactions with the polymer matrix so that the interfacial interaction between the polymer and nanotubes is dramatically improved.^[49-51] A notable drawback of covalent functionalization is the disruption of the extended π conjugation in nanotubes. This may have limited impact on thermal and mechanical properties, but the influence on electrical properties is known to be more profound because each covalent functionalization site scatters electrons.^[25,29,52]

The surface chemistry of nanotubes became more extensively studied after the discovery of an oxidation process for SWNTs involving ultrasonic treatment in a mixture of concentrated nitric and sulfuric acid.^[53] These processing conditions result in nanotube fragments with lengths in the range of 100 to 300 nm, whose ends and sidewalls are functionalized with a high density of various oxygen containing groups (mainly carboxyl groups). Chen et al. adopted this method to study the solution properties of SWNTs after attaching long chain octadecylamine to the open ends and sidewalls via formation of amide functionality.^[22] By using a similar method, Sano et al. fabricated nanotube rings from a ring closure reaction of end-functionalized nanotubes.^[54] Wong et al. demonstrated the capability of these oxidized nanotubes to be used in chemically selective imaging and nanometer probing of biological systems.^[55] Some other small molecules and ferritin/bovine serum albumin (BSA) proteins, shown in Figure 2.4, can also be successfully attached by chemically bonding to carboxyl-functionalized nanotubes.^[56]

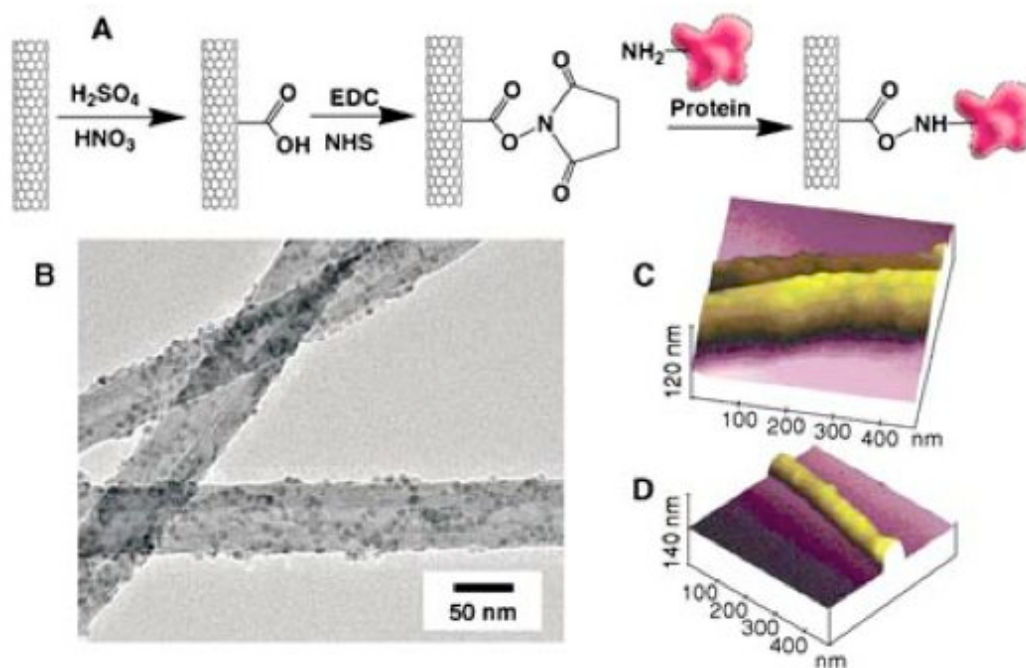


Figure 2.4. (A) Covalent binding of proteins to nanotubes via a diimide-activated amidation. (B) TEM image of ferritin-attached MWNTs. (C,D) AFM images of BSA-functionalized MWNTs (from Ref. 56).

Although the oxidation process that introduces carboxyl groups can be used to form stable chemical modification by amide or ester linkage, it has a relatively weak influence on the mechanical and electrical properties of the nanotubes. On the contrary, addition reactions enable the direct coupling of functional groups on the conjugated nanotube surface, which makes it possible to increase the degree of nanotube functionalization.^[25,52] Figure 2.5 shows a series of documented addition reactions based on pristine nanotubes, among which fluorination is well studied experimentally and theoretically.^[36] The highest degree of functionalization is approximately C_2F and the fluorine atoms can be detached using hydrazine in a 2-propanol nanotube suspension^[57]

or with heat.^[58] It was demonstrated that alkyl groups could replace fluorine atoms by using Grignard or organolithium reagents.^[59] This helps the solubility of these functionalized nanotubes in organic solvents and complete dealkylation can be realized by heating at 500°C in inert atmosphere, thus recovering the pristine nanotubes. In addition, several diamines^[60] or diols^[61] were also reported to react with fluorinated nanotube through substitution.

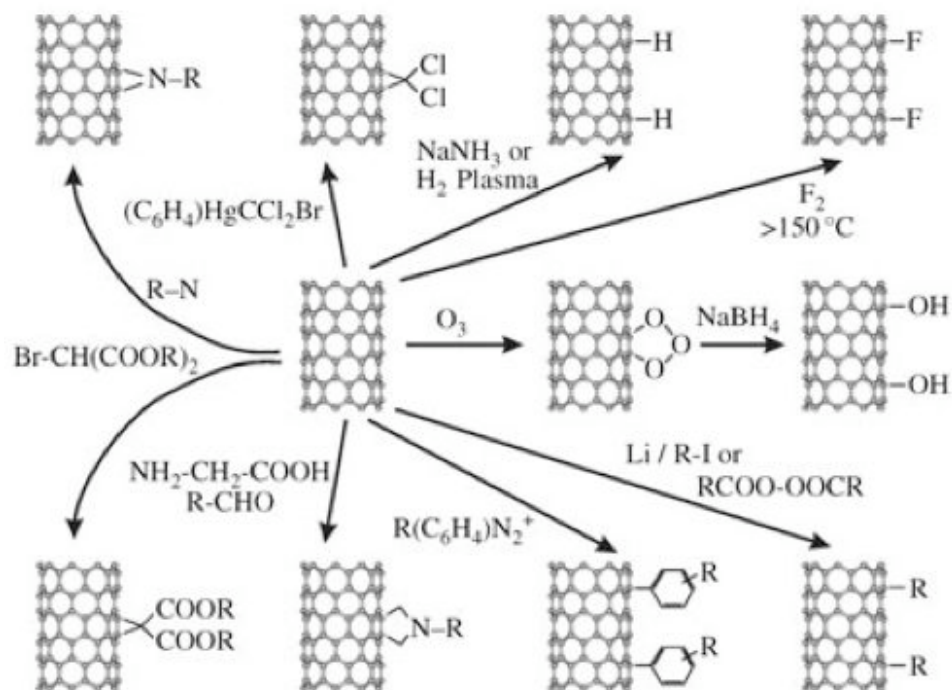


Figure 2.5. Some possible addition reactions for functionalization of carbon nanotubes (from Ref. 36).

Polymer chains can also be attached to the surface of nanotubes through two general approaches: “grafting from” and “grafting to”.^[62] The “grafting to” approach is based on attachment of pre-formed end-functionalized polymer molecules to functional groups on the nanotube surface via chemical reactions.^[63-66] An advantage of this method is that polymers with controlled mass and molecular weight distribution can be used. The limitation of this method is that the initial binding of polymer chains sterically prevents diffusion of additional macromolecules to the surface, which leads to a low grafting density. Some polymers that can be attached to nanotubes via the “grafting to” method include: monoamine-terminated poly(ethylene oxide) (PEO),^[63] poly(vinyl alcohol) (PVA),^[64] and chlorinated polypropylene (CPP).^[65] The “grafting from” approach is based on the initial attachment of the initiators onto the nanotube surface, which is followed by polymerization of appropriate monomers with the formation of the polymer molecules bound to the nanotube.^[67-71] The advantage of this technique is that composites with high grafting density can be prepared, however, it requires strict control of the amount of initiator and the conditions for the polymerization reaction. Polystyrene (PS),^[67] polyethylene (PE),^[68] poly(styrene-*b*-acrylic acid),^[69] and poly(methyl methacrylate)^[70] have been reported using this method.

2.2.2. Noncovalent Functionalization of Carbon Nanotubes

Noncovalent functionalization of nanotubes is widely used because this physical process leaves the nanotube structure intact and maintains the intrinsic properties of the nanotube. In general, nanotubes can be noncovalently functionalized by three exohedral

methods: surfactant, π - π stacking, and polymer wrapping.^[72-77] Molecular storage is an additional endohedral method used for non-covalent modification.^[78,79] Figure 2.6 highlights each of these techniques. Surfactants such as sodium dodecylsulfate (SDS) and sodium dodecyl benzene sulfonate (SDBS) are commonly used to stabilize nanotubes in water and it is believed that nanotubes are stable in the hydrophobic interiors of the corresponding micelles.^[80] This enables the liquid-phase spectroscopic characterization of nanotubes and makes them ready for wet-processing. Another surfactant that was found to successfully stabilize nanotubes is Gum Arabic,^[81] which is a water soluble polysaccharide produced by Acacia Senegal trees. More recently, a variety of surfactants have been used to stabilize nanotubes in this manner.^[82-86] It's worth noting that the nanotubes with open ends can also be functionalized via an endohedral approach, which means the inner cavity of nanotube offers space for the storage of guest molecules, such as C_{60} .^[87]

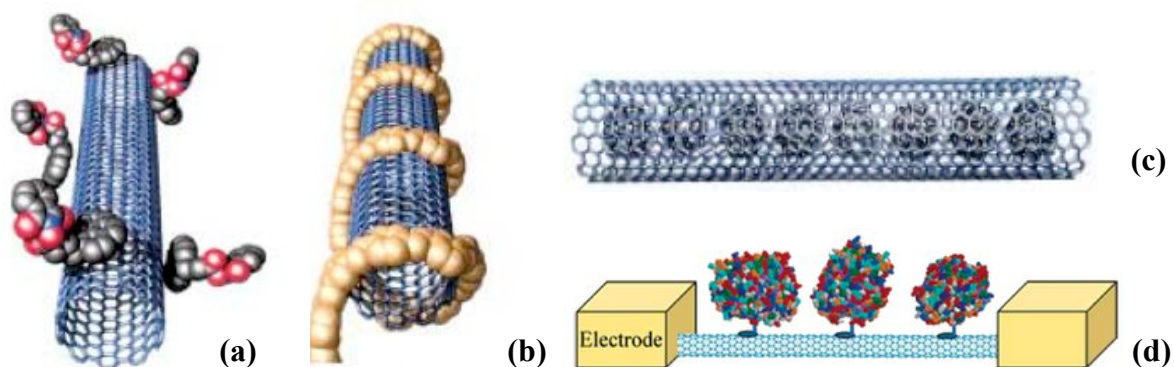


Figure 2.6. Schematic illustration of noncovalent nanotube functionalization through: (a) surfactant adsorption, (b) polymer wrapping, (c) endohedral storage of guest molecules (from Ref. 79), and (d) π - π stacking (from Ref. 89).

The π - π stacking mechanism is another technique used to non-covalently stabilize nanotubes in solvent (see Fig 2.6(d)). This method was first discovered by Chen et al.^[88] who noncovalently attached protein on the surface of a nanotube by using a pyrene-based anchor molecule. The bifunctional anchor was irreversibly adsorbed onto the hydrophobic nanotube surface via the pyrenyl group to form a fixation point and then the other end of the anchor reacted with the amine group on the protein to generate protein immobilization. The pyrenyl group is highly aromatic in nature and known to interact strongly with graphite layers via π - π stacking, so the strong interaction with nanotubes is also attributed to this mechanism. Besteman et al. used a similar method to make biosensors from enzyme-coated nanotubes (Fig. 2.6(d)) and demonstrated the capability of monitoring pH and enzymatic activity.^[89] SWNTs were also immobilized on SiO₂/Si substrate by this method.^[90] The π - π stacking interaction with nanotubes is

not limited to just pyrene derivatives. Short and rigid conjugated polymers made from poly(aryleneethynylene) (PPE) also show this π - π stacking phenomenon.^[91]

Finally, polymer wrapping was discovered by O'Connell et al., who showed that polyvinyl pyrrolidone (PVP) and polystyrene sulfonate (PSS) could be used to make aqueous SWNT suspension in g/l concentrations by helical wrapping of polymer chains on the nanotube surface.^[77] This results in nearly monolayer coverage of tightly associated polymer around individual SWNTs. The same group also demonstrated the fabrication of fluorescent SWNTs by wrapping fluorescently labeled PVP macromolecules,^[92] although the polymer formed a monolayer of only ~ 2.5 nm coiling around individual SWNT or nanotube bundles. This makes individual SWNTs visible using a fluorescent microscope and it is possible to directly observe SWNTs inside living cells. The spare polymer strands left over after wrapping form junctions between nanotubes, tying them together into new configurations, which may benefit assembly in nanotube devices. Some other polymers that can wrap around nanotubes include poly(acrylic acid) (PAA),^[93] amylase,^[94] peptides,^[95] porphyrin-based polymers,^[96] and single-stranded DNA (ssDNA).^[97]

2.3. Nanotube-Filled Polymer Composites

Carbon nanotubes are considered an ideal inclusion for polymer nanocomposites due to superior electrical, thermal, and mechanical properties, as mentioned above.^[98] The first nanocomposite application with nanotubes was reported in 1994 by Ajayan et al.^[99] and great enthusiasm now exists to explore the potential of this nanofiller. The

great challenge for nanotube composites is to transfer nanotube properties to the final composite, which requires better understanding of the relationship between nanotube microstructure, nanotube-polymer interface and final composite properties. Nanotubes naturally form bundles due to the strong intertubular van der Waals attraction and the exfoliation/dispersion characteristics are controlled by nanotube-polymer interaction. In most cases, an appropriate treatment of the carbon nanotube exterior is commonly applied to modify the interface with the polymer matrix to improve the properties of the final composites.^[20]

2.3.1. Electrical Properties of Polymer-Nanotube Composites

Nanotubes are often used to improve the electrical conductivity of polymer composites by several orders of magnitude with a very low concentration.^[100-105] The electrical conductivity as a function of nanotube loading follows a percolation power law:^[106]

$$\sigma = \sigma_0(V - V_c)^s \quad (1)$$

where σ is the experimental composite conductivity, σ_0 is a scaling factor that is comparable to the effective conductivity of the filler, V is the volume fraction of the filler, s is the power law exponent, and V_c is the percolation threshold, which is basically the amount of filler material at which the composite conductivity increases dramatically due to the formation of a network. The percolation threshold for spherical and randomly

dispersed filler is about 15 vol% for a 3-D network, while that for carbon nanotube-filled composites can be two or three order of magnitude lower due to the high aspect ratio.

In an initial study, Sandler et al. found that the electrical conductivity of a MWNT/epoxy composite reached 10^{-2} S/m with just 0.1 vol.% MWNT.^[107] This was compared with the electrical conductivity of traditional carbon black/epoxy composites and the nanotubes showed both significantly reduced percolation threshold and increased overall conductivity enhancement. Percolation threshold is the critical concentration of conductive filler required to form an “infinite” network in a polymer composite (i.e., the onset of electrical conductivity).^[108-110] For SWNT/polymer composites, the reported percolation threshold is in the range from 0.005 vol.% to 5 vol.%.^[104,111,112] The percolation threshold is typically higher for MWNTs,^[113-115] but a value as low as 0.0025 wt% has been reported for aligned MWNTs in epoxy.^[105]

Kim et al. examined the conductivities of SWNT/epoxy composites and the percolation threshold was found to be 0.074 wt% SWNTs.^[116] Yu et al. prepared MWNT/polystyrene (PS) composites by first dispersing MWNTs in water with sodium dodecyl sulfate (SDS) and mixed with different amount of PS latex, then freeze-dried the mixture and compression molded to form composite sheets.^[117] The percolation threshold was found to be 1.5 wt% MWNT and the maximum conductivity was about 1 S/m with 5.5 wt% nanotube loading. Jeon et al. fabricated SWNT/high density polyethylene (HDPE) composites through fast crystallization from dilute solution and reported a percolation threshold of 0.13 wt% SWNTs, which is the lowest value for nanotube/polyethylene composites.^[118] Du et al. made SWNT/poly (methyl

methacrylate) (PMMA) composites via coagulation method and found the percolation threshold to be about 0.39 wt%.^[119] These are just a glimpse of the many studies of electrical conductivity in nanotube-filled polymer composites.^[120-129]

Electrical conductivity and percolation threshold of nanotube/polymer composites are influenced by many factors such as aspect ratio, dispersion, and alignment.^[29] Bryning et al. prepared SWNT/epoxy composites with nanotubes made by the HiPco and laser oven processes, which have aspect ratios of ~150 and ~380, respectively.^[104] The composite containing nanotubes with higher aspect ratio was found to have lower percolation threshold. More than an 8-fold percolation threshold decrease in MWNT/epoxy composites was found by Bai et al., when the length of MWNT was increased from 1 to 50 μm .^[130] The addition of surfactant to the polymer matrix can improve the dispersion of nanotubes and hence benefit the conductivity of the resultant composites, which is especially true for the latex-based polymer matrix. Grunlan et al. dispersed SWNTs by Gum Arabic in water and subsequently mixed with poly (vinyl acetate) (PVAc) emulsion to make nanotube suspensions.^[131] Upon drying, the nanotubes have to stay in the interstitial space and the polymer particles will interdiffuse and coalesce to form a coherent film. The percolation threshold of the dried composites is about 0.038 wt% and electrical conductivity is shown in Figure 2.7(a). The nanotube microstructure created by this process is called a segregated network and its formation is illustrated in Figure 2.7(b). By using similar process, Regev et al. made SWNT/PS composites based on PS latex.^[132] With Gum Arabic, SWNTs can be successfully exfoliated into tiny bundles and dispersed uniformly in the latex suspension, as

evidenced by cryo-TEM imaging (see Figure 2.8). Electrical conductivity of these composites is found to be lower than the composite using SDS as surfactant in which the percolation threshold was found to be 0.28 wt% SWNT (1:1 weight ratio for SWNT and SDS).

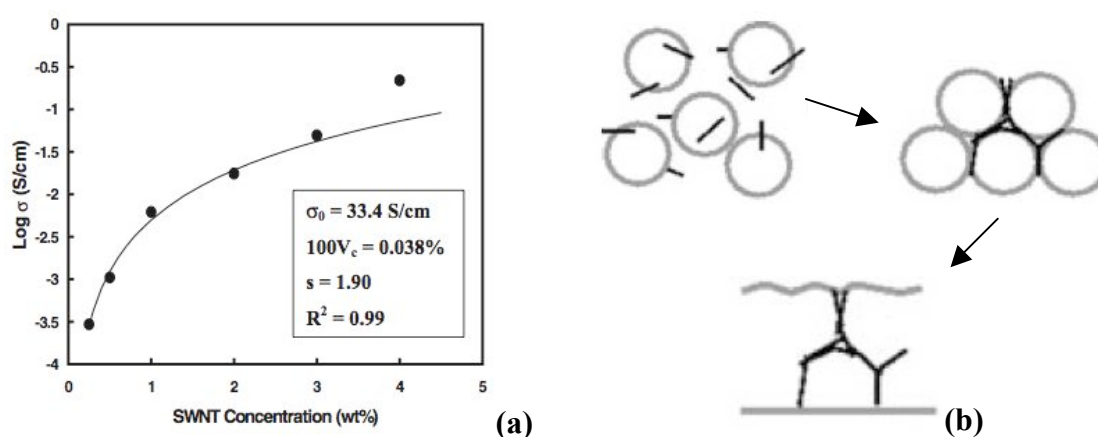


Figure 2.7. Electrical conductivity as a function of SWNT concentration in PVAc emulsion matrix (a), Schematic illustration of drying process for SWNT-filled emulsion (b): from uniform suspension containing both SWNTs and latex particle (upper left) to close-packed configuration when most of the water has evaporated (upper right) and eventually polymer particles coalesce to lock the SWNT dispersion and form a consistent film (lower center) (from Ref. 131).

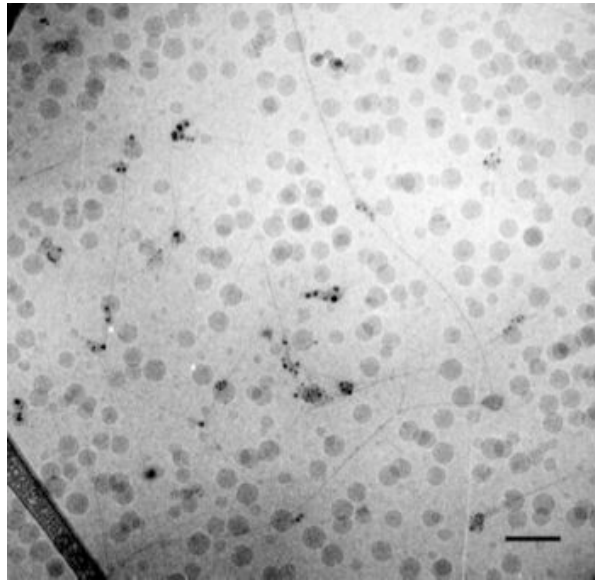


Figure 2.8. Cryo-TEM image of 1 wt% SWNT in an aqueous suspension containing 1 wt% Gum Arabic and 5 wt% of polystyrene latex. Scale bar: 100 nm (from Ref. 132).

The improved electrical conductivity for polymer materials with the addition of carbon nanotubes can lead to many applications such as electrostatic dissipation,^[133,134] electromagnetic interference shielding (EMI),^[135,136] ink-jet printing,^[137,138] and transparent conductive coating.^[139,140] Ramasubramaniam et al. tested the electrical conductivity of SWNT/polycarbonate and SWNT/PS composites by using poly (phenyleneethynylene) (PPE) as a surfactant.^[141] Figure 2.9 shows the conductivity for SWNT/PC composites, as well as the conductivity levels necessary for electrostatic dissipation, electrostatic painting and electromagnetic interference shielding (EMI). It was found that 0.3 wt% and 3 wt% SWNT loading in polycarbonate were sufficient for electrostatic dissipation and EMI shielding, respectively.

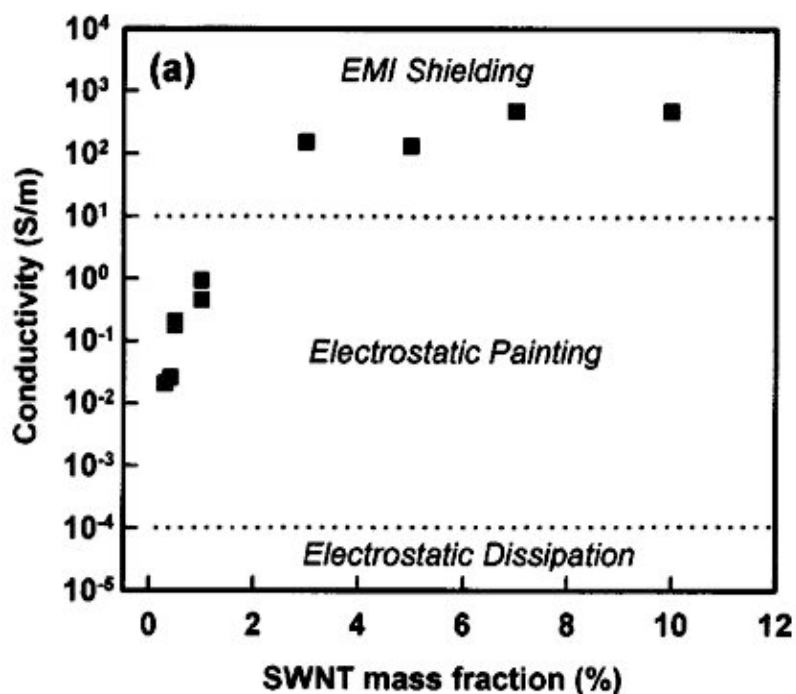


Figure 2.9. Electrical conductivity as a function of SWNT loading for SWNTs/PC composites. Dashed lines represent the approximate conductivity lower bound required for specific electrical applications (from Ref. 141).

2.3.2. Mechanical Properties of Polymer-Nanotube Composites

The use of nanotubes to improve polymer mechanical behavior is as studied as electrical conductivity.^[142-144] Oxidized and fluorinated SWNT were added to epoxy by Zhu et al.^[145,146] The nanotubes were first treated by a mixture of H_2SO_4/HNO_3 and HCl was then added to make carboxylic acid-functionalized SWNTs. These nanotubes were subsequently fluorinated at 150 °C for 12 h to obtain approximate C_2F stoichiometry. The fluorinated nanotubes were dispersed in DMF by sonication and the curing agent was added after evaporating DMF and subsequently degassed and cured. SEM images of the fracture surfaces (see Figure 2.10) for the samples with and without functionalization

show a transition from nonuniform dispersion (with pristine SWNT) to homogeneous dispersion (with functionalized SWNT). Compared to samples made with 1wt% pristine SWNT, composites reinforced by 1wt% functionalized SWNT show 18% and 24% improvement in tensile strength and elastic modulus, respectively. MWNTs/epoxy composite was also reported by attaching a curing agent to the nanotube surface.^[147] Tensile modulus, tensile strength, and break strain were increased by 28%, 104%, and 60%, respectively when 1wt% agent-functionalized MWNT/epoxy composite was cured by another curing agent.

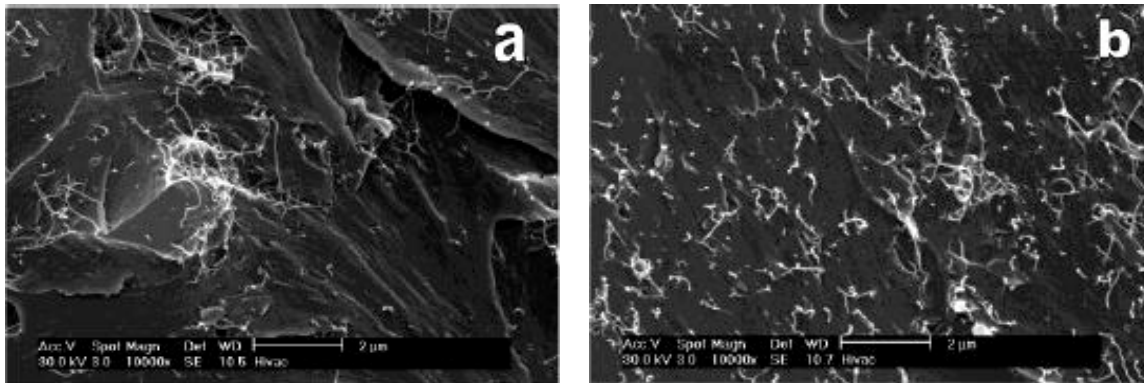


Figure 2.10. Fracture surface SEM images for epoxy composites reinforced by 1wt% pristine SWNT (a) and 1wt% functionalized SWNT (b) (from Ref. 145).

In some cases, in-situ radical polymerization has been applied to make nanotube-filled composites.^[148-150] Jia et al. used 2,2'-azobisisobutyronitrile (AIBN) as an initiator to start polymerization of PMMA off of MWNT surfaces by breaking the π -bonds and hence attaching polymer chains to the nanotubes.^[151] Unfortunately, only a limited increase in mechanical properties was observed for this system. This method was slightly modified by Velasco-Santos et al. who instead introduced oxidized and functionalized MWNT into the in-situ polymerization of MMA.^[152] This significantly increased tensile strength and toughness, as the addition of 1.5wt% functionalized MWNT improved toughness by 75%. In-situ polymerization was also used for preparation of carbon nanotube/polyamide (PA) composites.^[153,154] Additionally, Gao et al. used in-situ ring-opening polymerization of caprolactam to allow continuous spinning of SWNT/PA-6 fibers with typical fiber diameter and length of 200 μm and hundreds of meters, respectively (see Figure 2.11).^[155] For the range of SWNT loading studied (0.1 to 1.5 wt%), composites loaded with 0.2 wt% and 1.5 wt% SWNT showed the highest tensile strength (127% improvement) and Young's modulus (173% improvement).

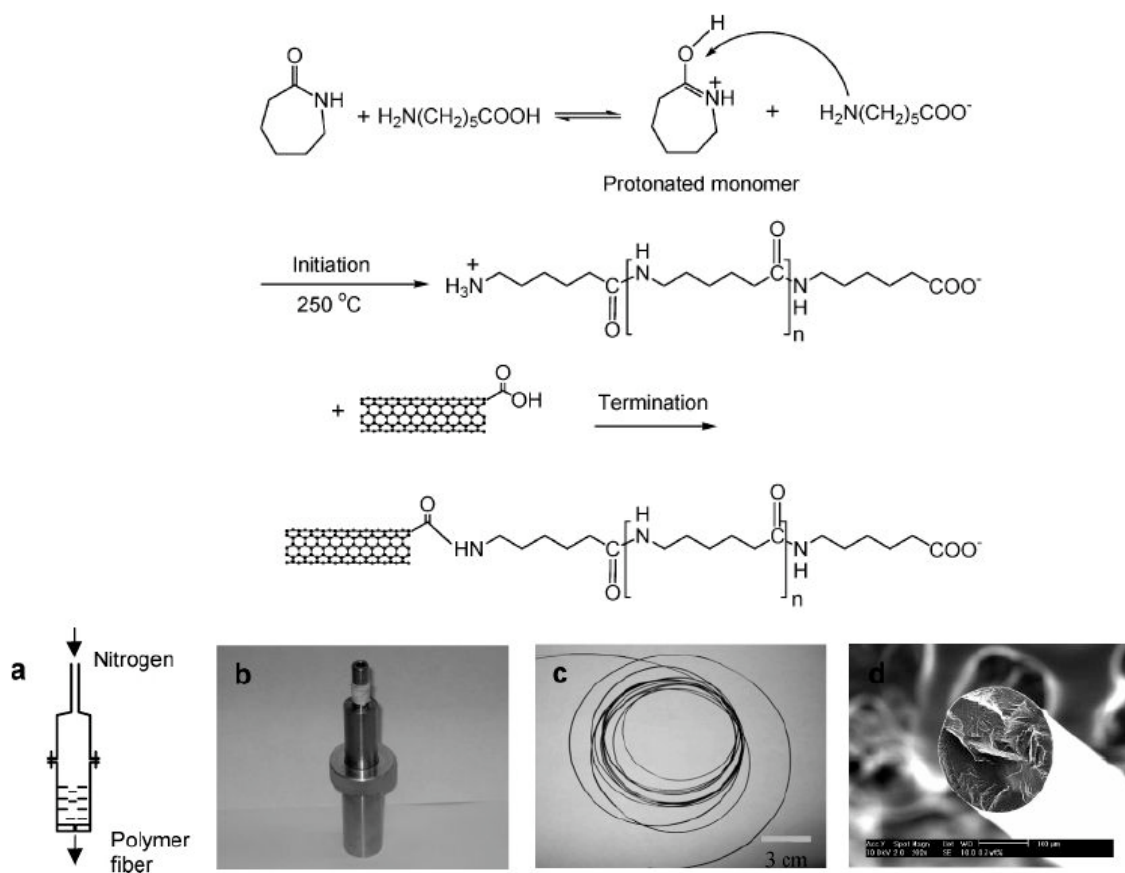


Figure 2.11. Top: Scheme of the preparation of SWNT/PA-6 composites via ring-opening polymerization of caprolactam. Bottom: Scheme of the spinneret setup (a); photograph of the setup (b); photograph of the composite fiber (c); SEM image of the cross-sectional fracture of the composite fiber (d) (from Ref. 155).

The first study using nanotube for reinforcement of solution based composites was by Shaffer and Windle,^[156] but very little increase in storage modulus was observed for the dried poly vinyl alcohol (PVA)/MWNTs composites. With 60 wt% addition of MWNT, the storage modulus increased from approximately 6 GPa for the neat polymer to 12 GPa. Cadek et al. examined Young's modulus and hardness for MWNT/PVA and

MWNT/poly (9-vinyl carbazole) (PVK) films by nanoindentation.^[157] The Young's moduli were found to increase from 7 GPa to 12.5 GPa and from 2 GPa to 6 GPa for 1 wt% MWNTs/PVA composite and 8 wt% MWNTs/PVK composite, respectively. Very recently, Wang et al. fabricated PVA tapes with highly aligned SWNTs and polymer chains after drawing the solution-cast films in the solid state.^[158] Remarkable increases in Young's modulus and tensile strength were observed with a small amount of nanotube loading. For example, the addition of 1 wt% SWNT led to a 200% increase in tensile strength.

2.3.3. Other Properties and Applications for Polymer-Nanotube Composites

Haggenmueller et al. studied the thermal conductivity of SWNTs/PE composites in terms of SWNT loading, the degree of PE crystallinity, and the PE alignment.^[159] It was observed that the SWNTs/PE composites made with high density PE (HDPE, ~78% crystalline) showed higher thermal conductivity than the composite made with low density PE (LDPE, ~33% crystalline). For example, an isotropic SWNT/HDPE composite with 20 vol.% has a thermal conductivity twice as high as the composite made with an LDPE matrix, reaching 3.5 W/mK. Melt fiber spinning of SWNT/HDPE composites with low nanotube loading enables the alignment for both nanotubes and PE crystallites and the thermal conductivity along the alignment direction increases with PE alignment, regardless of the nanotube loading. Other groups have also studied the thermal conductivity of nanotube/polymer composites.^[160,161]

Nanotube/polymer composites have been found to be good sensors. Loh et al. built multifunctional carbon nanotube/polyelectrolyte thin films through layer-by-layer assembly and tested the strain and corrosion sensing capability.^[162] The layer-by-layer method involves sequential dipping of a charged substrate in to opposite charged polyanion and polycation solutions to deposit a variety of species one monolayer at a time. Yu et al. used a similar approach to make polyethyleneimine/oxidized MWNTs multilayer films for humidity sensing.^[163] Wanna et al. studied MWNTs/polyaniline composites for carbon monoxide sensing.^[164] Zhang et al. fabricated sensors using SWNTs that were electrochemically functionalized with polyaniline, which are capable of sensing ammonia gas.^[165] Numerous nanotube-filled composites have been examined for their ability to sense temperature, humidity, and chemicals.^[166-170] It is this wide variety of property enhancements and applications that make the study of carbon nanotube filled composites so necessary.

CHAPTER III

COMPARISON OF NONCOVALENTLY AND COVALENTLY FUNCTIONALIZED CARBON NANOTUBES IN EPOXY

3.1. Introduction

In order to transfer the properties of nanotubes to the polymer composite, proper nanotube stabilization is needed. Improved dispersion, exfoliation, and compatibility of nanotubes can be achieved by using covalent^[22,25,29,35,48,52,70,145,154,171-180] or noncovalent approaches.^[29,35,52,74,76,80,131,177,181-183] Noncovalent functionalization requires the addition of a polymer,^[80,183] surfactant^[52,76,80,131,181] or secondary particle (e.g., clay)^[182] that interacts strongly enough with the nanotubes (and matrix/solvent) to break intertubular bonds. It is now understood that noncovalent stabilization can preserve the electrical properties of nanotubes.^[29,184] On the contrary, covalent functionalization can dramatically improve the interfacial interaction between the nanotubes and polymer matrix via direct chemical bonding, which is stronger than noncovalent interactions. Examples of covalent modification of nanotubes include oxidation,^[22,25,48,177] fluorination,^[25,57,145,174,178,179] in-situ polymerization,^[25,35,52,70,154] and polymer chain attachment.^[25,35,171,176,180] A notable drawback for covalent functionalization is the disruption of the surface conjugated π network, which leads to the reduction of electrical conductivity.^[35,185] This is especially true when a higher degree of functionalization is achieved, such as nanotube fluorination, which can reach approximately C_2F .^[57] For applications requiring electrical conductivity (EMI shielding,^[186] sensing,^[162]

electrostatic dissipation,^[187] etc.), damaging the nanotube's ability to transport electrons must be avoided.

Covalently functionalized nanotubes have been shown to simultaneously raise the percolation threshold in epoxy composites and improve mechanical properties.^[147,188] In one study, MWNTs were reacted with 3-glycidoxypropyltrimethoxysilane and subsequently introduced into an epoxy matrix.^[189] A uniform dispersion of nanotubes was achieved and the modulus increased about 12% over the sample containing unmodified nanotubes (for nanotube loading at 0.25 wt% or above), but electrical conductivity decreased by nearly 8 orders of magnitude relative to unfunctionalized MWNT-filled epoxies. Many studies have been carried out to understand the surface chemistry of nanotubes and their contribution to the property enhancement of the composite.^[36,48,190] Despite all of this work, there has not been a study to directly compare the effect of one agent that is covalently and noncovalently combined with nanotubes. This requires a molecule that can act as a surfactant and can also be covalently attached to the nanotube surface in a relatively simple way. In a recent study, the influence of nanotube covalent acid oxidation and non-covalent surfactant adsorption on the thermal and electrical properties of polyvinyl alcohol (PVA)/nanotube composites was studied.^[177] Unfortunately the two types of nanotube stabilization resulted in significant differences in composite composition, which made direct comparison of the two systems very challenging. Composites containing end functionalized carbon nanotubes have been reported and little effect on composite electrical conductivity was found due to nanotube functionalization.

The present study takes advantage of a recently developed technique to covalently attach polyethylenimine (PEI) to multi-walled carbon nanotubes (MWNTs).^[191] This “graft to” method maintains the intrinsic physical and chemical properties of the polymer after the reaction.^[62] Epoxy composites containing PEI covalently functionalized to nanotubes were compared to composites containing a physical mixture of PEI and MWNTs. In other words, the nanotubes and PEI used in both composites are identical. In one system PEI was used as a surfactant to aid the dispersion of nanotubes and in the other system PEI was chemically bonded to achieve the same purpose. The influence of interaction type (covalent or noncovalent) on the electrical and mechanical properties of the composites was directly evaluated. The results confirm that covalent bonding degrades conductivity, while enhancing dispersion and modulus relative to noncovalent bonding.

3.2. Experimental

3.2.1. Materials

Two types of multi-walled carbon nanotubes were used in this study. Low conductivity MWNTs (ID: 5-10 nm, OD: 20-30 nm, length: 10-30 μm) were purchased from Cheap Tubes (Brattleboro, VT). Higher conductivity MWNTs (ID: 5-10 nm, OD: 20-30 nm, length: 0.5-200 μm) and polyethylenimine (PEI) with a molecular weight of 10,000 g/mol were purchased from Aldrich (Milwaukee, WI). Bisphenol-F based epoxy resin (D.E.R. 354) with epoxide equivalent weight of 167–174 g/eq was provided by the

Dow Chemical Company (Midland, MI). 1-Methyl tetrahydrophthalic anhydride (ECA-100, Dixie Chemical) and an amine catalyst, N,N-dimethylbenzylamine ($\geq 99\%$, Aldrich) were used as the curing agent and catalyst, respectively.

3.2.2. Sample Preparation

Covalent attachment of PEI molecules to the surface of MWNTs was achieved using an established procedure.^[191] In a typical preparation, 2 g of MWNTs and 10 g of PEI were mixed in 100 ml of N,N-dimethylformamide (DMF) and the covalent functionalization occurred after sonication for 30 min, followed by stirring at 50 °C for 3 days. The reaction product was continuously washed by DMF, 1 M HCl, 1M NaOH, water, and methanol to remove any excess PEI. The product is oven dried for overnight before any epoxy composite fabrication.

The MWNT-filled composites were made by suspending an appropriate amount of nanotubes and PEI in 100 ml of acetone with sonication at 50W for 20 min using a VirTis Virsonic 100 Ultrasonic Cell Disrupter (SP Industries, Warminster, PA). Epoxy resin, curing agent, and amine catalyst were then dissolved in acetone and mixed with the MWNT suspension. This mixture was mechanically stirred for 5 min at 1720 rpm followed by 30 min at 3100 rpm and sonicated in a water bath for an hour. Acetone was removed by rotation evaporation at 60 °C and the mixture was cured in a glass mold for one hour at 95 °C, followed by three hours at 150 °C. The weight ratio of epoxy resin to the curing agent was kept at 5:4, while the amine catalyst was maintained at 1 wt% of the total solids.

3.2.3. Characterization

Sheet resistance ($<120,000 \Omega/\text{sq}$) of the epoxy composites was measured with a home-built four-point probe apparatus consisting of an Agilent E3644A DC power supply (Agilent Technologies, Inc., Englewood, CO), Keithley Model 2000 digital multimeter (Keithley Instruments, Inc., Cleveland, OH), and an SP4-62180TRS four-point probe head (Lucas Labs, Gilroy, CA). Composites with higher resistance ($>120,000 \Omega/\text{sq}$) were measured with a VOYAGER Surface Resistivity Meter (SRM)-100 (PINION Products Corp., Los Fresnos, TX). Dynamic mechanical analysis was done with a Q800 (TA Instruments, New Castle, DE) using a temperature ramp of $5 \text{ }^\circ\text{C}/\text{min}$ at a frequency of 1 Hz. Thermomechanical analysis was performed with a Q400 (TA Instruments, New Castle, DE) using a $5 \text{ }^\circ\text{C}/\text{min}$ temperature ramp. SEM images were taken by FEI Quanta 600 FE-SEM, which is supported by the NSF grant DBI-0116835, the VP for Research Office, and the TX Eng. Exp. Station.

3.3. Results and Discussion

3.3.1. MWNT Functionalization

Figure 3.1 shows the reaction scheme for covalent functionalization of MWNTs by PEI. It can be seen that after functionalization, the conjugated π network on nanotube surface is disrupted due to the breakup of double bonds and the branched PEI molecules are attached to the nanotube surface via amide bonding. Thermogravimetric analysis was carried out to determine the weight percentage of polymer after functionalization, as

shown in Figure 3.2. PEI exhibits a clear thermal degradation starting at ~ 300 °C and leaves almost no residue when the temperature reaches ~ 450 °C. For pristine MWNTs, there is negligible weight loss before ~ 650 °C, which suggests that the weight loss for the functionalized product between 300 °C and 450 °C is exclusively due to the degradation of PEI molecules chemically attached to the nanotube surface. Using this method, the degradation curve for the functionalized product was normalized to get rid of any influence of moisture and the reaction product was found to contain 8 wt% PEI, in the case of low conductivity MWNTs. The covalently functionalized MWNTs are denoted as C-MWNT-PEI, whereas the noncovalently functionalized nanotubes are denoted as N-MWNT-PEI. The same procedure used with the higher conductivity MWNTs resulted in 6 wt% PEI attachment.

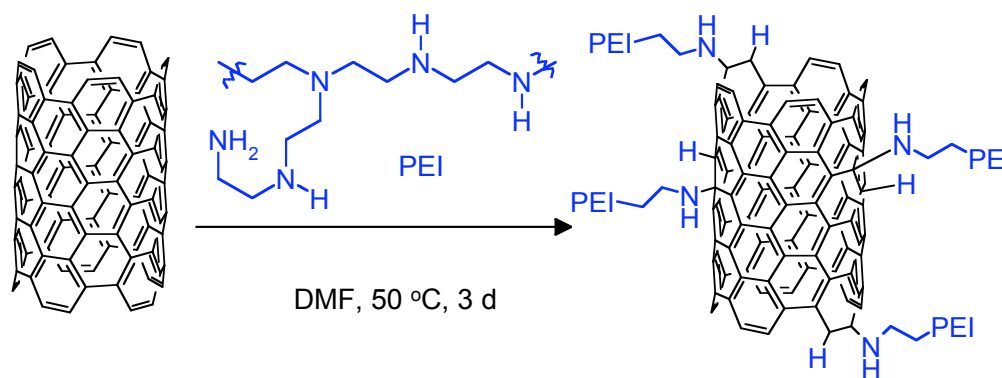


Figure 3.1. Reaction scheme for covalent functionalization of MWNT with PEI.

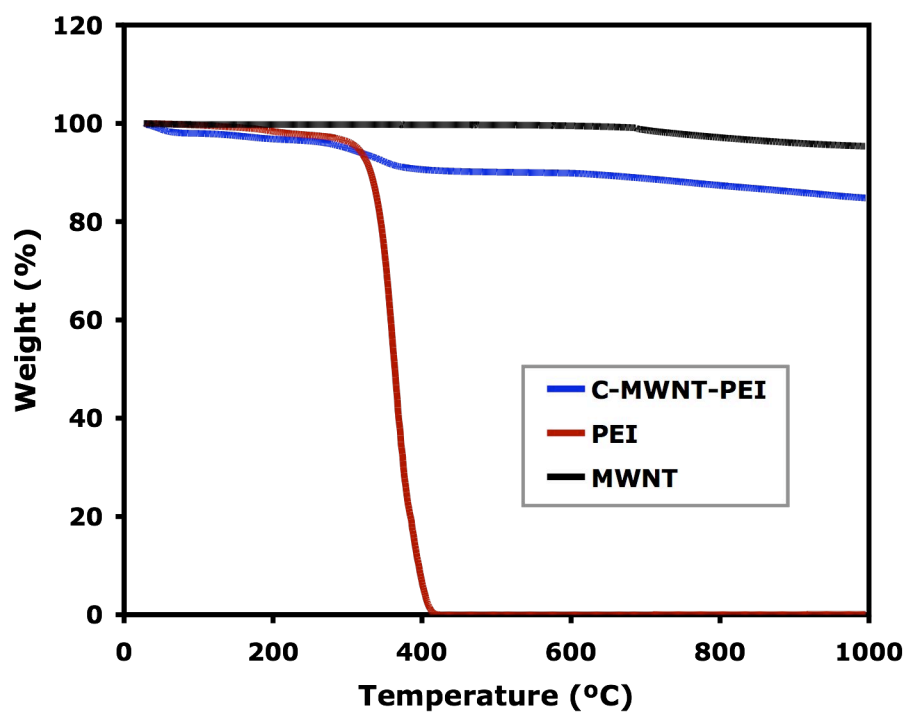


Figure 3.2. Weight loss as a function of temperature for pristine MWNTs, PEI, and the PEI-functionalized MWNTs (shown for low conductivity MWNTs).

3.3.2. Epoxy Composites Containing Low Conductivity MWNTs

Figure 3.3 shows SEM images of freeze-fractured cross-sections of epoxy containing 1 wt% of pristine MWNTs, N-MWNT-PEI, and C-MWNT-PEI. Without any functionalization, the nanotubes exist as numerous heavily aggregated bundles (Fig. 3.3(a, b)), while covalent functionalization dramatically improves the nanotube dispersion. At low magnification it is difficult to find any large nanotube aggregates (Fig. 3.3(e)). Nanotubes are also found to be better embedded into epoxy when covalently modified (Fig. 3.3(f)), which is evidenced by the lack of nanotube pullout from the matrix. At higher magnification, both unfunctionalized (Fig. 3.3(b)) and noncovalently functionalized (Fig. 3.3(d)) systems show characteristic holes that are artifacts of MWNT pullout. Noncovalently functionalized nanotubes are shown to have an intermediate level of dispersion (Fig. 3.3(c, d)). Although some aggregation is apparent, many of the nanotubes are exfoliated into relatively small bundles or even individual nanotubes. Noncovalent functionalization is expected to be less efficient due to lack of strong bonds holding the PEI at the nanotube surface. Covalent functionalization guarantees that all PEI is used for stabilization and there is no free polymer mixed into the epoxy matrix, which may lead to poorer dispersion and possible plasticizing of the matrix.

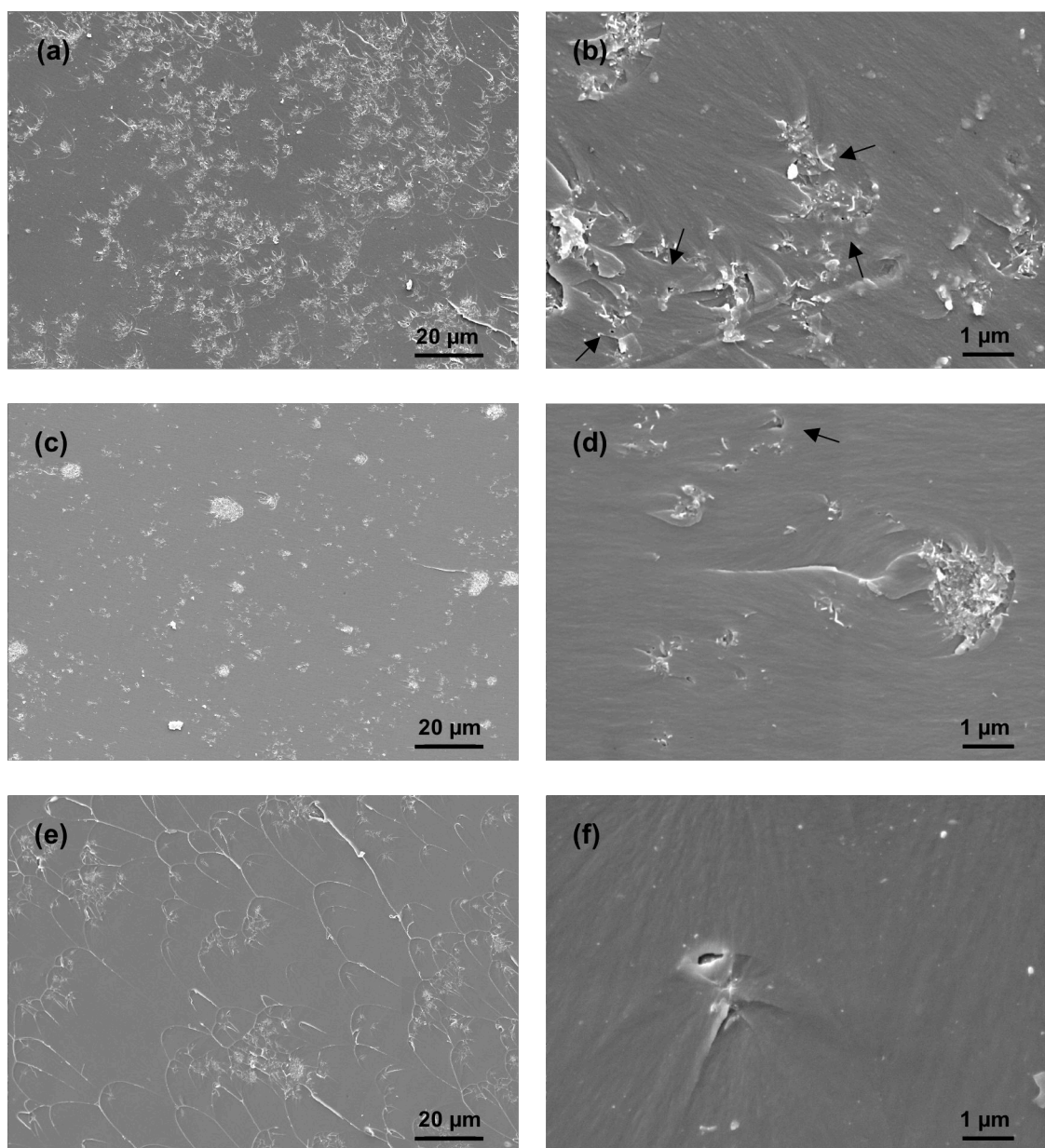


Figure 3.3. SEM images of freeze-fractured cross sections of epoxy composites containing 1 wt% MWNT (a, b), 1 wt% N-MWNT-PEI (c, d), and 1 wt% C-MWNT-PEI (e, f). These composites contain the MWNT that is stabilized by 8 wt% PEI. Arrows indicate points of MWNT pullout.

The changes in nanotube microstructure after functionalization have a dramatic influence on the electrical conductivity of these composites, as shown in Figure 3.4.

Both covalent and noncovalent functionalization of nanotubes reduce the electrical conductivity of the composites relative to those with no stabilization for MWNTs with 8 wt% PEI. Composites containing covalently functionalized nanotubes show no conductivity enhancement, even when the nanotube concentration reaches 1 wt%. This is believed to be due to the formation of chemical bonding on the surface of nanotubes during functionalization, which scatter electrons. Composites containing noncovalently functionalized nanotubes showed improved conductivity relative to C-MWNT-PEI/epoxy composites. A conductivity as high as 10^{-8} S/cm is realized when the composite has 1 wt% N-MWNT-PEI, which is nearly three orders of magnitude greater than C-MWNT-PEI. For all MWNT concentrations, the composites containing neat MWNT have the highest conductivity due to the aggregated nanotube microstructure and lack of insulating PEI to interfere with intertubular junctions. In the absence of PEI, the MWNT can efficiently transfer electrons to one another.

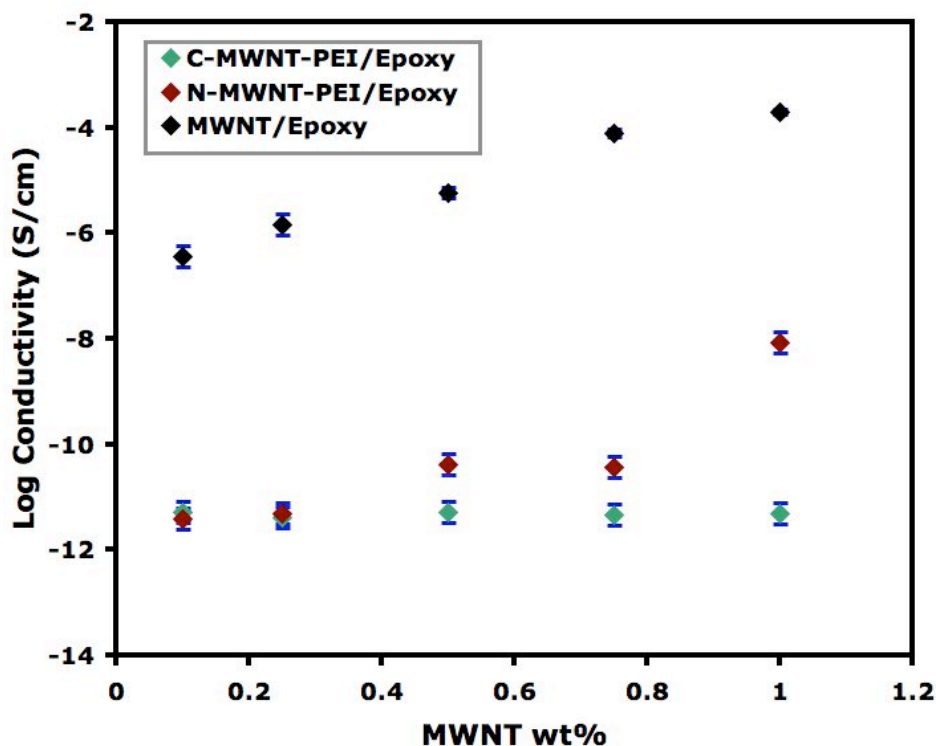


Figure 3.4. Electrical conductivity as a function of nanotube concentration for composites containing MWNT, C-MWNT-PEI, and N-MWNT-PEI, for low conductivity MWNTs with 8 wt% PEI attachment.

The dynamic mechanical properties of the composites containing 1 wt% pristine nanotubes, C-MWNT-PEI and N-MWNT-PEI are shown in Figure 3.5. All three samples exhibit similar glass transition temperature (~ 96 °C). The MWNT/epoxy composite is found to have nearly the same room temperature storage modulus as the N-MWNT-PEI/epoxy sample. Although better nanotube dispersion is observed after noncovalent nanotube functionalization (see Fig. 3.3), the nanotube/polymer interface is likely not as strong as the MWNT/epoxy sample due to the presence of adsorbed PEI molecules on the surface of nanotubes. It is possible that the contributions from better

nanotube dispersion and weakened nanotube/polymer interface cancel one another and result in a comparable storage modulus. The composite containing 1 wt% C-MWNT-PEI shows an 8 % improvement in storage modulus relative to the other two samples. This improvement is expected due to the greater nanotube/polymer interfacial interaction when all of the PEI molecules are covalently tethered to the surface of the nanotubes. It needs to be noted that it is also possible for PEI molecules to react with epoxy directly via the amine group.

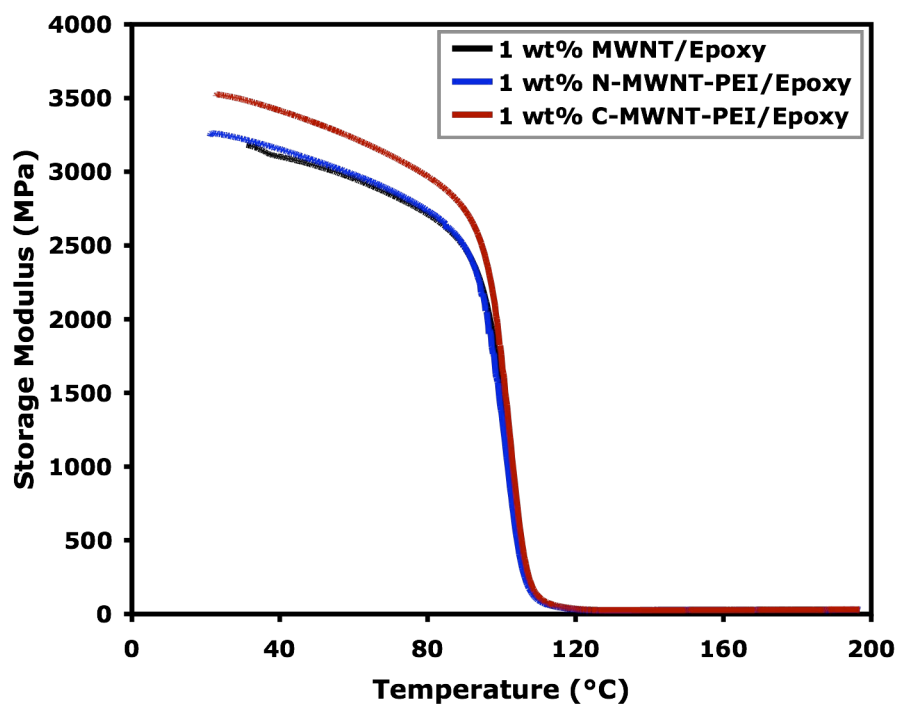


Figure 3.5. Storage modulus as a function of temperature for composites containing 1 wt% nanotubes.

Figure 3.6 shows the thermomechanical analysis of the composites containing 1 wt% nanotubes. It can be seen that all composites show similar glass transition temperature, near 110 °C, which is in relatively good agreement with the DMA results (see Fig. 3.5). The coefficient of thermal expansion (CTE) for the composite was determined according to the sample thickness and the slope of the thermal expansion curve. The CTE for N-MWNT-PEI/epoxy composite (before and after T_g) shows a slight increase as compared to the MWNT/epoxy (unfunctionalized) sample. This is believed to be due to the plasticizing effect of free PEI molecules. The C-MWNT-PEI/epoxy composite exhibits significantly reduced CTE relative to the MWNT/epoxy sample. The CTE values decreased from 71.6 $\mu\text{m}/(\text{m } ^\circ\text{C})$ to 64.3 $\mu\text{m}/(\text{m } ^\circ\text{C})$ and from 191.2 $\mu\text{m}/(\text{m } ^\circ\text{C})$ to 177 $\mu\text{m}/(\text{m } ^\circ\text{C})$ for the temperature ranges before and after T_g , respectively. It is very likely that this is due to the stronger interfacial interaction between epoxy and C-MWNT-PEI, which prevents the composite from expanding as rapidly over a given temperature range.

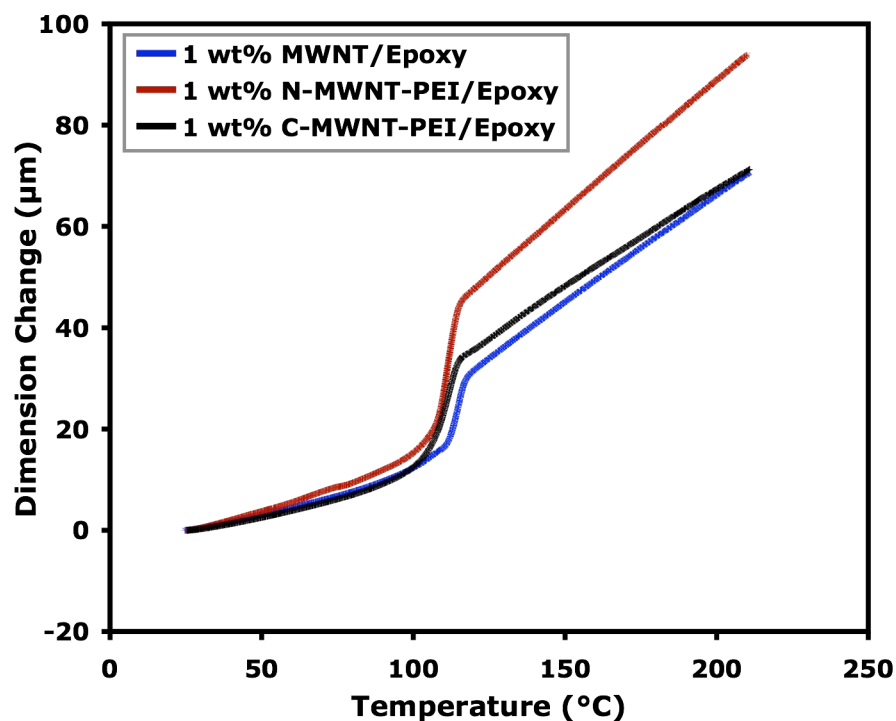


Figure 3.6. Thermal expansion of epoxy composites containing 1 wt% nanotubes.

3.3.3. Epoxy Composites Containing High Conductivity MWNTs

The nanotube dispersion for composites containing the high conductivity MWNTs, which have 6 wt% PEI attached, is shown in Figure 3.7. In this case, it is surprising to find that the N-MWNT-PEI demonstrates better nanotube dispersion than C-MWNT-PEI as evidenced by less nanotube aggregates and more exfoliated nanotubes. This is in contrast with the results for the composites containing low conductivity MWNTs. There are likely several contributing factors causing this discrepancy. First, the low conductivity MWNTs have greater PEI attachment that likely enhances dispersion. With greater functionalization (8 wt% PEI), the C-MWNT-PEI is more likely to have

better opportunity to interact with the epoxy matrix and result in a better dispersed nanotube network as compared to the MWNTs with lower PEI concentration. A second issue is the difference in length between the high and low conductivity nanotubes. The high conductivity MWNTs are nearly ten times as long, making it much easier for them to interact with one another. It is believed that this greater length increases the chance that PEI chains are actually covalently bonding multiple nanotubes together.

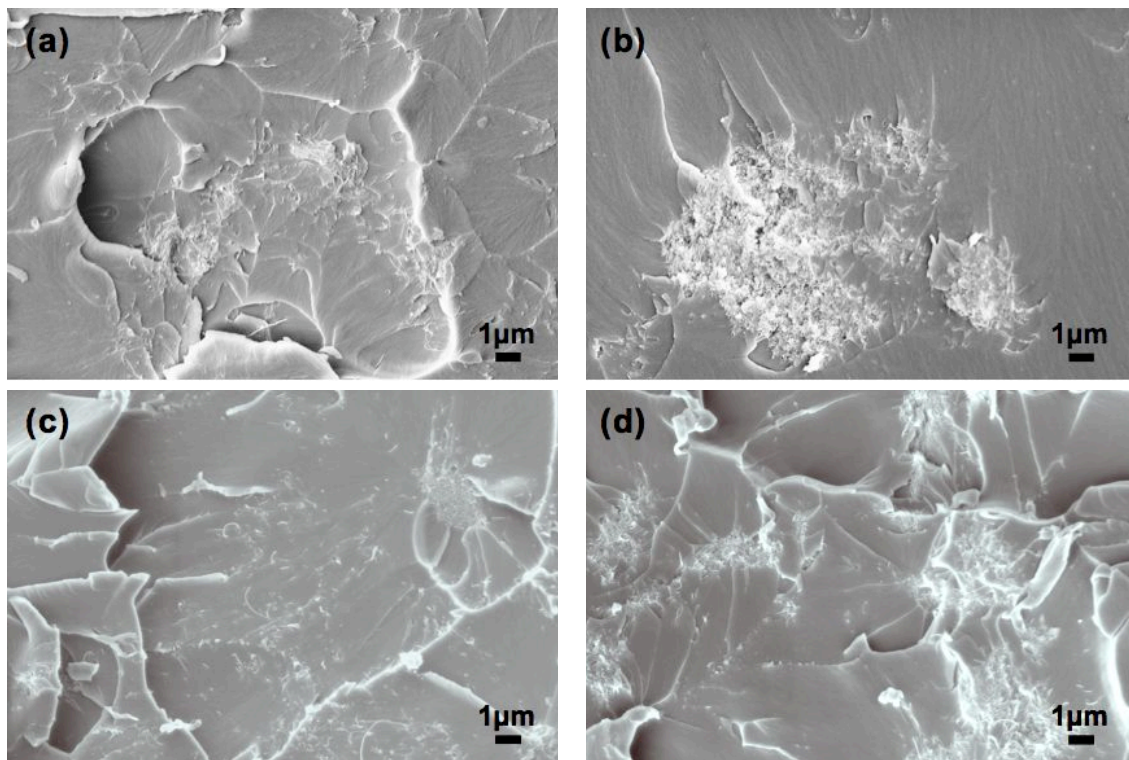


Figure 3.7. SEM images for epoxy composites containing 0.47 wt% MWNTs ((a) and (b)) and 0.94 wt% MWNTs ((c) and (d)). Image (a) and (c) are for N-MWNT-PEI while (b) and (d) are for C-MWNT-PEI.

When higher conductivity MWNTs are used, with reduced functionality (~6 wt% PEI), the conductivity differences between covalent and noncovalent composites are much more significant, as shown in Figure 3.8. In addition to having reduced PEI content, these nanotubes have a greater maximum length than those used in Fig. 3.4 (200 μm vs. 30 μm). Greater length is known to enhance conductivity due to the fewer junctions (or breaks) in a given electrical pathway.^[192] For the two nanotube loadings examined, the C-MWNT-PEI/epoxy samples exhibit lower conductivity relative to N-MWNT-PEI/epoxy and unfunctionalized composites. In this case, almost no conductivity disparity is observed between MWNT/epoxy and N-MWNT-PEI/epoxy samples. This result suggests that using higher conductivity nanotubes with lower PEI functionality maintains electrical conductivity when nanotubes are noncovalently functionalized. In systems where the matrix hinders network formation, it is likely that N-MWNT would provide greater conductivity.

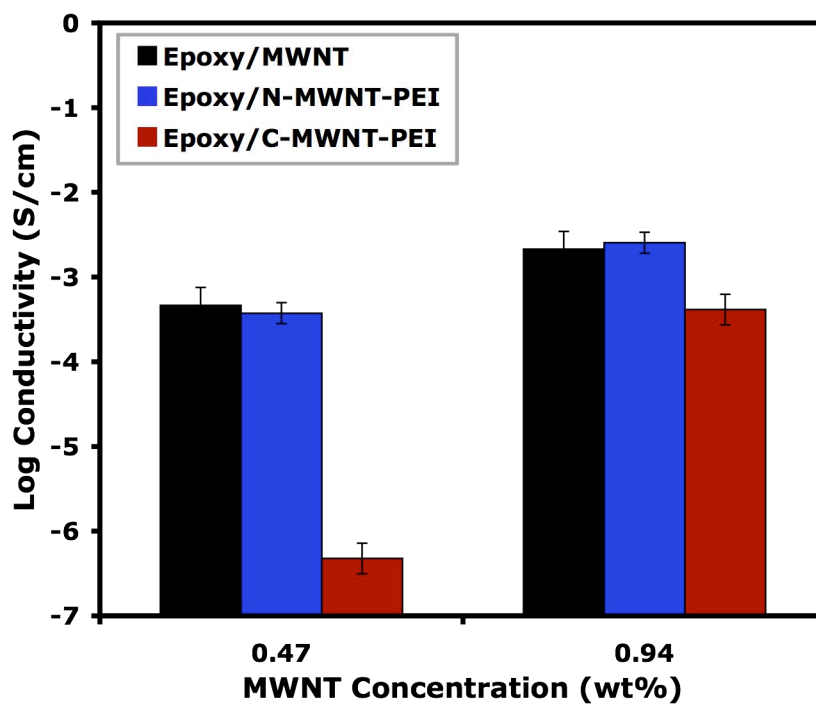


Figure 3.8. Electrical conductivity for the composites containing 0.47 wt% and 0.94 wt% MWNTs.

The dynamic mechanical properties of the composites containing C-MWNT-PEI and N-MWNT-PEI are shown in Figure 3.9. For nanotube loading of 0.94 wt% (Fig. 3.9(a)), the composite containing C-MWNT-PEI shows the highest modulus improvement by showing a storage modulus of 3.8 GPa. The sample containing just 0.94 wt% MWNT and 0.94 wt% N-MWNT-PEI exhibit storage modulus of 3.7 GPa and 3.5 GPa, respectively. The modulus enhancement after the addition of covalently functionalized MWNTs is due to the improved nanotube/epoxy interface that improves the load transfer characteristics of the composites. On the contrary, the sample with noncovalently functionalized MWNTs shows a reduced modulus as compared to the sample containing only 0.94 wt% nanotube. This suggests noncovalent functionalization could possibly decrease the contribution of nanotube addition to the modulus enhancement of the composite. The possible reason for this reduction is the plasticizing effect of free PEI molecules, but the differences amongst these composites is not great enough to warrant concern. The samples containing pristine MWNTs and N-MWNT-PEI exhibit similar glass transition temperature, while the composite containing C-MWNT-PEI shows decreased glass transition temperature, which is likely due to the nanotube aggregation (see Fig 3.7). The samples containing 0.47 wt% C-MWNT-PEI and 0.47 wt% N-MWNT-PEI show very similar storage moduli and glass transition temperature, as shown in Figure 3.9(b).

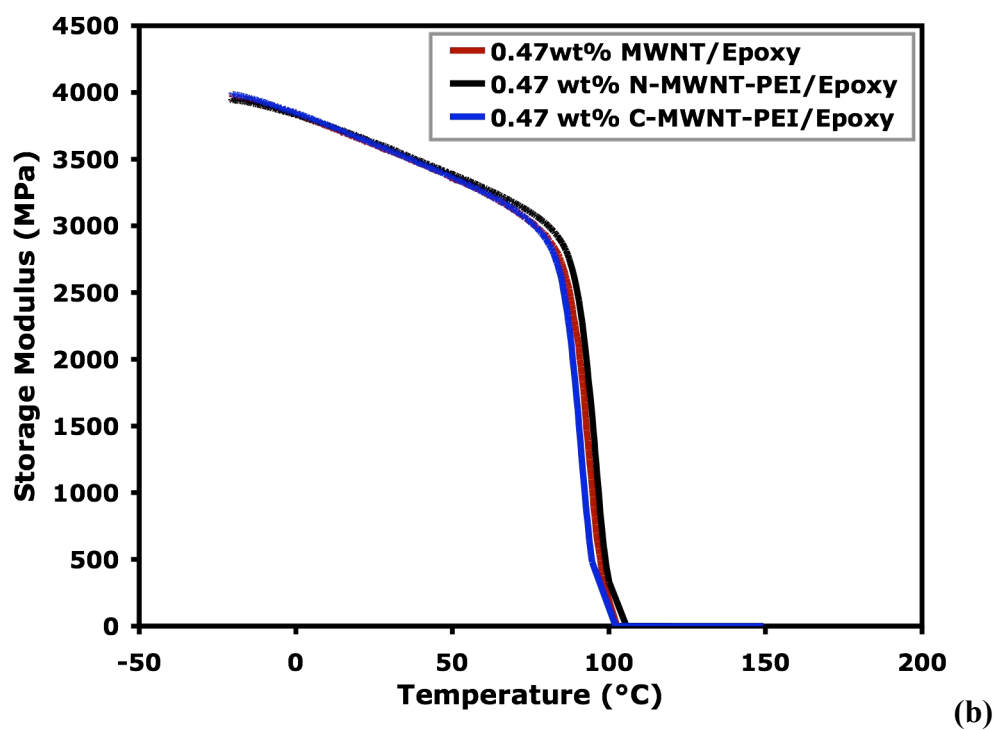
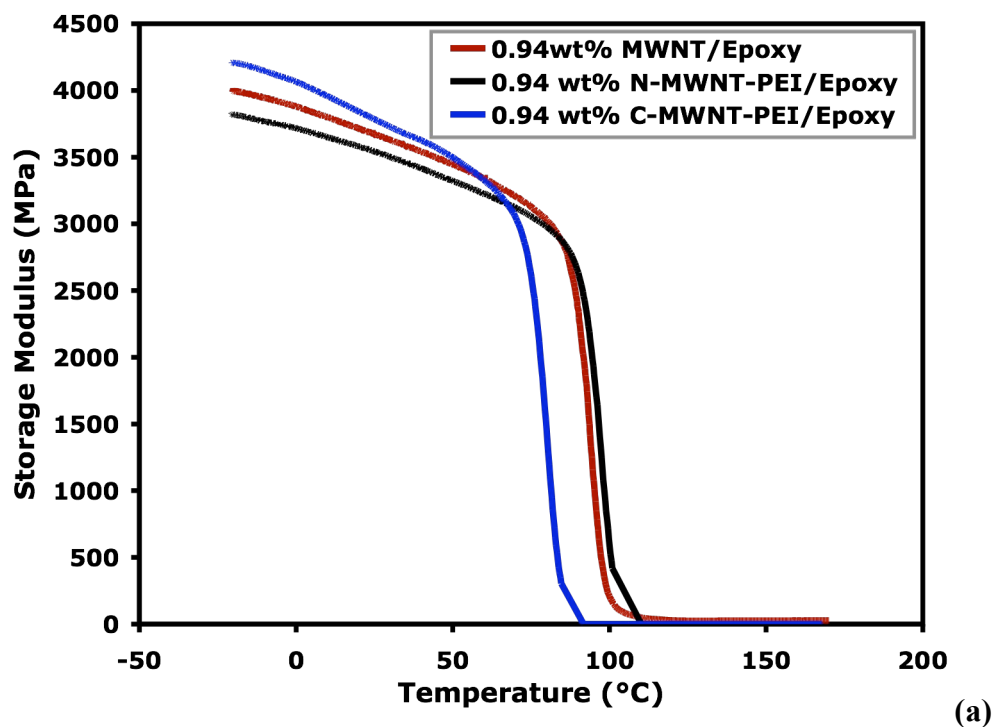


Figure 3.9. DMA for epoxy composites containing pristine MWNTs, N-MWNT-PEI, and C-MWNT-PEI at nanotube concentration of 0.94 wt% (a) and 0.47 wt% (b).

3.4. Conclusions

Polyethylenimine molecules were either chemically bonded or physically adsorbed on the surface of multi-walled carbon nanotubes to directly compare the influence of stabilization method on the microstructure and properties of epoxy composites. Composites were compositionally identical, with the only difference being whether MWNTs were covalently or noncovalently stabilized. For the composites containing lower conductivity MWNTs, both forms of functionalization produced improved nanotube dispersion, especially for the C-MWNT-PEI/epoxy composite. A decrease in electrical conductivity was observed for both samples, which is attributed to a weaker network for the better dispersed nanotubes. The C-MWNT-PEI/epoxy composite shows the lowest conductivity due to the disruption of the conjugated nanotube surface during functionalization, but an improved storage modulus is found simultaneously. When higher conductivity nanotubes (with lower PEI functionalization (~ 6 wt%)) are used, C-MWNT-PEI/epoxy composites are 10,000 times more resistive than their noncovalent counterparts. In this case, the noncovalent stabilization exhibits similar conductivity to unstabilized nanotubes. Storage modulus of the composites containing covalently functionalized nanotubes is also increased, relative to noncovalent, due to the stronger nanotube-polymer interaction. This study is the first direct comparison between covalent and noncovalent nanotube functionalization and its influence on the electrical and mechanical behavior of epoxy composites. Further work is needed to understand the influence of nanotube type and the ratio of stabilizing polymer to nanotube. These studies will serve to improve the ability of nanotubes to

enhance composite properties for applications that include EMI shielding, electrostatic dissipation, and conductive adhesives. Subsequent chapters explore other forms of noncovalent stabilization, using clay (Chapter IV) or pH-responsive polyelectrolytes (Chapter V), in an effort to enhance electrical conductivity and reduce percolation threshold. Any level of covalent functionalization will impair electrical conductivity, but it may be possible to enhance conductivity and mechanical behavior using noncovalent approaches.

CHAPTER IV

CLAY-ASSISTED DISPERSION OF CARBON NANOTUBES

4.1. Introduction

Clays are known to have a layered structure, in which the atoms in the layers are cross-linked by chemical bonds, while the atoms of adjacent layers interact by physical forces.^[193] The thickness of a single clay layer and the interlayer spacing are both in the single nanometer range. Clays are classified into structures such as kaolinite, smectite, and vermiculite, among which smectite is the most commonly used for polymer nanocomposites because of its high aspect ratio, large surface area, and high cation exchange capacity.^[194,195] For example, natural montmorillonite (a smectite) has a layer thickness of 1 nm and is composed of alumino-silicate platelets that have a chemical formulae of $\text{Al}_2\text{Si}_4\text{O}_{10}(\text{OH})_2 \cdot y\text{H}_2\text{O}$. The platelet carries a negative charge, which means that interlayer guest species must be positively charged (such as Na^+) to maintain electrical neutrality. Because the layers are held together by physical interactions (e.g., van der Waals forces), they can be intercalated by water or other organic molecules and hence expand their interlayer distance.^[196]

Clay-polymer composites are categorized into three types based on the extent of interlayer expansion: conventional composites (microcomposites), intercalated nanocomposites, and exfoliated nanocomposites,^[197] as shown in Figure 4.1. The distance between a unit layer and the next parallel unit layer is called the basal plane spacing, d . If the d value remains the same after the addition of clay to the polymer

matrix, the composite is a conventional microcomposite (Fig. 4.1(a)). If the interlayer space is filled by organic molecules, causing an increase in d value, but clay layers remain stacked, the composite is intercalated (Fig. 4.1(b)). If the clay layers are completely separated from one another and form disordered arrays, the composite is an exfoliated nanocomposite (Fig. 4.1(c)).^[198]

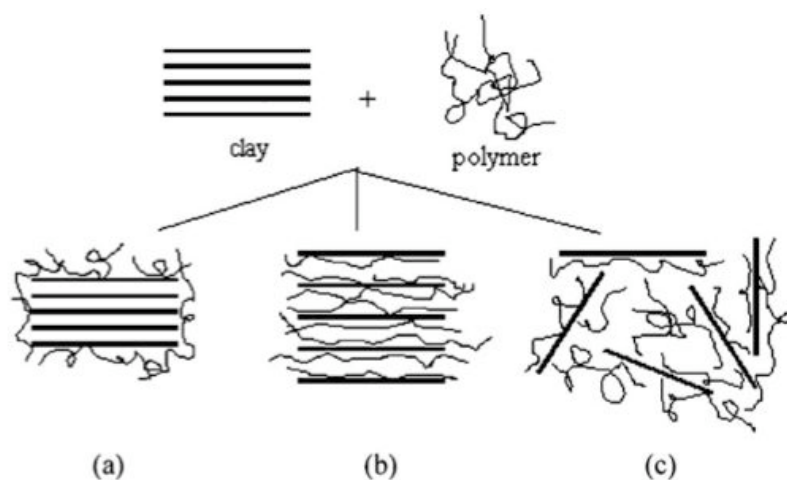


Figure 4.1. Schematic illustration of the three types of clay-polymer composites: conventional composite (a), intercalated nanocomposite (b), and exfoliated nanocomposite (c) (From Ref. 198).

The introduction of clay into a polymer matrix can significantly improve properties such as mechanical behavior,^[15,16] gas barrier,^[199,200] and flame retardancy.^[201,202] For example, 4.2 wt% of clay was found to increase the tensile strength of nylon 6 from 69 MPa to 107 MPa and double the tensile modulus, while

retaining the impact strength.^[203,204] An exfoliated clay/epoxy nanocomposite exhibited a 25% increase in storage modulus for both glassy and rubbery phases with just 5 wt% clay.^[205] For the barrier properties, the permeation coefficient of water vapor was reduced by 54% for a clay/polyimide composite with the addition of only 2 wt% montmorillonite.^[206] Flame retardancy, normally quantified by heat release rate, was reported to have a 40% reduction when 5 wt% organoclay (functionalized clay) was added to nylon 6.^[207]

In the present study, clay platelets were introduced into single-walled carbon nanotube (SWNT)/epoxy composites to improve nanotube dispersion, improve electrical conductivity and maintain mechanical performance. Unlike surfactant or polymer dispersants, clay is mechanically strong and known to have good dispersion/load transfer characteristics in a polymer matrix.^[13,15,16] Although charged ZrO_2 particles have been used to stabilize nanotubes in water,^[208] no polymer composite reinforced by nanotubes and another charged inorganic particle has been reported prior to this study. This study provides a new method to facilitate nanotube dispersion by adding a secondary filler. The clay/nanotube interaction is studied microscopically to understand how the addition of clay improves electrical conductivity. In other words, the focus here is to more effectively disperse nanotubes by using clay as a dispersing aid and ultimately improve nanocomposite properties.

4.2. Experimental

4.2.1. Materials

Raw SWNTs used for this study were produced by the HiPco process and contain 27wt% iron impurity (provided by Carbon Nanotechnologies, Houston, TX). Bisphenol-F based epoxy resin (D.E.R. 354, epoxide equivalent weight of 167-174 g/eq), 1-methyl tetrahydrophthalic anhydride curing agent (ECA-100), and N,N-dimethylbenzylamine ($\geq 99\%$) catalyst were obtained from The Dow Chemical Company (Midland, MI), Dixie Chemical (Houston, TX) and Aldrich (Milwaukee, WI), respectively. Natural montmorillonite clay (Cloisite[®] Na⁺) and organoclay (Cloisite[®] 15A and Cloisite[®] 30B) with cation exchange capacity (CEC) of 92.6 meq/100 g, 125 meq/100 g, and 90 meq/100 g, respectively, were provided by Southern Clay Products (Gonzales, TX).

4.2.2. Preparation of Nanotube Suspension and Nanocomposites

Aqueous suspensions of clay and SWNTs were prepared by introducing an appropriate amount of Cloisite[®] Na⁺ and SWNTs into glass vials, followed by sonication at 50 W for 20 min using a VirTis Virsonic 100 Ultrasonic Cell Disrupter (SP industries, Warminster, PA). The weight ratio of Cloisite[®] Na⁺ to SWNTs was kept at 10:1 and the concentration in water was 0.25 wt% and 0.025 wt%, respectively. This masterbatch was further diluted for different purposes such as digital imaging and cryo-TEM imaging.

SWNT/clay/epoxy composites were made by first suspending a given amount of SWNT and clay in 40 ml of acetone with sonication at 50 W for 20 min using the same

ultrasonic tool used for aqueous dispersions (described in preceding paragraph). Epoxy resin, curing agent, and amine catalyst were then dissolved in acetone and mixed with the SWNT/clay suspension. This mixture was mechanically stirred for 5 min at 1720 rpm followed by 30 min at 3100 rpm and sonicated in a water bath for one hour. Acetone was removed by rotation evaporation at 60 °C and the mixture was cured in a glass mold for one hour at 95 °C followed by three hours at 150 °C. The weight ratio of epoxy resin to the curing agent was kept at 5:4, while the amine catalyst was maintained at 1 wt% of the total solids. For example, the composite containing 0.1 wt% SWNT and 2 wt% clay has a weight ratio composition of 53.83/43.07/1/2/0.1 (epoxy resin/curing agent/amine catalyst/clay/SWNT).

4.2.3. Liquid Suspension and Nanocomposite Characterization

Electrical conductivity of nanocomposite panels was measured with a four-point probe system, as described in Chapter III. Composites with higher sheet resistance ($>120,000 \Omega/\text{sq}$) were unable to be measured by the four-point probe system and were measured with a Voyager Surface Resistivity Meter (SRM)-110 (Pinion Products Corp.). Digital photos of the aqueous SWNT/clay suspension were taken with an Olympus D-580 camera. Optical microscopy was performed with an Olympus BX60 operated in transmission mode under bright field and cross-polarized light conditions. Composite samples were polished down to 80 μm before imaging. Scanning electron microscopy was performed with a Zeiss 1530 VP FE-SEM (supported by the National Science Foundation under Grant No. DBI-0116835). Epoxy panels were soaked in liquid

nitrogen and fractured by hand to prepare cross-sectional surfaces, which were coated with 4 nm of platinum before imaging. Transmission electron microscopy of composite samples were obtained with a JEOL 1200 EX TEM. Raman spectroscopy was carried out with 632 nm laser excitation in a JYHoriba LabRam-IR system equipped with a CCD detector. Cryo-TEM imaging for the aqueous suspension of nanotubes and clay was performed with an FEI Tecnai G2 F20 FE-TEM containing a cryo-accessory. Samples were sonicated for 30 minutes and applied onto freshly glow-discharged homemade holey carbon grids, which were blotted and plunge frozen using an FEI Vitrobot. Vitrified specimens were transferred under liquid nitrogen to a GATAN 626 cryo-specimen holder and imaged under low-dose conditions by a GATAN Ultrascan 1000 CCD camera at 200 kV. Dynamic mechanical analysis (DMA) of the nanocomposites was carried out with an RSA III (TA Instruments, New Castle, DE), equipped with a three-point bending fixture, using a temperature ramp of 2 °C/min and a frequency of 1 Hz.

4.3. Results and Discussion

4.3.1. Clay-Nanotube Interaction in Water

Before studying the interaction between SWNTs and clay in nanocomposites, their interaction in water was examined. Figure 4.2 shows the digital images of glass vials containing aqueous suspensions of only SWNTs (right vial) and a SWNT/montmorillonite clay mixture (left vial). The SWNT concentration for both containers are the same, at 0.00025 wt%, and the weight ratio between clay and nanotubes is 10:1. The vial containing only nanotubes shows very little nanotube stability, even right after sonication, as evidenced by visible nanotube chunks in almost clear liquid (Fig. 4.2(a), right vial). This is in good agreement with studies by others^[209] and is due to the hydrophobic characteristics of pristine nanotubes. In contrast to this lack of nanotube solubility in water, the vial containing the SWNT/clay mixture shows a uniform dark brownish liquid without any visible aggregates right after sonication (Fig. 4.2(a), left vial). This suggests that clay aids the dispersion of nanotubes in water, much like a surfactant like sodium dodecyl sulfate (SDS).^[181,210]

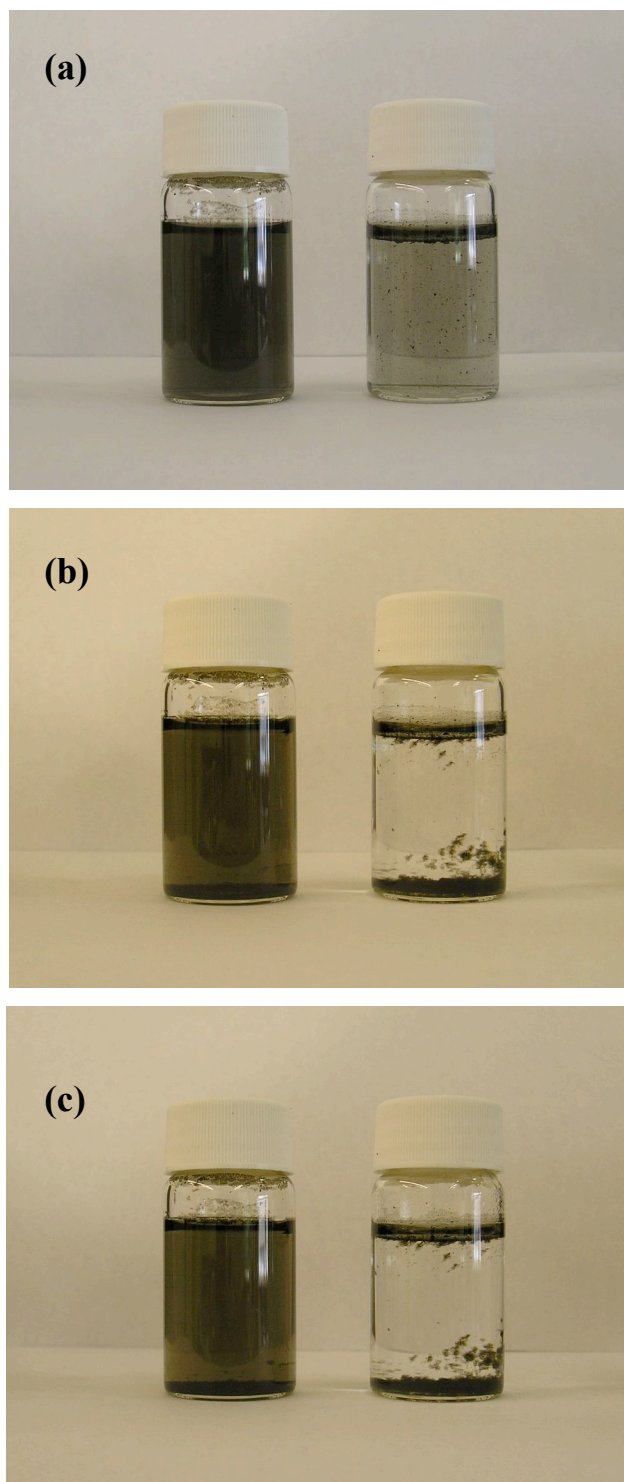


Figure 4.2. Digital images of SWNT suspensions in water with a 10:1 weight ratio of clay to SWNTs (left) and without any clay (right). Images were taken right after sonication (a), one day after sonication (b), and one week after sonication (c).

Although incomplete, the clay stabilization of SWNT is relatively long lasting. In the absence of clay, all the nanotubes phase separated in less than one day at ambient conditions (Fig. 4.2(b), right vial). The liquid is transparent and nanotubes either precipitated to the bottom of the vial or stayed at the top of the liquid surface. With clay addition, the liquid maintained the dark brownish color, but it became lighter as compared to the as-produced sample (Fig. 4.2(b), left vial). Nanotubes did settle to the bottom of the vial, but the amount of precipitation was much less than the liquid without clay. One week after the initial preparation of the suspensions, there is no visible change for the liquid without clay and the vial containing both clay and nanotubes maintained a homogeneous dark supernatant indicative of well-suspended nanotubes. The supernatant did lighten somewhat with time, but a significant amount of SWNT appeared to stay suspended over a week. A recent study of clay-stabilized suspensions of nanotubes suggests that there is an attraction between the Lewis base character of the nanotubes and the weak acid character of the clay platelet faces.^[209,211] This hypothesis seems to be supported by cryo-TEM images of these suspensions.

Figure 4.3 shows nanotubes and clay particles in water that were imaged with cryo-TEM. The long ropes in the image are nanotubes and the black dots on the surface of the nanotubes are metal catalyst particles, which were used during the synthesis of these nanotubes and still present due to lack of purification. Clay layers are shown as short, rigid, and parallel lines in this image, as indicated by the arrows. Their length is much shorter than the nanotube bundles and this is likely because larger clay particles were removed during TEM sample preparation. This image reveals that the clay exists in

small stacks, which are composed of just a few layers of platelets. In all cases, the clay layers stay very close to the vicinity of the nanotubes, which suggests there are strong interactions keeping them together. This clay/nanotube interaction, or affinity, seems to be due to more than weak van der Waals forces. There is likely a Lewis base-acid interaction (SWNT surfaces are known to have Lewis base character).^[212] It is this interaction that is believed responsible for significant electrical conductivity enhancement in nanotube-filled epoxy, as described in Section 4.3.2.

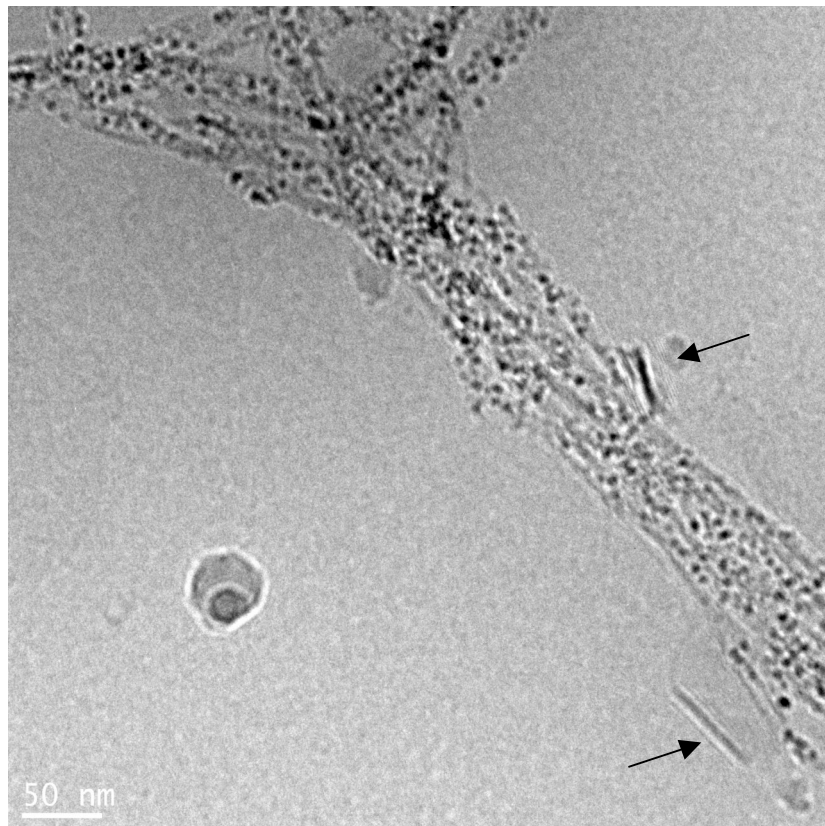


Figure 4.3. Cryo-TEM image of an aqueous suspension containing both nanotubes and clay.

Raman spectroscopy is another useful technique to study nanotube dispersion, especially in the tangential mode region (G-band), as shown in Figure 4.4. The G-band splits into two main components, a G^+ line at higher frequency (typically $\sim 1590\text{ cm}^{-1}$) and a G^- line at lower frequency (between 1530 and 1560 cm^{-1}), which is due to the C-C bonds in SWNT having higher force constants in the direction parallel to the tube length (G^+) than in the orthogonal direction (G^-).^[213,214] The G^- line has an asymmetric Breit-Wigner-Fano (BWF) lineshape that results from interference scattering between an electronic continuum in metallic tubes and the G^- Raman-active band.^[215,216] A diminished BWF lineshape and reduced intensity of G^- are generally found when a better dispersed nanotube suspension is realized.^[217,218] For the SWNT suspension in water, the peak of G^+ is shifted from 1597 cm^{-1} , when there is no clay, to 1590 cm^{-1} after clay addition, which indicates the vibration for the carbon atoms along the axis of the nanotube is reduced. In other words, the presence of clay hinders the molecular vibration of nanotubes and thus suggests interactions between nanotubes and clay. It is also noted that the intensity for the G^- and BWF bands are dramatically reduced after clay inclusion, which means more nanotubes were dispersed in water and this is in good agreement with the observation in Fig. 4.2. Similar results were reported by other aqueous suspensions containing nanotubes by using Raman.^[219,220]

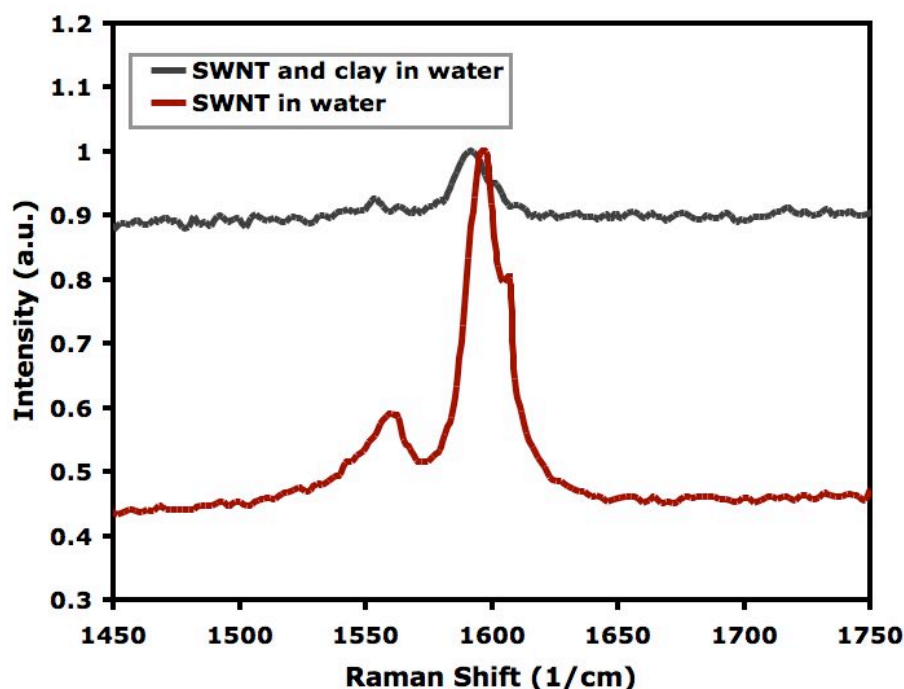


Figure 4.4. Raman spectra of aqueous suspensions of SWNT, with and without clay.

4.3.2. Electrical Conductivity of Epoxy Containing SWNT and Clay

The effect of natural clay (Cloisite[®] Na⁺) addition to the electrical conductivity of nanocomposites containing SWNTs is shown in Figure 4.5. It can be seen that for the two systems (with and without 2 wt% clay), the conductivity increases exponentially with increasing SWNT concentration. At every SWNT concentration, the composites with 2 wt% clay show higher conductivity than the corresponding composites without clay. The disparity is greatest at low SWNT concentration where the composite with 0.05 wt% SWNT shows a 4.3 order of magnitude increase in conductivity when 2 wt% clay was introduced. The conductivity data was fitted with the classic percolation power

law and it is found that the system without clay shows a percolation threshold of 0.05wt% SWNT, while the 2 wt% clay-filled system is 0.01wt% SWNT. Typical SWNT epoxy composites have thresholds greater than 0.05 wt%,^[116,186,188] but V_c as low as 0.00005 wt% SWNTs has been achieved through controlled aggregation.^[104] The combination of low percolation threshold and high conductivity (>0.001 S/cm with 0.1 wt% SWNT) exhibited here is among the best ever reported for SWNT-filled epoxy nanocomposites.

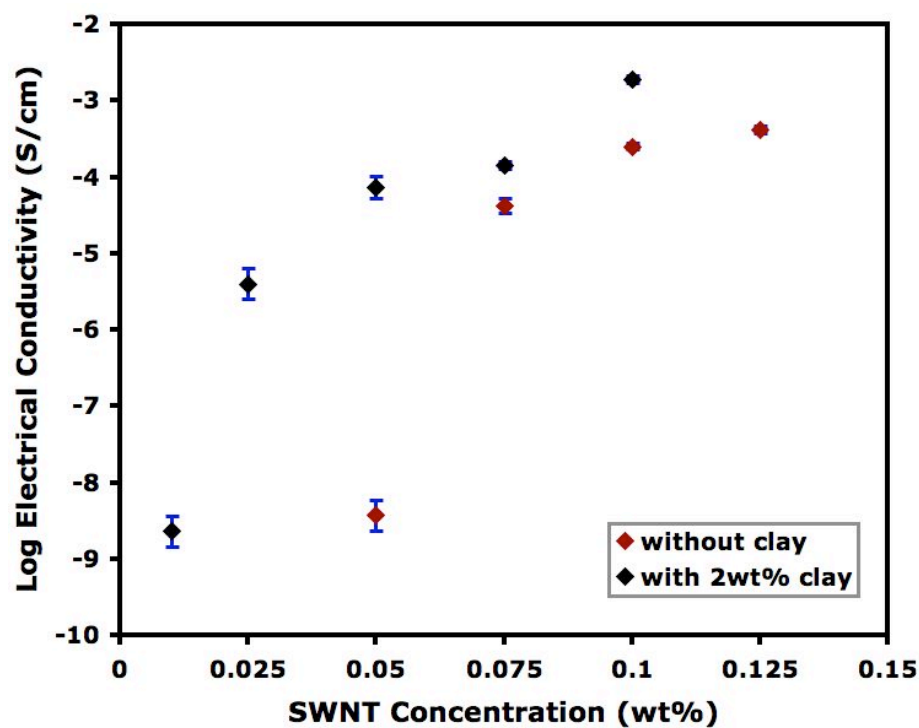


Figure 4.5. Electrical conductivity as a function of single-walled carbon nanotube loading for epoxy nanocomposites, with and without 2 wt% clay (Cloisite[®] Na⁺).

In an effort to better understand the contribution of clay to the electrical conductivity of the nanocomposites, the SWNT concentration was kept constant at 0.05 wt% and the clay concentration was varied, as shown in Figure 4.6. Significant conductivity enhancement was observed for all the samples and the composite with 0.2 wt% Cloisite[®] Na⁺ shows slightly higher conductivity than the samples with 2 and 5 wt% Cloisite[®] Na⁺. This may be attributed to the interference between SWNT network and the dispersed clay particles whose concentration dramatically exceeds that of the SWNTs. It is expected that some electrical conductivity will be sacrificed if a higher concentration of clay is added, however, higher loading of clay is preferable for other properties (e.g., barrier). Adding clay to the nanocomposites provides the opportunity to balance electrical conductivity improvement and other property enhancements that require the introduction of clay. Composites containing functionalized clay, 0.2 wt% Cloisite[®] 15A and Cloisite[®] 30B, also show a significant improvement in electrical conductivity, but not as good as natural clay. It is worth noting that an epoxy composite containing vapor grown carbon fibers (VGCF) and clay shows increasing conductivity with increasing amount of clay addition for 1 and 2.5 wt% VGCF composites,^[221] although the maximum achievable conductivity is only 10^{-5} S/cm. Carbon fibers are orders of magnitude larger ($d = 150$ nm and $L \geq 10$ μ m for VGCF) than single-walled carbon nanotubes, which increases their percolation threshold (> 1 wt%) and weakens inter-particle contacts in VGCF-filled composites.

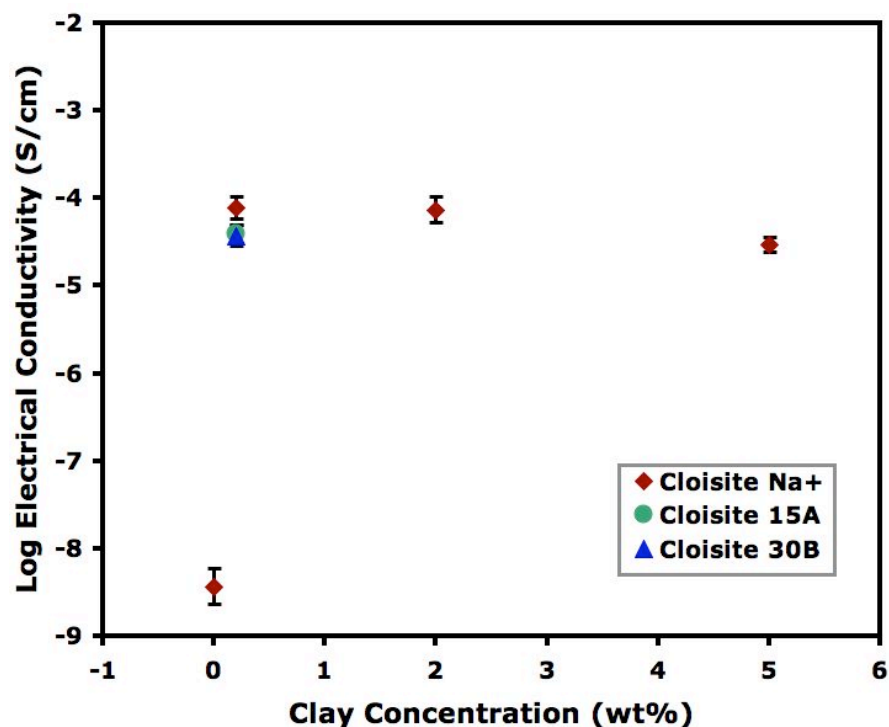


Figure 4.6. Electrical conductivity as a function of clay concentration for epoxy nanocomposites containing 0.05 wt% SWNT.

4.3.3. Nanotube Dispersion in Epoxy Containing Nanotubes and Clay

It is well accepted that the performance of composites is directly related to the dispersion and microstructure of the filler materials. In this study, the dispersion of nanotubes and clay are characterized by optical microscopy, SEM, and TEM. Figure 4.7 shows optical microscope images for epoxy samples containing SWNT and clay. In the absence of clay, nanotubes tend to be poorly dispersed and a highly aggregated morphology is observed (Fig. 4.7(a)). Aggregated SWNT clusters are irregularly shaped and have sizes ranging from 5 to 50 μm . An effective three-dimensional network cannot

be constructed because of the poor connection among the aggregates. In contrast, the composite with 2 wt% clay significantly improves the SWNT dispersion by showing more SWNT rich area (dark area) with the same SWNT concentration (Fig. 4.7(c)). Simultaneously, the SWNT network became fully connected, as evidenced by measurable conductivity, due to better contact amongst the SWNT clusters. From Figure 4.6, it is clear that clay clusters cannot be seen with an optical microscope under the current magnification with bright field conditions (Fig. 4.7(e)), but cross-polarized light can be applied to resolve them as well-dispersed bright aggregates (Fig. 4.7(d) and (f)). Figure 4.7(d) is the optical microscope image for the sample containing both 0.05 wt% SWNT and 2 wt% clay under cross-polarized light. The clay morphology is quite similar to the sample with clay only and nanotubes seem to have little effect on the clay dispersion in epoxy. Figures 4.7(b), (d), and (f) are taken at the same positions as Figures 4.7(a), (c), and (e), which provides the opportunity to study the dispersion of SWNT and clay simultaneously.

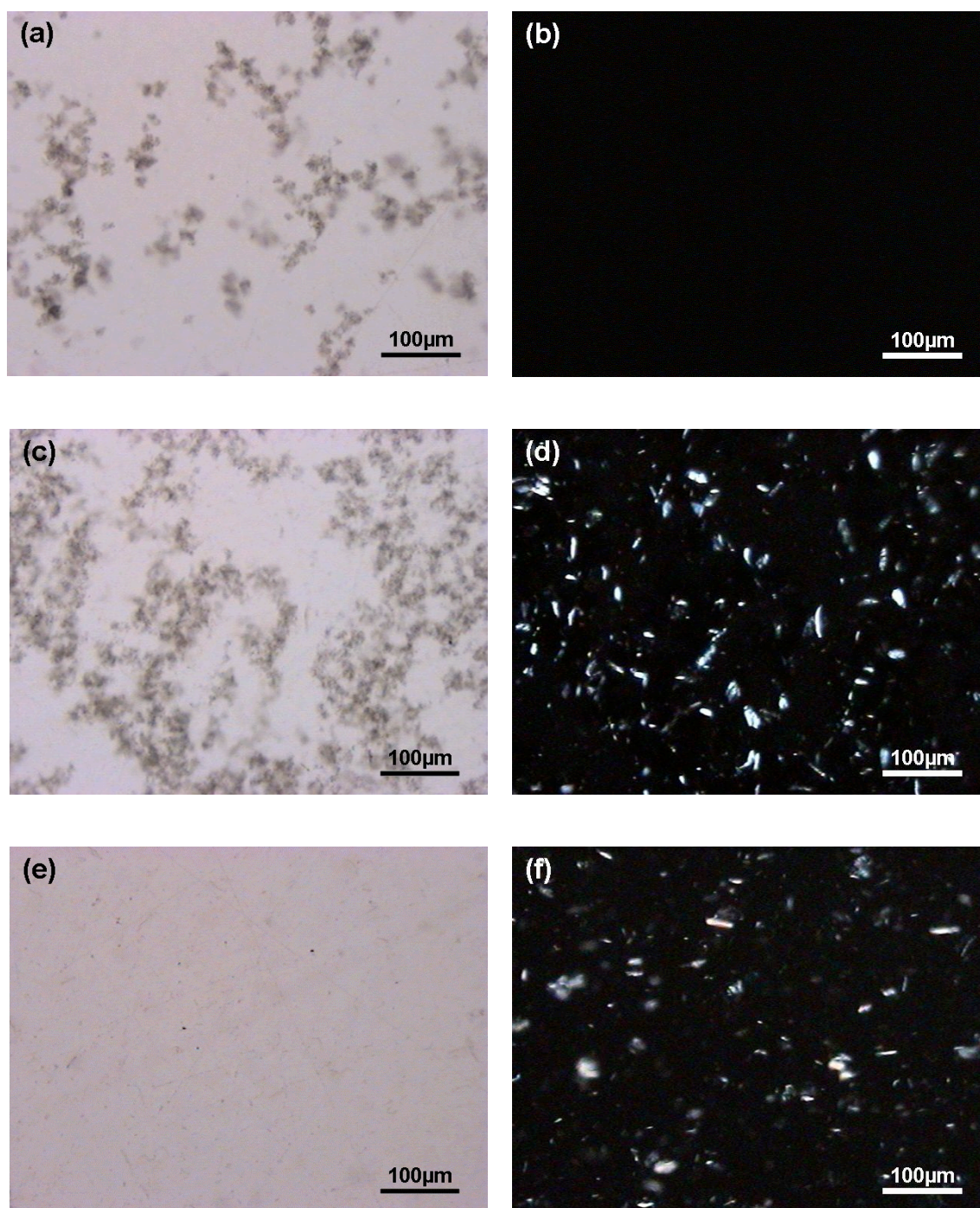


Figure 4.7. Optical microscopy images of epoxy composites containing: 0.05 wt% SWNT (a), 0.05 wt% SWNT and 2 wt% clay (c), and 2 wt% clay (e) under bright field light condition. Images (b), (d), and (f) are the same respective positions, but under cross-polarized light condition.

The epoxy composite panel (~ 2.5 mm thick) containing 0.05 wt% SWNT exhibited a dark greenish color with many visibly embedded fine clusters, while the one with the additional 2 wt% clay appears uniformly black to the naked eye. This is because more nanotubes were exfoliated from the large aggregates with the help of clay and blocked more light that is trying to pass through the panel. This difference in nanotube dispersion and network structure is a key factor contributing to the dramatic increase in conductivity with the introduction of clay.

Figure 4.8 shows SEM images for the freeze-fractured cross-sections of the composites containing 0.1 wt% SWNT. In the absence of clay, nanotubes tend to form larger aggregates relative to the sample containing 2 wt% clay. Relatively larger SWNT aggregates are more easily observed in the composite without clay (Fig. 4.8(a)), as indicated by arrows. Similar aggregates are hard to find for the clay-containing composite (Fig. 4.8(b)), although some small aggregates are likely present. This SWNT microstructure is not the most favorable one for mechanical reinforcement, but it is a step toward better three-dimensional SWNT network construction.

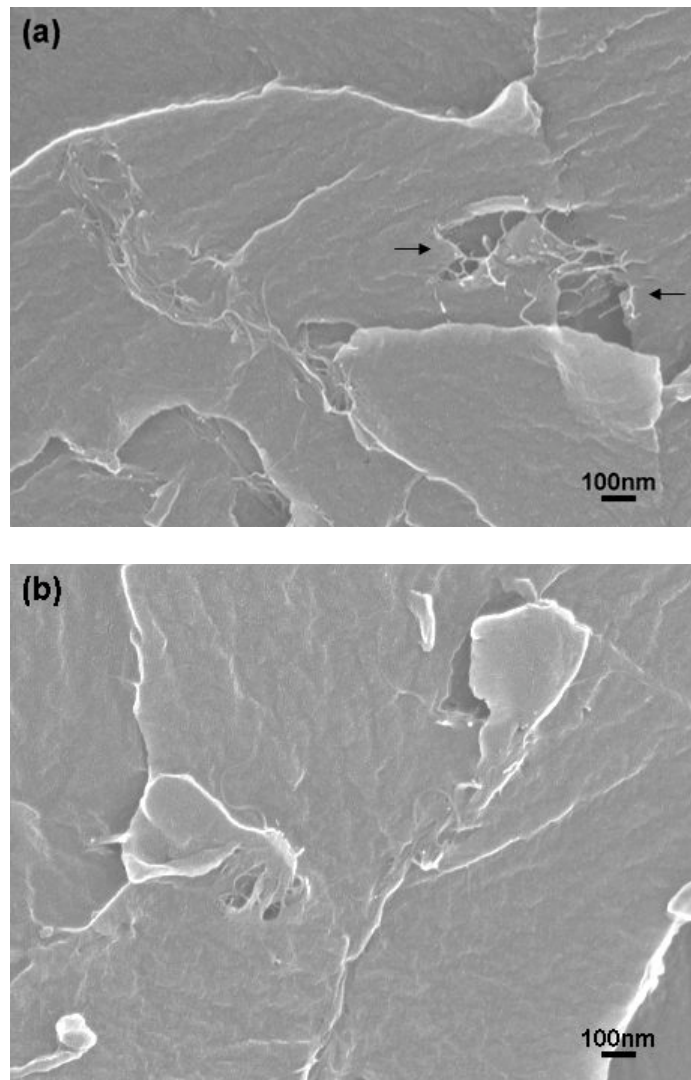


Figure 4.8. Cross-sectional SEM images of epoxy nanocomposites containing 0.1 wt% SWNTs (a) and both 0.1 wt% SWNTs and 2 wt% clay (b).

Although the dispersion of nanotubes can be revealed by SEM, the nanotube-clay interaction is still not directly observed due to the invisibility of clay. As a result, the nanocomposite containing 0.1 wt% SWNTs and 2 wt% clay, which can provide information regarding the dispersion of both nanotubes and clay simultaneously, was

imaged by TEM. In Figure 4.9, it is clear that clay platelets form large aggregates that have dimensions ranging from hundreds of nanometers to micrometers. Moreover, almost no noticeable intercalation of clay layers is found, which indicates that putting clay particles into epoxy results in a microcomposite in terms of clay dispersion. Carbon nanotubes are a lot more difficult to find under TEM, partially because of the low nanotube concentration studied. Even so, tiny nanotube bundles were found near the clay aggregate, as shown by the arrows. Other nanotube bundles can be observed further up on this large clay aggregate. This further demonstrates that there is an affinity between these two fillers and clay forms microcomposites whether nanotubes are present or not, while nanotubes can form a better dispersed nanocomposite (in terms of nanotube dispersion) with the addition of clay.

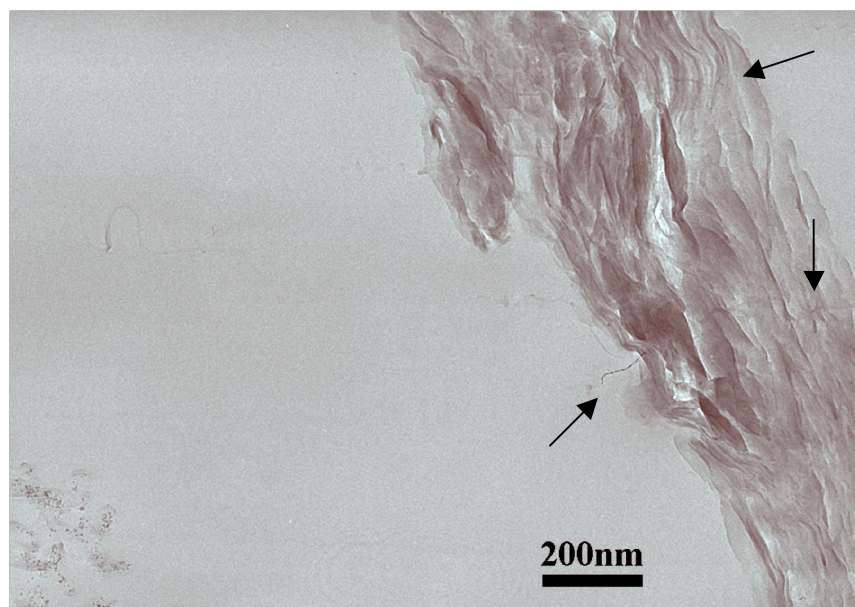


Figure 4.9. TEM image of the epoxy composite containing 0.1 wt% SWNT and 2 wt% clay.

There are several reasons why clay improves SWNT network formation and electrical conductivity in these composites. First, the addition of clay increases the viscosity of the composite mixture prior to cure, making it more difficult for nanotubes to migrate and re-aggregate following sonication. Another factor is the excluded volume created by the micron-scale clay clusters that effectively creates a segregated network of nanotubes.^[131] Finally, and perhaps most importantly, the nanotubes seem to interact more strongly with clay than epoxy. This SWNT-clay interaction can be visualized using partially polarized light in an optical microscope, as shown in Figure 4.10(a). Under these conditions, the epoxy matrix is gray in color, while clay is seen as bright clusters and SWNT is black. Nearly all of the clay aggregates are surrounded by a sea of SWNTs in this image (Fig. 4.10(a)), which suggests that there is a strong affinity between these two particles. Nanotubes are not observed in open areas that have little or no clay. This templated dispersion of SWNT is shown schematically in Figure 4.10(b). Dispersion of clay particles in epoxy remains unchanged in the presence of nanotubes (compare Fig. 4.7(d) and (f)), but SWNT dispersion is dramatically influenced by the presence of the clay (compare Fig. 4.7(a) and (c)). Lack of adequate clay exfoliation is the most likely reason for the negligible improvement in composite modulus with added clay. Negatively-charged surfactants and polymers are known to have strong affinity for nanotubes,^[76,222] so it is not surprising that anionic montmorillonite also shows a favorable interaction. Even with this attraction, the SWNTs maintain their strong inter-tubular attractions that produce a conductive network.

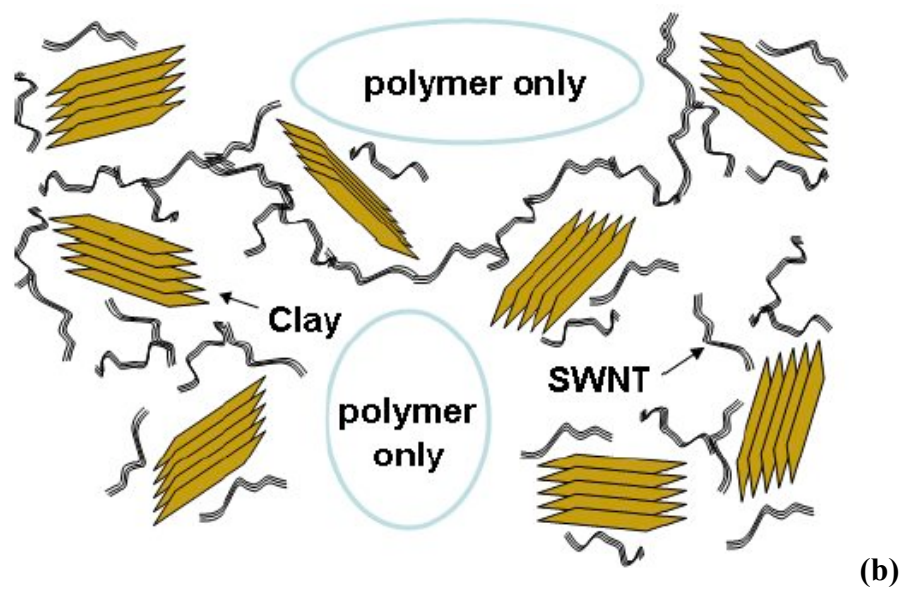
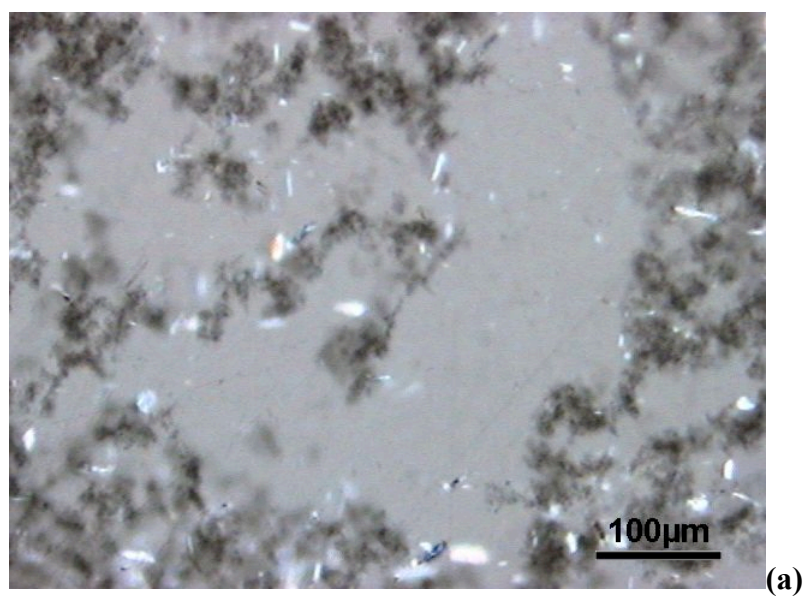
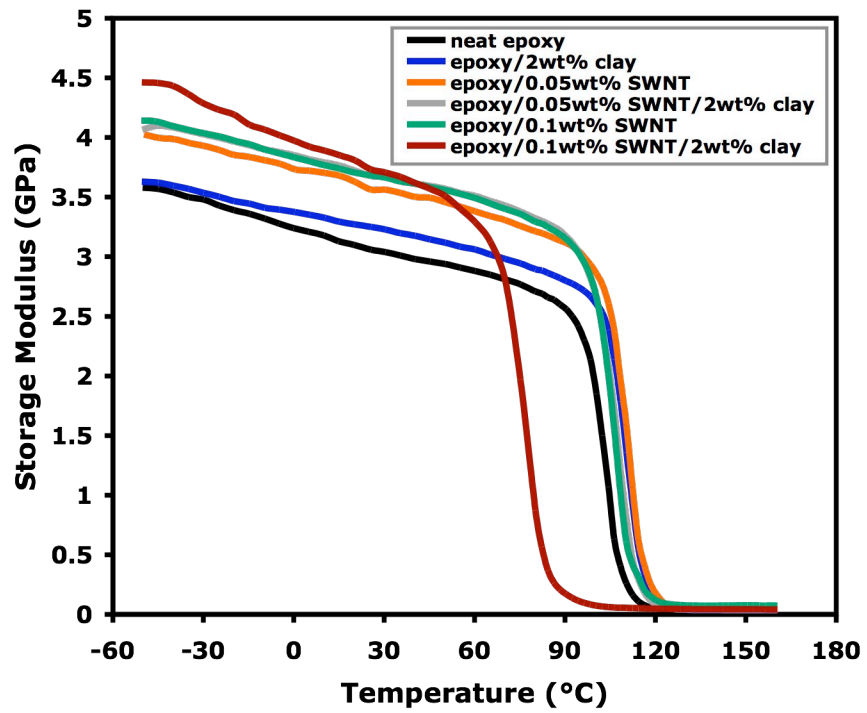


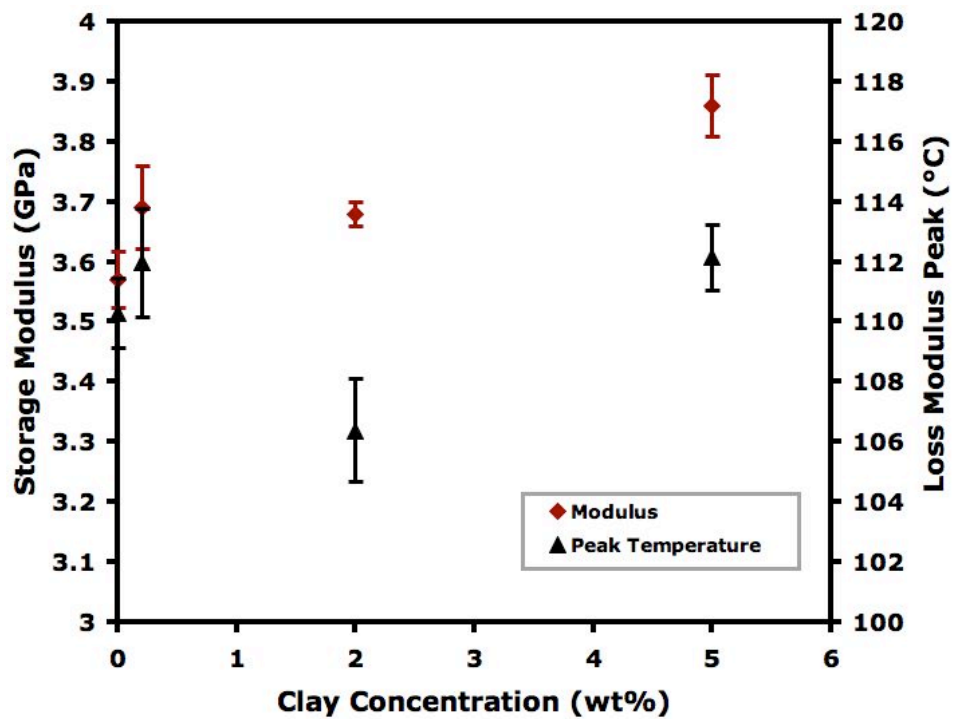
Figure 4.10. Optical microscope image of an epoxy composite containing 0.05 wt% SWNT and 2 wt% clay under partially polarized light (a) and schematic of clay-assisted dispersion of SWNT (b).

4.3.4. Mechanical Properties

The thermo-mechanical behavior of these composites was studied using dynamic mechanical analysis (DMA), as shown in Figure 4.11(a). At room temperature (25 °C), the storage moduli of the composites increase with increasing SWNT concentration. The introduction of 2 wt% clay further increases the storage modulus for a given amount of SWNT. The samples with 0.05 wt% SWNT and 0.1wt% SWNT show 16.7% and 20.3% higher storage modulus than neat epoxy, respectively. The samples containing 2 wt% clay and same amount of SWNT (0.05 wt% and 0.1 wt%) exhibit 20.3% and 21.9% improvement, respectively. The ability of clay to carry some load in the presence of SWNT is due to the nearly unaffected clay dispersion. Glass transition temperature of each composite, taken as the peak in loss modulus, is shown in Figure 4.11(b). All composites show slightly higher glass transition temperature than neat epoxy, except the sample with 0.1 wt% SWNT and 2 wt% clay, which lowered the T_g by 24 °C. One possible reason for this is a reduced crosslink density due to the interference between nanofillers and epoxy during curing.^[223,224] Clay contribution to the modulus of the composites was studied by testing samples with 0.05 wt% SWNT and different clay concentration (Fig. 4.11(b)). All composites containing clay show higher modulus than those without clay, although the improvement is relatively small due to the aggregated nature of the clay. Composites with 0.2 wt% and 2 wt% clay have quite similar modulus, while the addition of 5 wt% clay can increase the storage modulus from 3.57 GPa, when there is no clay, to 3.86 GPa.



(a)



(b)

Figure 4.11. Storage modulus as a function of temperature for clay/SWNT/epoxy composites (a) and as a function of clay concentration for composites containing 0.05 wt% SWNT (b).

4.4. Conclusions

In the SWNT concentration range studied (0.01 - 0.1 wt%), the addition of clay effectively improves the dispersion of SWNT in an epoxy matrix. The SWNT morphology can be changed from a discontinuous set of aggregated clusters, when there is no clay, to a continuous three-dimensional nanotube network. The percolation threshold for the composites without clay is 0.05 wt% SWNT, while the addition of 2 wt% clay reduces this value to 0.01 wt%. Furthermore, all the samples containing both nanotubes and clay particles show improved electrical conductivity relative to composites containing only nanotubes and it was also demonstrated that organoclay particles could also improve the conductivity dramatically, but not to the same extent as unmodified clay. Optical microscopy showed that clay platelets are highly aggregated whether SWNT was present or not, which suggests that clay formed a microcomposite in the epoxy matrix and there is little influence of SWNT on the clay microstructure. For the mechanical properties of the SWNT/epoxy composites, the storage modulus was increased when a higher concentration of SWNT was added, but the addition of clay did not significantly increase storage modulus.

Clay particles were also found to stabilize nanotubes in water. Although some precipitation occurred over time, the aqueous suspensions of nanotubes and clay remained stable for weeks. Cryo-TEM revealed that nanotubes remain in the vicinity of clay platelets and a similar phenomenon is observed for the epoxy nanocomposites, as evidenced by optical microscopy and TEM. This is due to the interaction between nanotubes and clay, which is the primary driving force for clay-assisted dispersion of

nanotubes.

The use of an insulating particle that fulfills the same function traditionally reserved for surfactants is a significant breakthrough. It is important to note that composite electrical conductivity is enhanced and mechanical properties are simultaneously improved, which is unusual for traditional stabilizers. Other properties, such as flame suppression and gas barrier, may also be enhanced due to the inclusion of clay. These composites are rendered truly multifunctional with the presence of these two fillers whose synergy generates an ideal microstructure, which makes this study an important step toward helping nanocomposites to achieve their potential. Another useful method to control nanoparticle dispersion is using weak polyelectrolytes, as described in Chapter V.

CHAPTER V

MICROSTRUCTURE TAILORING OF CARBON NANOTUBES BY PH-RESPONSIVE POLYMERS

5.1. Introduction

Interest in single-walled carbon nanotubes (SWNTs) remains strong because of their small size,^[45] high modulus,^[225] high intrinsic electrical conductivity^[226] and high thermal conductivity.^[33] SWNTs hold significant promise for imparting electrical conductivity, mechanical strength, and thermal conductivity to polymeric materials.^[227] Despite this potential, the ability to stabilize nanotubes in solution remains a significant hurdle to their widespread use. This has led to significant research efforts on the use of noncovalent stabilizing agents and chemical modification of the nanotube to impart solubility.^[61,76,81,173] Once stabilized, these nanotubes lend themselves to chemical modification, spectroscopic study, and/or incorporation into ink-based systems. Solubilized nanotubes are currently being studied for use in drug and gene delivery applications.^[228] Solid films of SWNT-filled polymers are being studied for a variety of uses such as thermal management^[229] and humidity sensing.^[163]

The present work demonstrates a method for controlling the microstructure of carbon nanotubes in both aqueous solution and dry composite films using poly(acrylic acid) (PAA) and other pH responsive polymers.^[222,230] These weak polyelectrolytes transition between neutral and fully charged states with changing pH. Changing charge density as a function of pH causes the polymer chain to transition between tightly coiled

and highly extended conformations, as shown in Figure 5.1 for poly(acrylic acid). With pH as a stimulus, nanotubes suspended in aqueous PAA solution can be switched reversibly between a more bundled state (at high pH) and a more exfoliated state (at low pH). Both states are relatively stable, but viscosity measurements suggest that nanotube exfoliation deteriorates as pH is increased. It is also found that nanotube microstructure changed after drying the suspensions. The better dispersed nanotubes at a low pH suspension eventually showed a more aggregated microstructure in the dried film, which indicates that the status of nanotube exfoliation could be influenced by the presence of water (from suspension to dried composite film). This study lays the groundwork for tailoring the dispersion of nanotubes in solid and liquid systems and hence adjust their properties (electrical, mechanical, etc.).

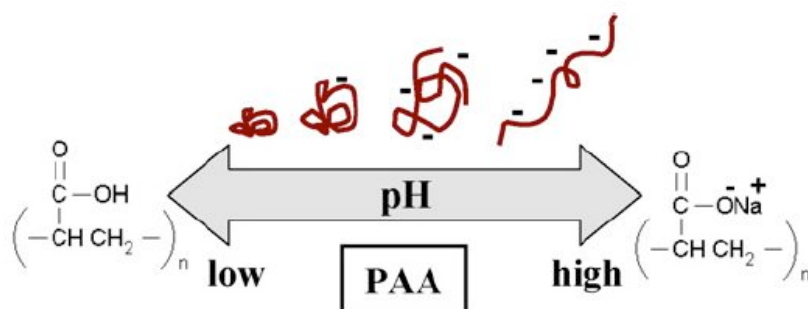


Figure 5.1. Influence of pH on conformation of poly(acrylic acid) (PAA) (from Ref. 230).

5.2. Experimental

5.2.1. Materials

Raw SWNTs used for this study were produced by the HiPco process and contain 27wt% iron impurity (provided by Carbon Nanotechnologies, Houston, TX). Poly(acrylic acid) (PAA, $M_w=100,000$), poly(allylamine hydrochloride) (PAH, $M_w=70,000$) and branched polyethylenimine (BPEI, $M_n=10,000$) were purchased from Aldrich (Milwaukee, WI) and used without further purification. Poly(methacrylic acid) (PMAA) with a molecular weight of 100,000 was obtained from Polysciences, Inc. (Warrington, PA).

5.2.2. Sample Preparation and Characterization

Dry SWNTs were combined with 1 wt% polymer solution by sonicating with a VirTis Virsonic 100 ultrasonic cell disrupter (SP industries, Warminster, PA) for 10 minutes at 50 W. The suspension pH was adjusted with 10 M NaOH or 10 M HCl followed by a 10-min sonication period. Viscosities were measured at room temperature with a Brookfield cone/plate LV DV-III Viscometer (Brookfield, Middleboro, MA). This viscometer has an accuracy of ± 0.65 cP at a rotational speed of 38.4 s^{-1} and ± 0.16 cP at a rotational speed 154 s^{-1} . Solid composite films were made by drying aqueous SWNT suspensions in plastics molds under ambient conditions. Electrical conductivity of the composite films were measured by a home-made four-point probe apparatus, as described in Chapter III. Digital images of the nanotube suspensions were recorded by a

Canon Powershot 500 digital camera after 30 min centrifugation at 5000 rpm with a Fisher Scientific accuSpin 400 (Pittsburgh, PA). Cryo-TEM images were obtained at the University of Minnesota's Characterization Facility (Minneapolis, MN). SEM acquisition was supported by National Science Foundation under Grant No. DBI-0116835 for the Zeiss 1530 VP FE-SEM (Carl Zeiss, Inc., Thornwood, NY) used to image dry composite films.

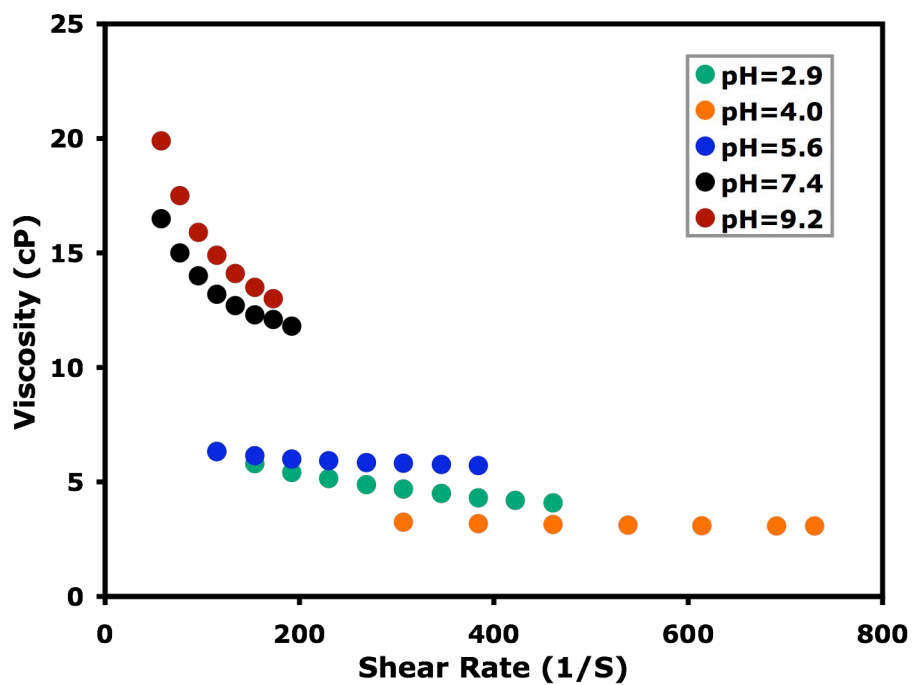
5.3. Results and Discussion

5.3.1. Reversible Microstructure Tailoring of Nanotubes with Poly(acrylic acid)

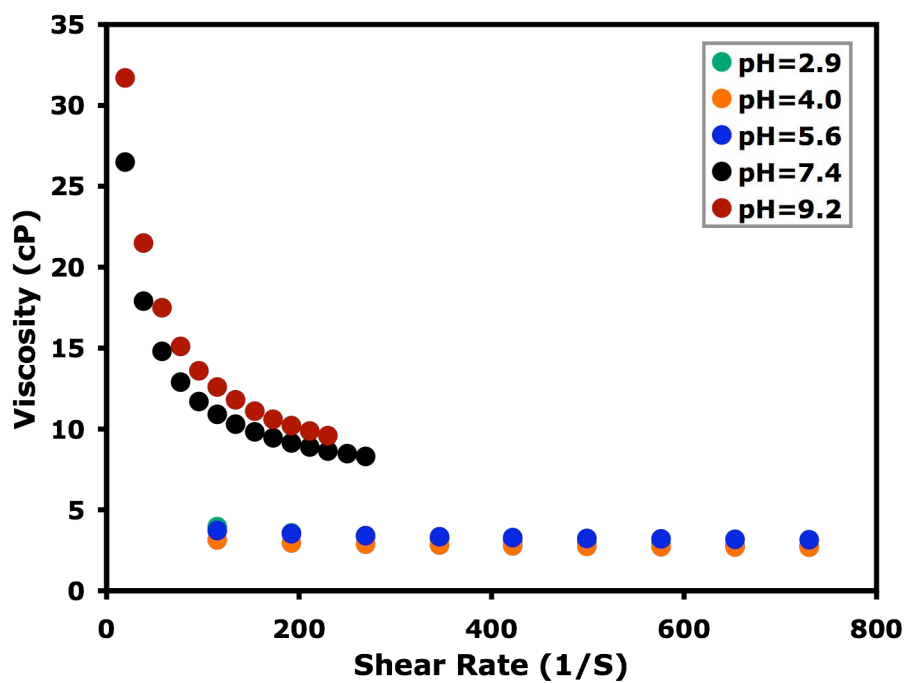
Poly(acrylic acid) is a protonated (neutral) weak polyacid at low pH that exhibits significant intramolecular hydrogen bonding and a highly coiled conformation. Figure 5.1 shows the changes in ionization and conformation that PAA undergoes with changing pH. Changing charge density as a function of pH causes the polymer chain to transition between tightly coiled and highly extended conformations. Higher charge density causes the polymer chain to repel itself, resulting in a more extended conformation. It is this combination of changes in polymer chemistry and conformation that alter its interaction with carbon nanotubes and produces macroscopic changes in suspension viscosity, as described below.

Single-walled carbon nanotubes were combined with an aqueous solution of PAA using sonication. The viscosity–pH relationship for suspensions containing 1 wt% PAA and 0.111 wt% SWNT under different shear rates is shown in Figure 5.2. Without

any adjustment, this suspension has a pH of 2.9 and a water-like viscosity (< 5 cP). Viscosity increases gradually as pH is increased, until a discontinuous increase at pH 7.4 that is likely where a significant conformational change occurs. This is not surprising because PAA charge density changes from 30 to 80% between pH 6 and 8.^[231] Increasing the shear rate reduces the viscosity at high pH, suggesting break up of SWNT networks. Even so, the viscosity of the suspension at pH 9.2 is still much higher than at lower pH due to the increased degree of ionization and effective binding of water molecules. Figure 5.3 shows the suspension viscosity as a function of pH to better highlight the influence of pH on viscosity. When the pH of the suspension is reduced from pH 9.2 back to pH 2.9, the viscosities follow the same trend with shear rate and a water-like viscosity is again observed at pH values lower than 7.4, which indicates reversibility for this system. A slight hysteresis is observed when decreasing viscosity, which is likely due to an increase in ionic strength of the suspension that will alter the level of conformational change in the polymer. A solution containing only 1 wt% PAA in the absence of carbon nanotubes shows relatively little change in viscosity as a function of pH, as shown in Figure 5.4. Furthermore, it should be noted that this polymer solution is Newtonian rather than shear thinning.



(a)



(b)

Figure 5.2. Viscosity as a function of shear rate for suspensions containing 0.11 wt% SWNT and 1 wt% PAA as pH is progressively increased (a) and then decreased (b) to demonstrate reversibility.

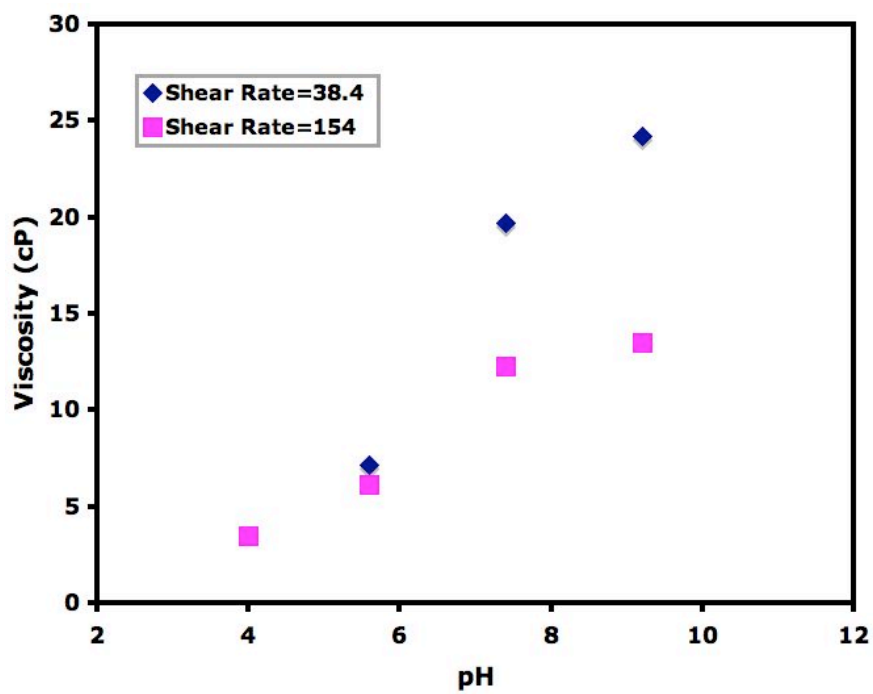


Figure 5.3. Viscosity as a function of pH for suspensions containing 0.11 wt% SWNT and 1 wt% PAA.

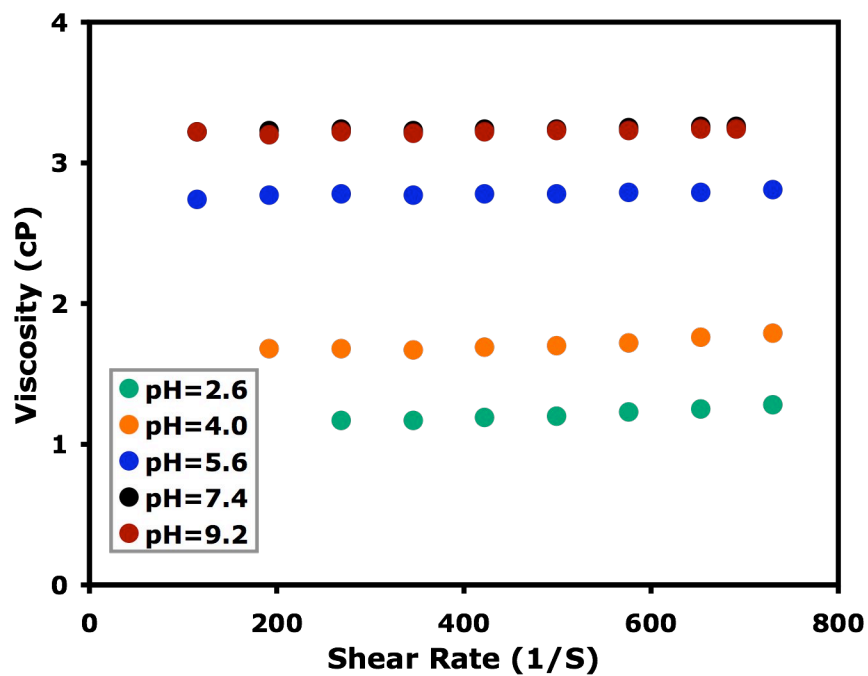


Figure 5.4. Viscosity as a function of shear rate for 1 wt% neat PAA aqueous solution.

Initially it was believed that higher viscosity at high pH was the result of better dispersed nanotubes that interacted more strongly with PAA in its highly-charged state,^[222] but cryo-TEM micrographs of the vitrified PAA solutions at pH 2.9 and 9.2 (Figs. 5.5(a) and (b), respectively) show that at low pH the SWNTs are completely exfoliated.^[230] At high pH the SWNTs are only partially exfoliated (Fig. 5.5(b)), but the suspension is not phase-separated. Efficient exfoliation is possible when enough inter-tube steric repulsion is induced by the dispersant. When PAA is neutralized at low pH, it adopts a coiled conformation (Figs. 5.1 and 5.5(c)). As the pH is increased, the poly(acrylic acid) chains are elongated, which reduces its physical size if associating with nanotubes with its longest dimension parallel to the tube axis, as shown schematically in Figure 5.5(d). In this case, it is more difficult for the polymer to generate the level of steric repulsion required for overcoming the van der Waals interaction between the nanotubes. As a result, the exfoliation is not complete and the SWNTs become more bundled.

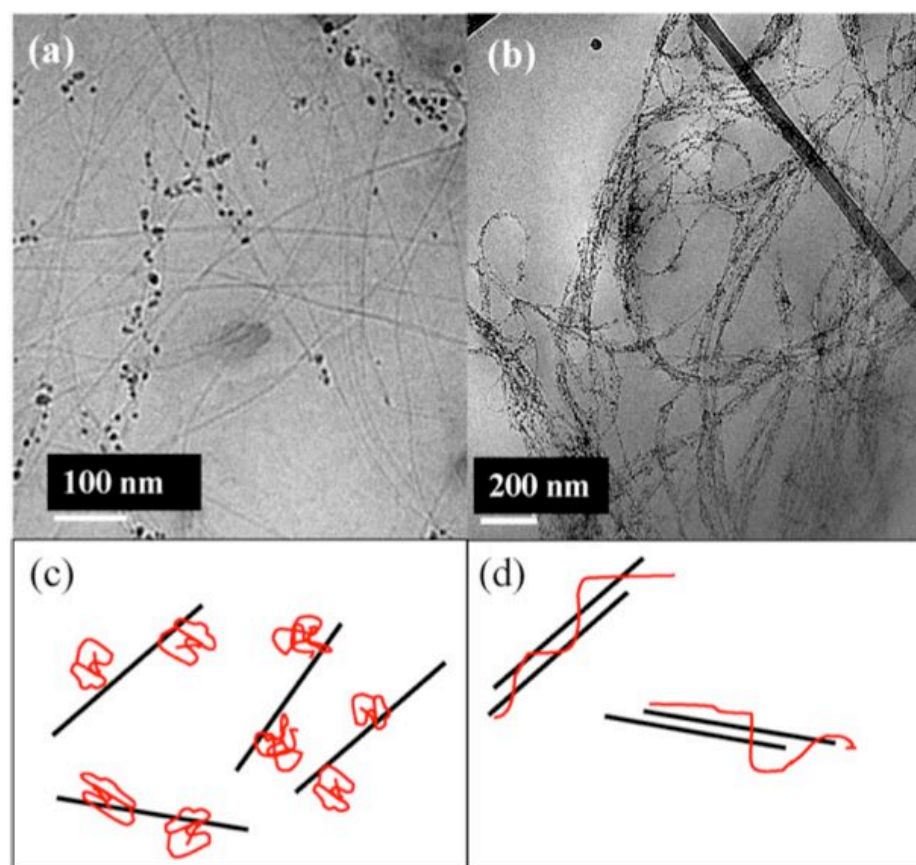


Figure 5.5. Cryo-TEM imaging of aqueous suspensions containing 0.11 wt% SWNT and 1 wt% PAA at pH (a) 2.9 and (b) 9.2, and respective schematic representations of the SWNT (black) and the polymer (red) (c, d). This figure is from Ref. 230.

The stability of the nanotube suspensions at varying pH was tested using centrifugation at 5000 rpm for 30 min, as shown in Figure 5.6. At low pH, the suspensions maintain a uniform black color although a small amount of precipitation is observed. Suspension stability was significantly reduced near neutral pH, where almost all nanotubes settle out of the mixture, leaving a transparent light gray supernatant at pH 7.4. When the pH was increased to 9.2, the supernatant became a colorless water-like

liquid, which suggests complete SWNT precipitation from water. Nanotube suspension stability is directly related to nanotube-polymer interaction and nanotube exfoliation. At low pH, nanotubes are better exfoliated due to stronger interaction with the neutralized polymer coils, which prevent SWNTs from aggregating and precipitating. When the pH is increased, nanotubes form aggregates and bundles, which are bulkier and only weakly interacting with the extended polymer chains.

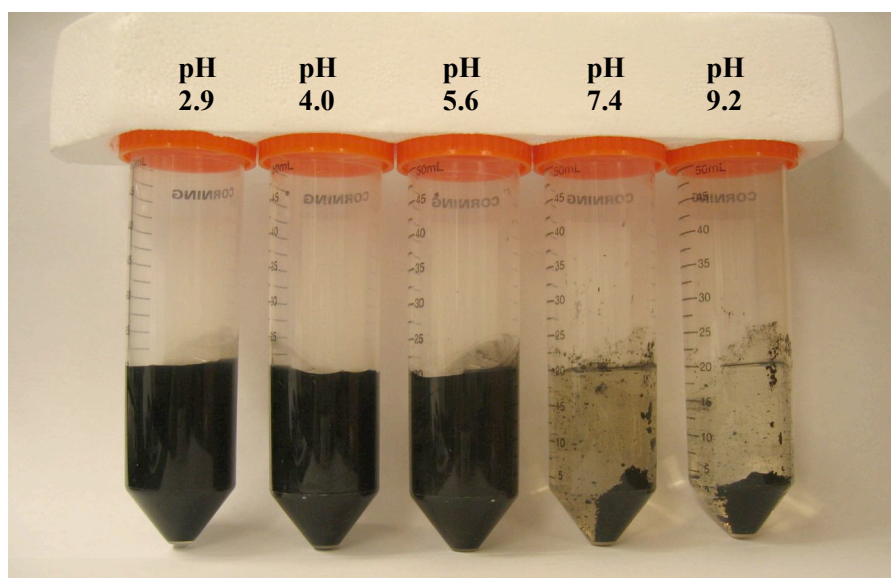


Figure 5.6. Digital image of nanotube suspensions, containing 0.011 wt% SWNTs and 0.1 wt% PAA at different pH after centrifugation.

Composite films were made by drying the nanotube suspensions under ambient conditions, resulting in PAA containing 10 wt% SWNTs. Figure 5.7 illustrates the microstructural changes of these dried suspensions as the pH is increased from 2.9 to 9.2

and then decreased back to the starting value. During the increase in pH, the nanotubes become progressively less aggregated and better embedded within the PAA matrix. There is a distinct transition between the microstructure at pH=5.6 and that at pH=7.4. At lower pH values the freeze-fractured surfaces in Figure 5.7 are relatively coarse and in many cases the nanotubes are pulled out of the matrix. This seems to indicate a weak PAA-SWNT interaction and has been observed in other SWNT-filled composites. Ropes on the order of 20 nm or more are clearly visible and aggregated with other ropes (see the arrows in the cross section at pH=4.0 as an example). At elevated pH this same suspension dries to form much smoother films with better nanotube exfoliation and no evidence of nanotube detachment from the polymer matrix, which suggests a much stronger SWNT-PAA interaction. Nearly individual nanotube strands can be observed in the cross section made with a pH=9.2 suspension. Features as fine as those indicated by the arrows cannot be observed at lower pH.

This same coarsening of the microstructure and weakening of the nanotube-polymer interface is observed as the pH is decreased from 9.2 to 2.9. Qualitative differences between microstructures of composites as pH is increasing or decreasing are likely due to changes in ionic strength of the suspension that accompany pH changes. Lower magnification images of dried suspensions containing 1 wt % SWNT are shown in Figure 5.8 to further highlight the coarse-to-fine microstructural transition that occurs in going from low to high pH. At low pH (Figure 5.5(a)), relatively large aggregates are observed throughout the composite cross section and many of these bundles were pulled out of the PAA matrix during the freeze-fracture process (examples are indicated by arrows). Aggregation of nanotubes is also observed at high pH (Figure 5.4(b)), but it is much more diffuse in appearance with no evidence of nanotube pullout. The overall freeze-fractured surface is smooth at high pH, whereas at low pH it is relatively coarse. These microstructural differences have a significant impact on composite behavior.

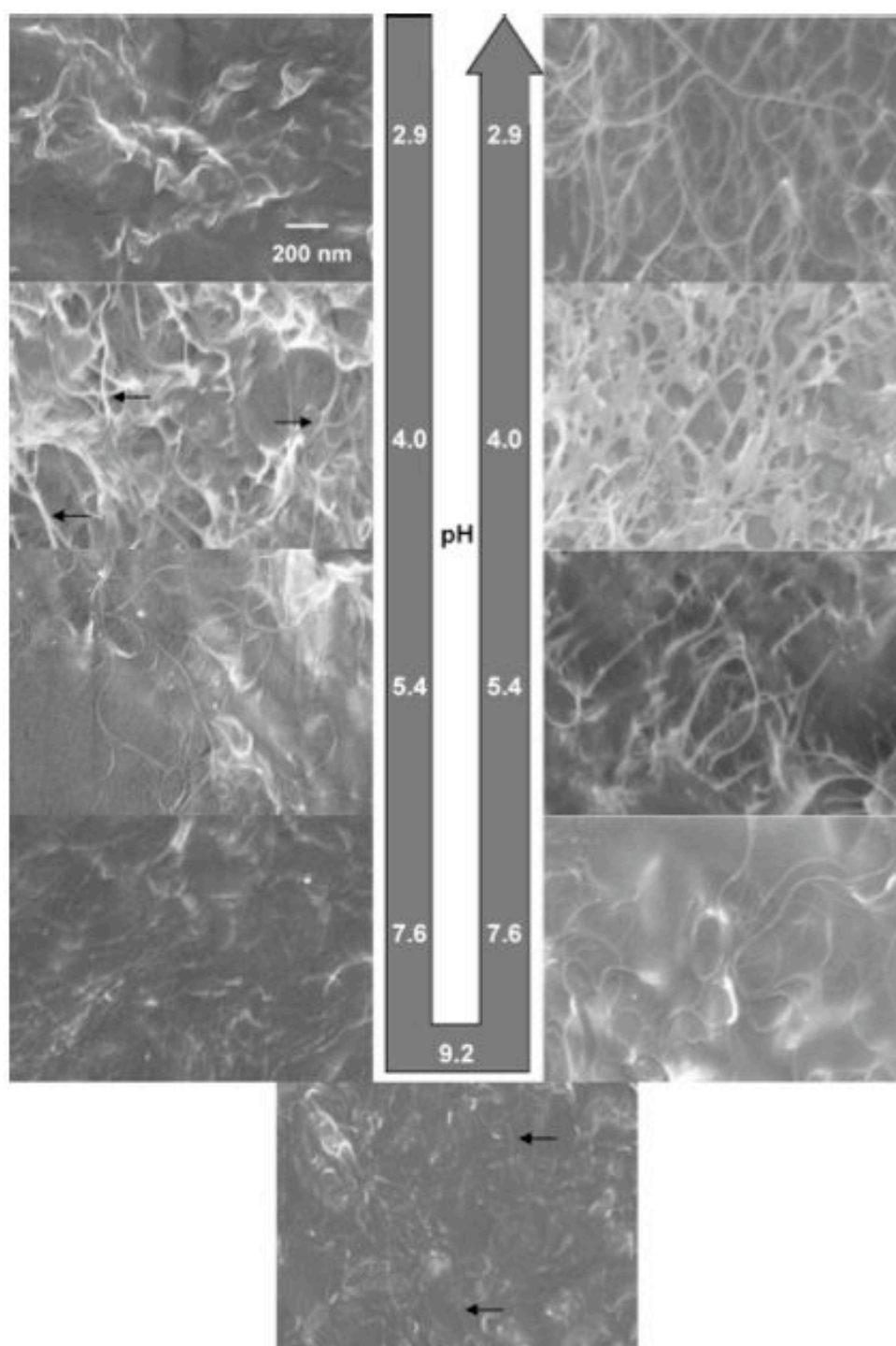


Figure 5.7. Freeze-fractured cross sections of dried suspensions, having 10 wt% SWNT in PAA, as pH is increased from 2.9 to 9.2 and then decreased back to 2.9. This figure is from Ref. 222.

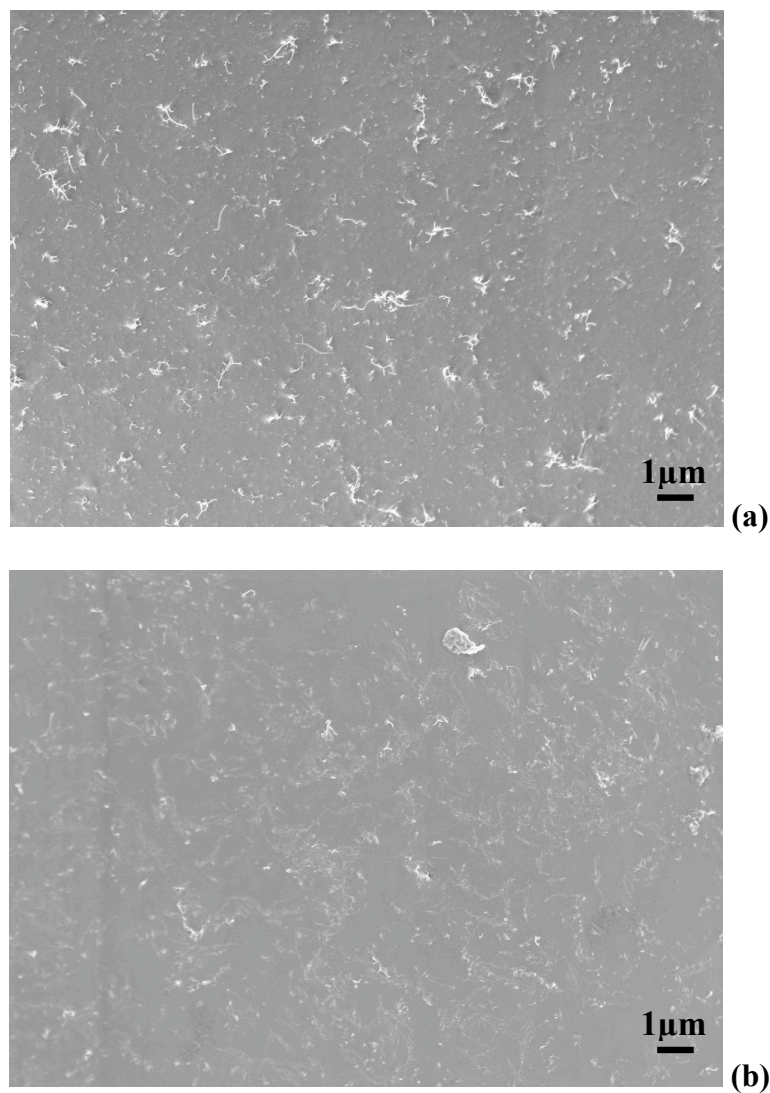


Figure 5.8. Freeze-fractured cross sections of PAA containing 1 wt% SWNT. Composites were prepared from aqueous mixtures with a pH of 2.9 (a) and 9.2 (b). These images are from Ref. 222.

Figure 5.9 demonstrates the influence of pH-induced microstructure on composite electrical conductivity. Both composite systems, prepared from suspensions

of pH=2.9 and 9.2, exhibit an exponential increase in conductivity with increasing SWNT concentration. The percolation threshold is obtained by fitting the percolation power law to the experimental data, as illustrated in Chapter III. At low pH, the composites show a relatively high percolation threshold (~ 0.45 wt%) and the threshold is an order of magnitude lower for the high pH system (~ 0.046 wt%). The reason for this difference in percolation is that at high pH, stronger nanotube/polymer interaction leads to better nanotube dispersion and thus the conductive network will be formed at lower nanotube concentration. Despite having a high percolation threshold, the low-pH composites are able to achieve a higher maximum electrical conductivity as the SWNT concentration increases. This improved conductivity at greater SWNT content is due to higher effective nanotube conductivity. In the low pH system, there are stronger tube-to-tube (more intimate) contacts due to the weak polymer-nanotube interface shown in Fig. 5.8(a). At high pH, the poly(acrylic acid) interacts more strongly with the SWNTs and the nanotubes are better dispersed, which leads to smaller diameter bundles. The network formed by these smaller nanotube bundles creates more nanotube-nanotube contacts, as compared to the network with larger nanotube bundles (at low pH). Because of contact resistance, the system with less nanotube-nanotube contact (larger bundles) will show higher maximum electrical conductivity. Additionally, the stronger polymer-nanotube interaction at low pH reduces the effective nanotube conductivity and weakens tube-to-tube junctions. These assertions are also supported by the values of the preexponential terms for these two systems, which are two orders of magnitude apart and suggest that effective nanotube conductivity at low pH is much better than that at

high pH. Differences are also observed in the thermal and mechanical behavior of these composites, but these differences are masked by changes intrinsic to neat PAA.

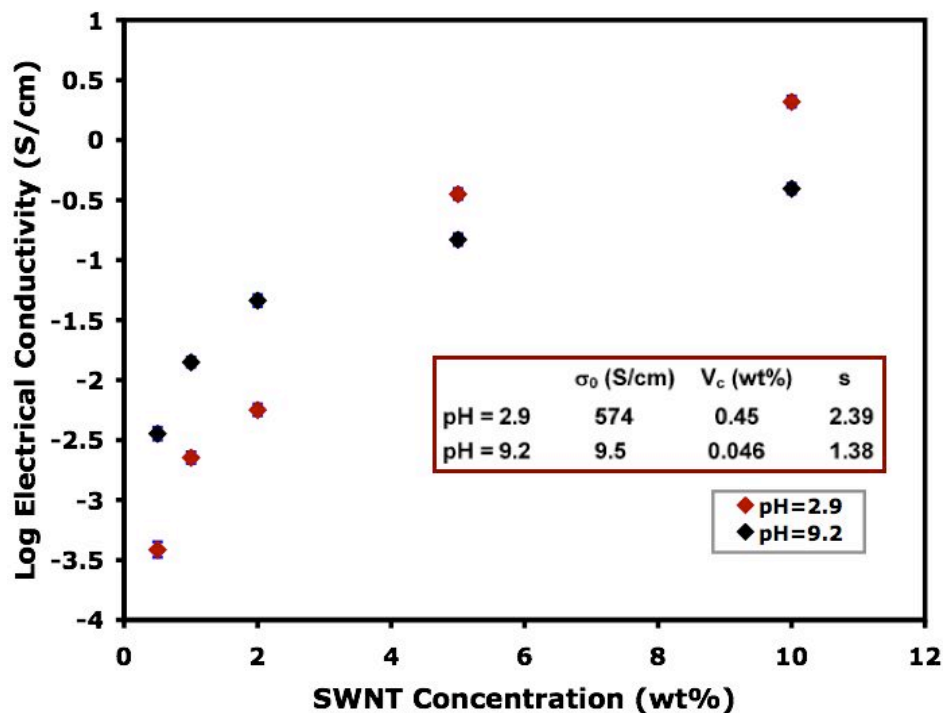


Figure 5.9. Electrical conductivity as a function of nanotube concentration for PAA composites prepared from aqueous suspensions at a pH of 2.9 and 9.2. The results are fitted using the percolation power law (Eq. 1), resulting in the parameters shown for each data set. The R^2 values for the curve fit are 0.9999 and 0.9978 for pH of 2.9 and 9.2 films, respectively.

5.3.2. Microstructure Tailoring of Nanotubes with Poly(allylamine hydrochloride)

Poly(allylamine hydrochloride) (PAH) is a weak polybase that is uncharged at high pH and becomes more extended at low pH as its positive charge density increases, as shown in Figure 5.10.^[230] Figure 5.11 shows viscosity as a function of shear rate for

SWNTs stabilized with PAH at varying pH values.^[232] These suspensions have the same nanotube concentration (0.11 wt%) as the PAA system shown in Figure 5.2. Similar shear thinning was found for low pH suspensions, where PAH molecular chains are well extended. The viscosity value steadily decreases with increasing pH until a value of about 3.4 cP is reached at a pH of 10.2. As pH is increased, PAH loses positive charge density and becomes more coiled. In a general sense, this change in conformation and viscosity as a function of pH is the opposite of that seen with PAA. This shear rate-viscosity relationship is re-plotted as a function of suspension pH, as shown in Figure 5.12. Cryo-TEM micrographs of the SWNT/PAH suspensions, at both low and high pH, show a bundled network similar to Fig 5.5(b). This suggests that the PAH-based suspension has a much weaker transition as a function of pH, which may be due to greater water-solubility and a reduced amount of chain coiling over this pH range. Additionally, the changes in viscosity do not appear to be completely reversible for PAH, which may indicate a stronger interaction with the SWNTs that prevents the necessary charge transfer.

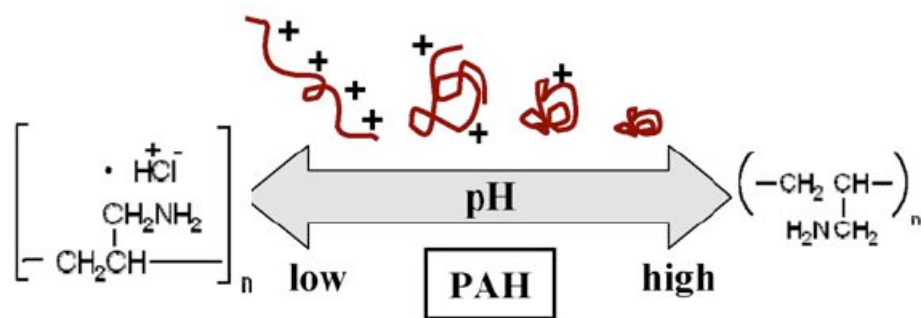


Figure 5.10. Influence of pH on conformation of poly(allylamine hydrochloride) (PAH) (from Ref. 230).

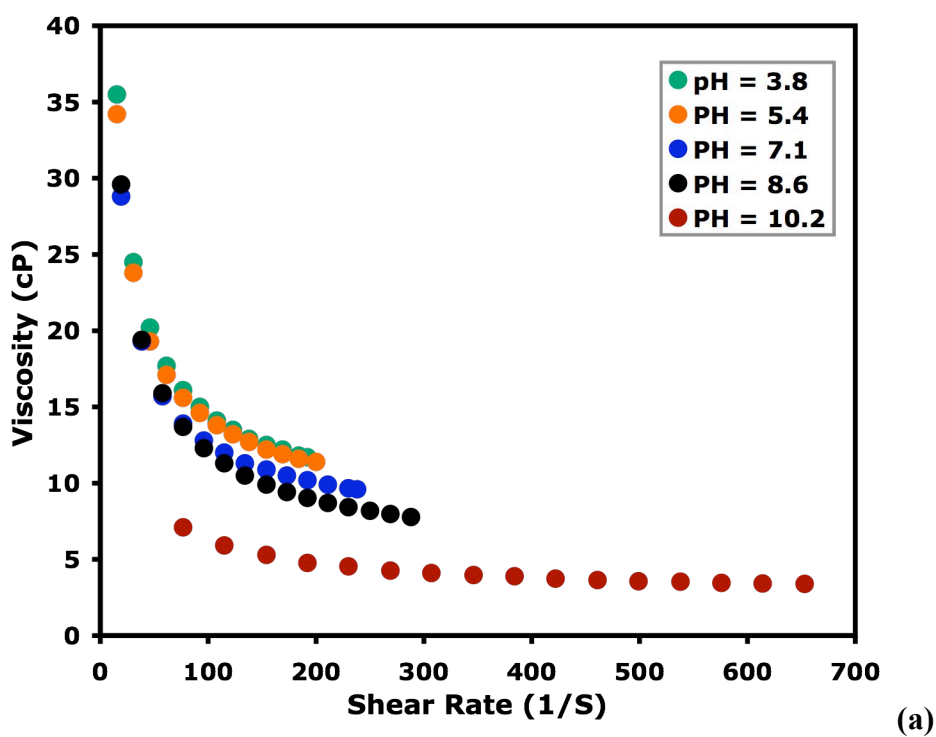


Figure 5.11. Viscosity as a function of shear rate for suspensions containing 0.11 wt% SWNT and 1 wt% PAH as pH is progressively increased (a) and then decreased (b).

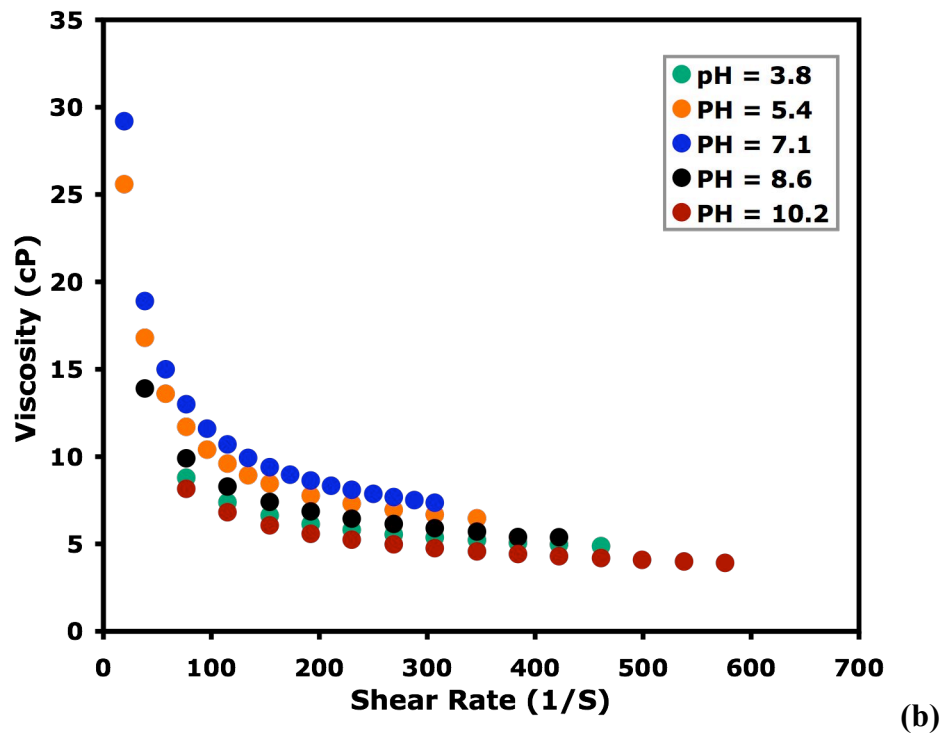


Figure 5.11. Continued

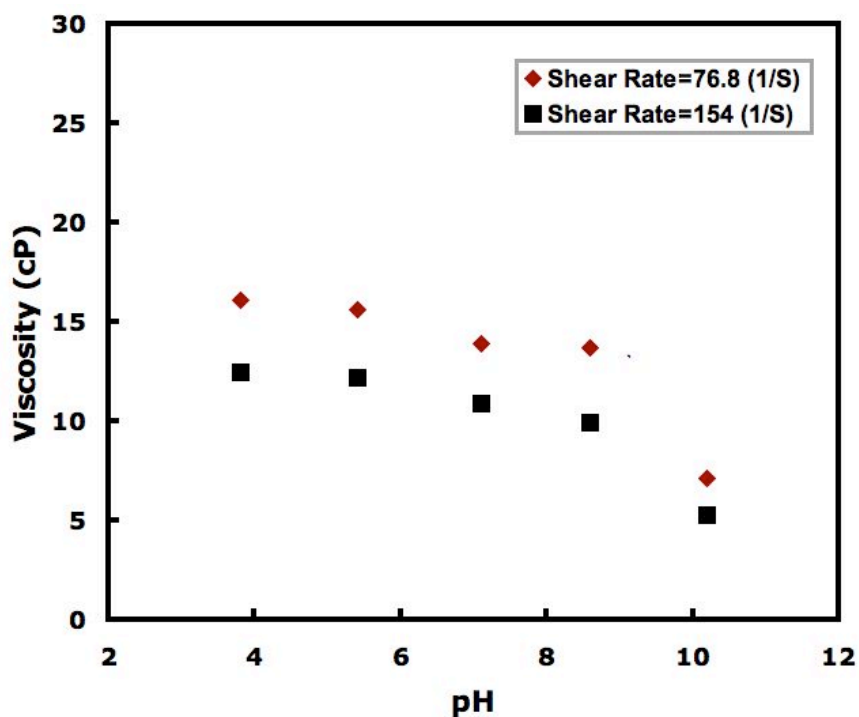


Figure 5.12. Viscosity as a function of pH for suspensions containing 0.11 wt% SWNT and 1 wt% PAH.

Cross-sectional SEM images for the dried PAH films containing 10 wt% SWNT are shown in Figure 5.13. The composites that are dried from suspensions at pH=3.8 and 10.2 both exhibit heavily networked nanotubes. The nanotubes in the low pH composite (Fig 5.13(a)) are heavily bundled and largely pulled out from the PAH matrix, which indicates a weaker nanotube-polymer interaction. An improved dispersion of nanotubes is observed for the high pH composite (Fig 5.13(b)), in which almost all nanotubes are well embedded in the matrix with a decreased bundle diameter. Higher magnification SEM images of the same composites provide a better view of nanotube exfoliation.

Without pH adjustment (Fig 5.13(c)), the majority of the nanotube bundles forming the network are in the range of 20-30 nm in diameter, while the nanotubes in the high pH composite (Fig 5.13(d)) have bundle diameters less than 10 nm. It is worth noting that for SWNT/PAA composite films, better nanotube exfoliation occurs when the polymer chain is more extended and having higher degree of ionization, which is not consistent with the results of SWNT/PAH films. One possible reason is the type of the charges (positive vs negative). PAA is progressively more negatively charged as pH increases and nanotubes are found to have good interaction with negatively charged dispersing aids, which enhance the exfoliation of nanotubes in PAA. On the contrary, PAH gets less positively charged as pH increases and it seems that the neutral polymer interacts more strongly with nanotubes than the positively charged version, while negatively-charged polymer (e.g. PAA) could have stronger interaction than neutral polymer. It should also be noted that the outer wall of a nanotube has a Lewis base character, which would make it more attracted to acidic species.

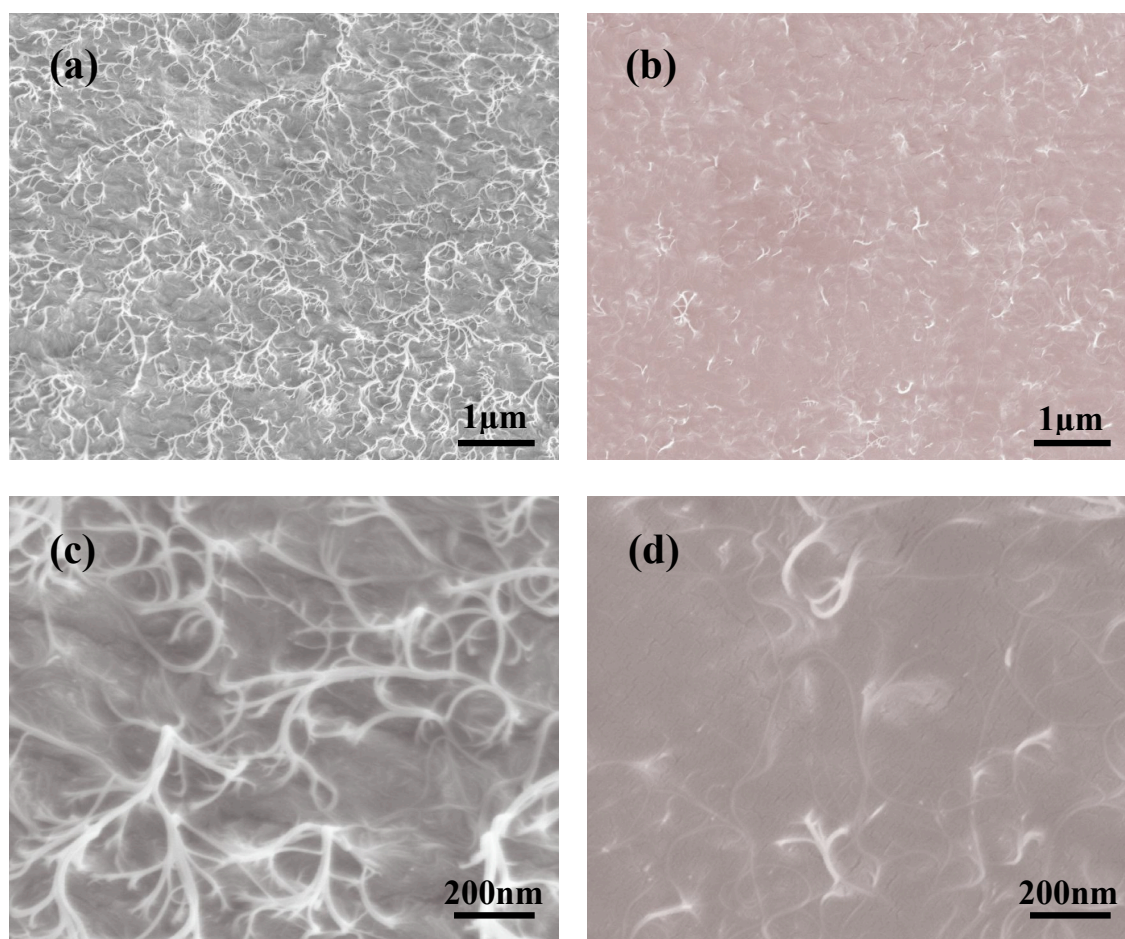


Figure 5.13. Freeze-fractured cross-sectional micrographs for PAH films containing 10 wt% SWNT that are dried from suspensions at a pH of 3.8 (a, c) and 10.2 (b, d).

The pH-adjustable nanotube microstructure for these SWNT/PAH composite films affects their electrical conductivity, as shown in Figure 5.14. All composites have the same nanotube concentration (10 wt%), but are dried from suspensions with different pH. Conductivity decreases two orders of magnitude as pH is increased from 3.8 to 10.2. This conductivity difference can also be seen from the SEM images (Fig 5.13). At low pH (Figures 5.13(a) and (c)), the nanotube network is stronger due to the thicker SWNT

bundles that are well connected, thus making the electron transfer more efficient. The nanotube network at high pH is weaker due to better exfoliation and weakly connected bundles, which deteriorate the electrical conductivity. This is in good agreement with the SWNT/PAA composites where the composite with better nanotube exfoliation (at high pH) shows lower electrical conductivity than the composite with large bundles (at low pH).

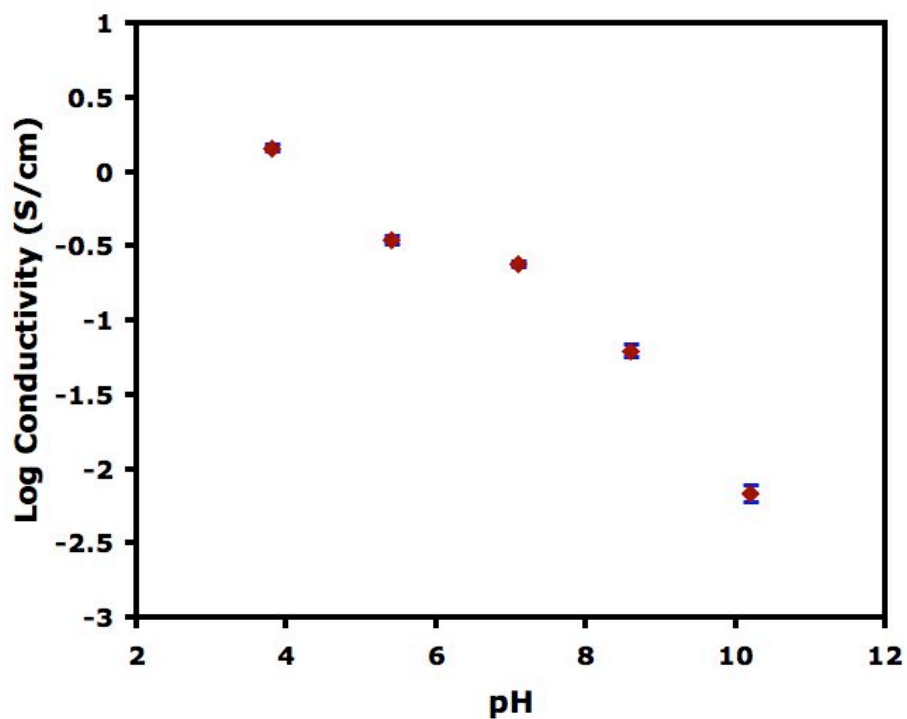


Figure 5.14. Electrical conductivity as a function of pH for dried PAH films containing 10 wt% SWNTs.

5.3.3 Microstructure Tailoring of Nanotubes with Other pH-Responsive Polymers

Poly(methyl acrylic acid) (PMAA) and branched polyethylenimine (BPEI) are also studied for their interaction with nanotubes. PMAA has similar chemical structure as PAA but with one more methyl group on the repeating unit on the backbone. The pH-dependent conformational change and degree of ionization adjustment for PMAA are also similar to PAA. Figure 5.15 shows the cryo-TEM images for PMAA aqueous suspension containing 0.11 wt% SWNTs. At low pH, where PMAA has more coiled conformation, nanotubes are better dispersed. Whereas at high pH, larger nanotube bundles are formed, which is in good agreement with the SWNT/PAA study. BPEI can also stabilize nanotubes in water for both low and high pH but the cryo-TEM images for suspensions at low and high pH show little difference, as shown in Figure 5.16. The possible reason for this is the branched molecular structure for BPEI as compared to the linear structure for PAA and PMAA.

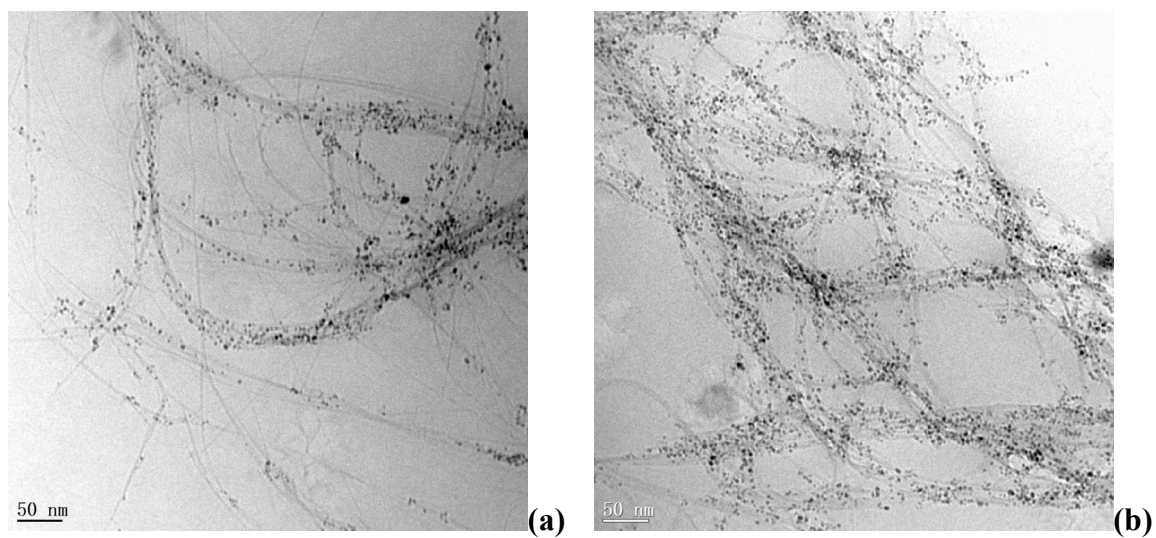


Figure 5.15. Cryo-TEM images for PMAA suspensions containing 0.11 wt% SWNTs at pH 3 (a) and pH 9 (b).

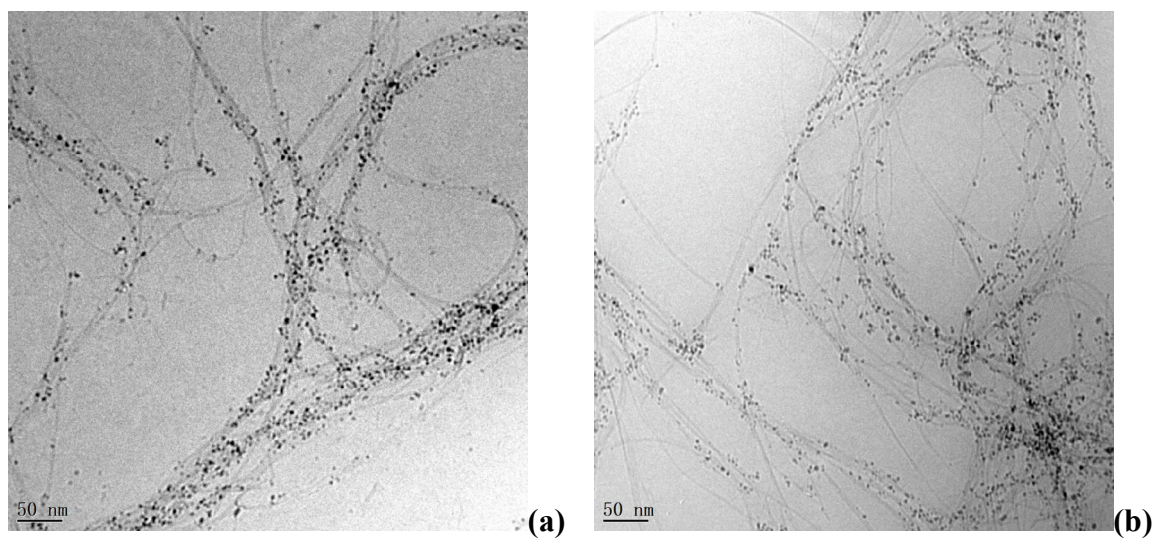


Figure 5.16. Cryo-TEM images for BPEI suspensions containing 0.11 wt% SWNTs at pH 4 (a) and pH 10 (b).

5.4. Conclusions

PAA was found to have reversible interaction with carbon nanotubes as a function of pH. Aqueous suspensions of SWNTs exhibit reversible viscosity change as pH is increased from the original (acidic) pH and then decreased back to the original value. The suspension viscosity changed from Newtonian behavior to non-Newtonian behavior when the pH was progressively increased, with an order of magnitude increase in viscosity observed for the high pH suspension. The structure of the dispersion was evaluated with cryo-TEM, which shows that nanotubes are well exfoliated at low pH and more aggregated (bundled) when the suspension pH is increased. This pH dependent dispersion of nanotubes also influences the suspension stability and it is found that the suspensions containing better exfoliated nanotubes are more stable. When the SWNT/PAA suspensions were dried to make composite films, it was unexpected to see that the well exfoliated nanotube microstructure for low pH suspension is not maintained in the solid film. At this point, it is believed that chemical interactions dominate microstructure during drying and polymer geometry (i.e. conformation) dominates in aqueous suspensions. Electrical conductivity can also be adjusted by the changing the pH prior to drying. A reduced percolation threshold and decreased maximum electrical conductivity were observed for high pH composite films due to the pH-induced microstructure.

SWNT/PAH composites also show pH-dependent interaction. The suspension viscosity is not as completely reversible as the SWNT/PAA system. SEM images for dried composite films verified that better nanotube exfoliation occurs when the film is

dried at high pH. This is not in good agreement with the result of SWNT/PAA and a possible reason is the different type of charges (positive vs negative). The electrical conductivity of the films are largely influenced by pH as well. For the 10 wt% SWNT in PAH films, there is a two orders of magnitude decrease in conductivity when the pH is increased from 3.8 to 10.3. In aqueous suspensions, PMAA shows pH-dependent dispersion of nanotubes that is very similar to PAA and BPEI shows little adjustment of nanotube microstructure as a function of pH.

CHAPTER VI

CONCLUSIONS AND FUTURE RESEARCH PLAN

Various methods for controlling the microstructure of carbon nanotubes in polymer composites were studied, along with their electrical, thermal and mechanical properties. More attention was paid to noncovalent functionalization of nanotubes due to the fact that covalent functionalization hurts the electrical conductivity of the composites. Experiments were carried out to compare composites containing covalently and noncovalently functionalized nanotubes, which illustrated how electrical conductivity suffers from covalent functionalization. In a related study, clay particles were used as a rigid dispersing aid and found to have strong interaction with carbon nanotubes in both water and epoxy nanocomposites. Significant electrical conductivity and mechanical property enhancements were simultaneously achieved in clay-nanotube-epoxy composites. Some pH-responsive polymers (i.e., weak polyelectrolytes) were also studied as a means to control interaction with nanotubes. The resulting composites showed tunable electrical properties as a function of polymer pH and the state of nanotube dispersion in water was reversible for some system. Inability to control nanotube dispersion remains a key hurdle for their use in practical applications.

6.1. Conclusions

6.1.1. Comparison of Noncovalent and Covalent Functionalization (Chapter III)

Epoxy composites, containing polyethylenimine covalently and noncovalently attached to multi-walled carbon nanotubes, were fabricated and compared in terms of electrical and mechanical behavior. The composites have identical concentrations of polyethylenimine and nanotubes, but different interaction between the two components. For the two kinds of nanotubes used, the electrical conductivity of the composites is always decreased when nanotubes were covalently functionalized. The composites containing noncovalently functionalized nanotubes either maintain electrical conductivity (for the high conductivity nanotubes) or decrease in conductivity (for the lower conductivity nanotubes) relative to composites with unfunctionalized tubes. The mechanical properties of the composites are improved with covalently functionalized nanotubes for both low and high conductivity nanotubes (longer tubes are more conductive), while the composites containing noncovalently functionalized nanotubes showed decreased or similar modulus for high and low conductivity nanotubes, respectively. Grafting covalent bonds to the sidewall of a carbon nanotube destroys the conjugated network and reduces conductivity, but it allows for a stronger interface between the nanotube and polymer matrix that improves mechanical behavior. This study confirms that electrical conductivity of the composites is reduced after covalent nanotube functionalization, which leads to the study of noncovalent interaction with

nanotubes for the rest of this dissertation. A primary focus of this dissertation is electrical conductivity of polymer-nanotube composites.

6.1.2. Clay Assisted Dispersion of Single-Walled Carbon Nanotubes (Chapter IV)

Montmorillonite clay nanoparticles strongly interact with single-walled carbon nanotubes in water and epoxy. Nanotubes can be dispersed in the presence of clay in an aqueous suspension, resulting in a dark brownish liquid. In the absence of clay, the nanotubes settle out of suspension immediately. This strong clay-nanotube interaction in water was confirmed with cryo-TEM and Raman spectroscopy. The reason for this interaction is Van de Waals forces and possibly Lewis acid-base interaction between nanotubes (base) and clay particles (acid). For all nanotube concentrations studied, the electrical conductivity of epoxy composites containing both nanotubes and clay is higher than composites containing just nanotubes. Furthermore, the percolation threshold is reduced from 0.05 wt% nanotube to 0.01 wt% for the composites containing nanotubes with 2 wt% clay. Nanotube dispersion is dramatically improved with clay, as evidenced by a transition in nanotube dispersion from a discontinuous set of aggregated clusters, when there is no clay, to a continuous three-dimensional nanotube network in the presence of clay. The dispersion of clay particles seems unchanged whether nanotubes are present or not, which suggests that although clay particles can indeed improve nanotube dispersion, there is little effect of clay dispersion due to the introduction of nanotubes. The addition of clay particles can also improve the storage modulus of composites containing only nanotubes. When the nanotube concentration is fixed, higher

loading of clay particles shows improved storage modulus, which provides the possibility to make composites with both improved electrical and mechanical properties by using this technique.

6.1.3. Weak Polyelectrolyte Control of Nanotube Dispersion (Chapter V)

The interaction between single-walled carbon nanotubes and poly(acrylic acid) (PAA) is found to be reversible as a function of pH. As the pH of a SWNT-PAA aqueous suspension is increased from three to nine, the suspension viscosity increases accordingly by an order of magnitude. When the pH of the suspension is reduced, the viscosity decreases reversibly and this behavior is related to the state of nanotube dispersion in water. At low pH, the nanotubes are better exfoliated, as evidenced by cryo-TEM images and greater suspension stability while sitting under ambient conditions. This pH-dependent nanotube dispersion and viscosity behavior is due to the conformation and degree of ionization adjustment by pH for the polyelectrolytes. For dried composite films made from these suspensions, the high pH composites show a reduced percolation threshold and a decrease in ultimate electrical conductivity, which is due to the pH-induced microstructure adjustment for the nanotubes. Poly(allylamine hydrochloride) (PAH) also showed pH dependent nanotube-polymer interaction but the suspension viscosity is not completely reversible as compared to the SWNT-PAA system. A possible reason is that as-received PAH has more ion than as-received PAA and this ion concentration difference remains when the pH is adjusted. Other pH-

responsive polymers were also tested (e.g. PEI), but these systems are not as tailorable as PAA and PAH.

6.2. Future Work

6.2.1. Covalently Functionalized Nanotubes with Intrinsically Conductive Polymers

Composites containing covalently functionalized nanotubes are normally found to have reduced electrical conductivity, but improved mechanical properties. It would be ideal if the electrical conductivity can be improved without harming the mechanical behavior. Grafting intrinsically conductive polymers (ICP) on the nanotube surface may be one possible solution. A skin of ICP on the surface of a carbon nanotube has already been reported,^[233] but this involved in-situ polymerization in presence of noncovalently stabilized SWNT. Grafting the ICP would result in covalently bonded polymer molecules on the surface of nanotubes, although the loss in conductivity would be minimized due to the conductive nature of the grafted polymer. Figure 6.1 shows how this ICP grafted nanotube could be produced. Purified SWNTs were first dispersed by single stranded DNA in water and then the monomer (3-aminophenylbronic acid hemisulfate salt, ABA) and potassium fluoride were introduced. The reaction was initiated by $(\text{NH}_4)_2\text{S}_2\text{O}_8$ and 0.05 M H_2SO_4 and kept at 0 °C for 7 hours and at 4 °C for 43 hours. Poly(3,4-ethylene-dioxythiophene)-poly(styrene sulfonate) (PEDOT-PSS) is one possible candidate for this study.^[234] Because PEDOT-PSS is also frequently used in

device fabrication, such as organic light-emitting diodes,^[235] the attachment of PEDOT-PSS on nanotubes will be more applicable to build devices.

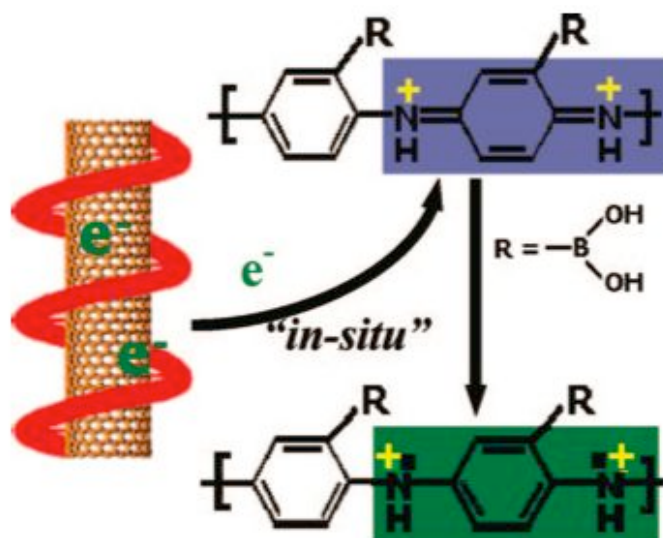


Figure 6.1. Schematic illustration of single stranded DNA functionalized SWNTs that subsequently attached with poly(aniline boronic acid) (PABA) (from Ref. 233).

6.2.2. Nanotube Interaction with Stimuli-Responsive Polymers

There are a variety of other polymers that respond to stimuli other than pH, such as temperature (e.g., poly(N-isopropylacrylamide) (PNIPAAm))^[236] and light (e.g., poly(aryl ether ketone amide) (PAEKA))^[237]. Chemical structures for PNIPAAm and PAEKA are shown in Figure 6.2. PNIPAAm has a lower critical solution temperature (LCST), at which it undergoes a reversible volume phase transition caused by the coil-

to-globule transition. The LCST for PNIPAAm is around 32 °C and the polymer solution experiences phase transition from a soluble to an insoluble state above the critical temperature. The PAEKA shown in Fig.6.2 contains an azobenzene structure in its backbone, which can be switched reversibly from a *cis* to a *trans* isomer when exposed to different wavelengths of UV or visible light. Moreover, the development in atom transfer radical polymerization (ATRP)^[238] makes it possible to produce other copolymers containing PNIPAAm (e.g. PNIPAAm-poly(Z-lysine)).^[239] The interaction between nanotubes and these copolymers will also be interesting.

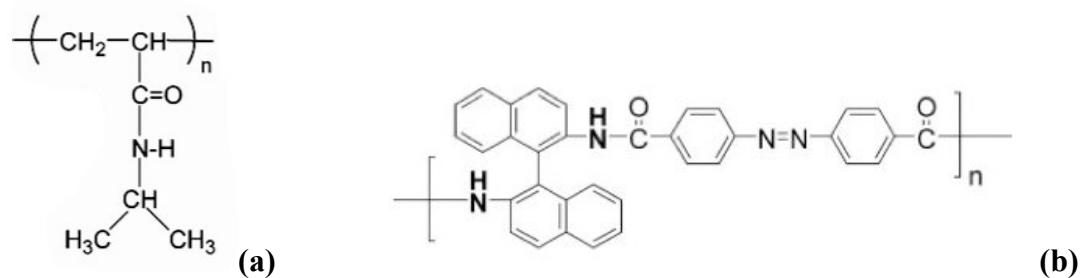


Figure 6.2. Chemical structures for PNIPAAm (a) and PAEKA (b). (from Ref. 236 and 237, respectively).

REFERENCES

- [1] J. Pyun, *Polymer Reviews* **2007**, *47*, 231.
- [2] R. Sengupta, S. Chakraborty, S. Bandyopadhyay, S. Dasgupta, R. Mukhopadhyay, K. Auddy, A. S. Deuri, *Polym. Eng. Sci.* **2007**, *47*, 1956.
- [3] V. Thomas, M. Namdeo, Y. M. Mohan, S. K. Bajpai, M. Bajpai, *Journal of Macromolecular Science Part a-Pure and Applied Chemistry* **2008**, *45*, 107.
- [4] L. J. Lee, C. C. Zeng, X. Cao, X. M. Han, J. Shen, G. J. Xu, *Compos. Sci. Technol.* **2005**, *65*, 2344.
- [5] H. Althues, J. Henle, S. Kaskel, *Chem. Soc. Rev.* **2007**, *36*, 1454.
- [6] A. J. Crosby, J. Y. Lee, *Polymer Reviews* **2007**, *47*, 217.
- [7] L. F. Drummy, Y. C. Wang, R. Schoenmakers, K. May, M. Jackson, H. Koerner, B. L. Farmer, B. Mauryama, R. A. Vaia, *Macromolecules* **2008**, *41*, 2135.
- [8] P. M. Ajayan, L. S. Schadler, P. V. Braun, *Nanocomposite Science and Engineering*; WILEY-VCH Verlag GmbH & Co. KGaA: Weinheim, 2003.
- [9] J. K. Kim, C. G. Hu, R. S. C. Woo, M. L. Sham, *Compos. Sci. Technol.* **2005**, *65*, 805.
- [10] S. Anilkumar, M. G. Kumaran, S. Thomas, *J. Phys. Chem. B* **2008**, *112*, 4009.
- [11] A. A. Katbab, A. N. Hrymak, K. Kasmadjian, *J. Appl. Polym. Sci.* **2008**, *107*, 3425.
- [12] S. Arunvisut, S. Phummanee, A. Somwangthanaroj, *J. Appl. Polym. Sci.* **2007**, *106*, 2210.

- [13] E. P. Giannelis, *Adv. Mater.* **1996**, *8*, 29.
- [14] J. M. Garces, D. J. Moll, J. Bicerano, R. Fibiger, D. G. McLeod, *Adv. Mater.* **2000**, *12*, 1835.
- [15] K. Wang, L. Wang, J. Wu, L. Chen, C. He, *Langmuir* **2005**, *21*, 3613.
- [16] K. Wang, L. Chen, J. Wu, M. L. Toh, C. He, A. F. Yee, *Macromolecules* **2005**, *38*, 788.
- [17] P. Brocorens, S. Benali, C. Broekaert, F. Monteverde, H. E. Miltner, B. Van Mele, M. Alexandre, P. Dubois, R. Lazzaroni, *Langmuir* **2008**, *24*, 2072.
- [18] S. Montserrat, F. Roman, J. M. Hutchinson, L. Campos, *J. Appl. Polym. Sci.* **2008**, *108*, 923.
- [19] F. Gao, *Materials Today* **2004**, *7*, 50.
- [20] F. Hussain, M. Hojjati, M. Okamoto, R. E. Gorga, *Journal of Composite Materials* **2006**, *40*, 1511.
- [21] S. Iijima, *Nature* **1991**, *354*, 56.
- [22] J. Chen, M. A. Hamon, H. Hu, Y. S. Chen, A. M. Rao, P. C. Eklund, R. C. Haddon, *Science* **1998**, *282*, 95.
- [23] T. W. Ebbesen, P. M. Ajayan, *Nature* **1992**, *358*, 220.
- [24] X. Lu, Z. F. Chen, *Chem. Rev.* **2005**, *105*, 3643.
- [25] D. Tasis, N. Tagmatarchis, A. Bianco, M. Prato, *Chem. Rev.* **2006**, *106*, 1105.
- [26] P. M. Ajayan, *Chem. Rev.* **1999**, *99*, 1787.
- [27] S. Kim, S. Pal, P. M. Ajayan, T. Borca-Tasciuc, N. Koratkar, *J. Nanosci. Nanotechnol.* **2008**, *8*, 416.

- [28] A. Nikitin, X. L. Li, Z. Y. Zhang, H. Ogasawara, H. J. Dai, A. Nilsson, *Nano Lett.* **2008**, *8*, 162.
- [29] M. Moniruzzaman, K. I. Winey, *Macromolecules* **2006**, *39*, 5194.
- [30] A. Oberlin, M. Endo, T. Koyama, *J. Cryst. Growth* **1976**, *32*, 335.
- [31] S. J. Tans, A. R. M. Verschueren, C. Dekker, *Nature* **1998**, *393*, 49.
- [32] H. W. C. Postma, T. Teepen, Z. Yao, M. Grifoni, C. Dekker, *Science* **2001**, *293*, 76.
- [33] E. Pop, D. Mann, Q. Wang, K. Goodson, H. Dai, *Nano Lett.* **2006**, *6*, 96.
- [34] S. Berber, Y. K. Kwon, D. Tomanek, *Phys. Rev. Lett.* **2000**, *84*, 4613.
- [35] J. N. Coleman, U. Khan, Y. K. Gun'ko, *Adv. Mater.* **2006**, *18*, 689.
- [36] K. Balasubramanian, M. Burghard, *Small* **2005**, *1*, 180.
- [37] P. J. F. Harris, *Int. Mater. Rev.* **2004**, *49*, 31.
- [38] J. T. Hu, T. W. Odom, C. M. Lieber, *Acc. Chem. Res.* **1999**, *32*, 435.
- [39] H. J. Dai, *Acc. Chem. Res.* **2002**, *35*, 1035.
- [40] W. K. Maser, E. Munoz, A. M. Benito, M. T. Martinez, G. F. de la Fuente, Y. Maniette, E. Anglaret, J. L. Sauvajol, *Chem. Phys. Lett.* **1998**, *292*, 587.
- [41] H. W. Zhu, C. L. Xu, D. H. Wu, B. Q. Wei, R. Vajtai, P. M. Ajayan, *Science* **2002**, *296*, 884.
- [42] S. A. Chesnokov, V. A. Nalimova, A. G. Rinzler, R. E. Smalley, J. E. Fischer, *Phys. Rev. Lett.* **1999**, *82*, 343.
- [43] T. Guo, P. Nikolaev, A. Thess, D. T. Colbert, R. E. Smalley, *Chem. Phys. Lett.* **1995**, *243*, 49.

- [44] H. J. Dai, *Carbon Nanotubes* **2001**, 80, 29.
- [45] P. Nikolaev, M. J. Bronikowski, R. K. Bradley, F. Rohmund, D. T. Colbert, K. A. Smith, R. E. Smalley, *Chem. Phys. Lett.* **1999**, 313, 91.
- [46] J. N. Coleman, U. Khan, W. J. Blau, Y. K. Gun'ko, *Carbon* **2006**, 44, 1624.
- [47] A. N. Khlobystov, D. A. Britz, G. A. D. Briggs, *Acc. Chem. Res.* **2005**, 38, 901.
- [48] J. L. Bahr, J. M. Tour, *J. Mater. Chem.* **2002**, 12, 1952.
- [49] G. D. Xu, B. Zhu, Y. Han, Z. S. Bo, *Polymer* **2007**, 48, 7510.
- [50] H. Kitano, K. Tachimoto, Y. Anraku, *J. Coll. Inter. Sci.* **2007**, 306, 28.
- [51] S. M. Yuen, C. C. M. Ma, C. L. Chiang, C. C. Teng, Y. H. Yu, *J. Polym. Sci. A: Polym. Chem.* **2008**, 46, 803.
- [52] N. Grossiord, J. Loos, O. Regev, C. E. Koning, *Chem. Mater.* **2006**, 18, 1089.
- [53] J. Liu, A. G. Rinzler, H. J. Dai, J. H. Hafner, R. K. Bradley, P. J. Boul, A. Lu, T. Iverson, K. Shelimov, C. B. Huffman, F. Rodriguez-Macias, Y. S. Shon, T. R. Lee, D. T. Colbert, R. E. Smalley, *Science* **1998**, 280, 1253.
- [54] M. Sano, A. Kamino, J. Okamura, S. Shinkai, *Science* **2001**, 293, 1299.
- [55] S. S. Wong, E. Joselevich, A. T. Woolley, C. L. Cheung, C. M. Lieber, *Nature* **1998**, 394, 52.
- [56] E. Katz, I. Willner, *Chemphyschem* **2004**, 5, 1085.
- [57] E. T. Mickelson, C. B. Huffman, A. G. Rinzler, R. E. Smalley, R. H. Hauge, J. L. Margrave, *Chem. Phys. Lett.* **1998**, 296, 188.
- [58] P. E. Pehrsson, W. Zhao, J. W. Baldwin, C. H. Song, J. Liu, S. Kooi, B. Zheng, *J. Phys. Chem. B* **2003**, 107, 5690.

- [59] R. K. Saini, I. W. Chiang, H. Q. Peng, R. E. Smalley, W. E. Billups, R. H. Hauge, J. L. Margrave, *J. Am. Chem. Soc.* **2003**, *125*, 3617.
- [60] J. L. Stevens, A. Y. Huang, H. Q. Peng, L. W. Chiang, V. N. Khabashesku, J. L. Margrave, *Nano Lett.* **2003**, *3*, 331.
- [61] L. Zhang, V. U. Kiny, H. Q. Peng, J. Zhu, R. F. M. Lobo, J. L. Margrave, V. N. Khabashesku, *Chem. Mater.* **2004**, *16*, 2055.
- [62] P. Liu, *Eur. Polym. J.* **2005**, *41*, 2693.
- [63] M. Sano, A. Kamino, J. Okamura, S. Shinkai, *Langmuir* **2001**, *17*, 5125.
- [64] Y. Lin, B. Zhou, K. A. S. Fernando, P. Liu, L. F. Allard, Y. P. Sun, *Macromolecules* **2003**, *36*, 7199.
- [65] R. Blake, Y. K. Gun'ko, J. Coleman, M. Cadek, A. Fonseca, J. B. Nagy, W. J. Blau, *J. Am. Chem. Soc.* **2004**, *126*, 10226.
- [66] J. N. Coleman, M. Cadek, R. Blake, V. Nicolosi, K. P. Ryan, C. Belton, A. Fonseca, J. B. Nagy, Y. K. Gun'ko, W. J. Blau, *Adv. Funct. Mater.* **2004**, *14*, 791.
- [67] M. S. P. Shaffer, K. Koziol, *Chemical Communications* **2002**, 2074.
- [68] X. Tong, L. Chang, H. M. Cheng, H. C. Zhao, Y. Feng, X. Q. Zhang, *J. Appl. Polym. Sci.* **2004**, *92*, 3697.
- [69] H. Kong, C. Gao, D. Y. Yan, *J. Mater. Chem.* **2004**, *14*, 1401.
- [70] H. Kong, C. Gao, D. Y. Yan, *J. Am. Chem. Soc.* **2004**, *126*, 412.
- [71] S. H. Qin, D. Q. Qin, W. T. Ford, J. E. Herrera, D. E. Resasco, S. M. Bachilo, R. B. Weisman, *Macromolecules* **2004**, *37*, 3965.

- [72] G. D. Zhan, X. H. Du, D. M. King, L. F. Hakim, X. H. Liang, J. A. McCormick, A. W. Weimer, *J. Am. Ceram. Soc.* **2008**, *91*, 831.
- [73] S. D. Bergin, V. Nicolosi, H. Cathcart, M. Lotya, D. Rickard, Z. Y. Sun, W. J. Blau, J. N. Coleman, *Journal of Physical Chemistry C* **2008**, *112*, 972.
- [74] V. Z. Poenitzsch, D. C. Winters, H. Xie, G. R. Dieckmann, A. B. Dalton, I. H. Musselman, *J. Am. Chem. Soc.* **2007**, *129*, 14724.
- [75] H. Ali-Boucetta, K. T. Al-Jamal, D. McCarthy, M. Prato, A. Bianco, K. Kostarelos, *Chemical Communications* **2008**, 459.
- [76] V. C. Moore, M. S. Strano, E. H. Haroz, R. H. Hauge, R. E. Smalley, J. Schmidt, Y. Talmon, *Nano Lett.* **2003**, *3*, 1379.
- [77] M. J. O'connell, P. Boul, L. M. Ericson, C. Huffman, Y. H. Wang, E. Haroz, C. Kuper, J. Tour, K. D. Ausman, R. E. Smalley, *Chem. Phys. Lett.* **2001**, *342*, 265.
- [78] Y. Lin, M. J. Meziani, P. Sun, *J. Mater. Chem.* **2007**, *17*, 1143.
- [79] A. Hirsch, *Angewandte Chemie-International Edition* **2002**, *41*, 1853.
- [80] D. A. Britz, A. N. Khlobystov, *Chem. Soc. Rev.* **2006**, *35*, 637.
- [81] R. Bandyopadhyaya, E. Nativ-Roth, O. Regev, R. Yerushalmi-Rozen, *Nano Lett.* **2002**, *2*, 25.
- [82] S. M. Bachilo, M. S. Strano, C. Kittrell, R. H. Hauge, R. E. Smalley, R. B. Weisman, *Science* **2002**, *298*, 2361.
- [83] M. J. O'connell, S. M. Bachilo, C. B. Huffman, V. C. Moore, M. S. Strano, E. H. Haroz, K. L. Rialon, P. J. Boul, W. H. Noon, C. Kittrell, J. P. Ma, R. H. Hauge, R. B. Weisman, R. E. Smalley, *Science* **2002**, *297*, 593.

- [84] X. Y. Gong, J. Liu, S. Baskaran, R. D. Voise, J. S. Young, *Chem. Mater.* **2000**, *12*, 1049.
- [85] H. Wang, W. Zhou, D. L. Ho, K. I. Winey, J. E. Fischer, C. J. Glinka, E. K. Hobbie, *Nano Lett.* **2004**, *4*, 1789.
- [86] K. Yurekli, C. A. Mitchell, R. Krishnamoorti, *J. Am. Chem. Soc.* **2004**, *126*, 9902.
- [87] B. W. Smith, M. Monthieux, D. E. Luzzi, *Nature* **1998**, *396*, 323.
- [88] R. J. Chen, Y. G. Zhang, D. W. Wang, H. J. Dai, *J. Am. Chem. Soc.* **2001**, *123*, 3838.
- [89] K. Besteman, J. O. Lee, F. G. M. Wiertz, H. A. Heering, C. Dekker, *Nano Lett.* **2003**, *3*, 727.
- [90] J. Zhu, M. Yudasaka, M. F. Zhang, D. Kasuya, S. Iijima, *Nano Lett.* **2003**, *3*, 1239.
- [91] J. Chen, H. Y. Liu, W. A. Weimer, M. D. Halls, D. H. Waldeck, G. C. Walker, *J. Am. Chem. Soc.* **2002**, *124*, 9034.
- [92] V. V. Didenko, V. C. Moore, D. S. Baskin, R. E. Smalley, *Nano Lett.* **2005**, *5*, 1563.
- [93] A. H. Liu, I. Honma, M. Ichihara, H. S. Zhou, *Nanotechnology* **2006**, *17*, 2845.
- [94] O. K. Kim, J. T. Je, J. W. Baldwin, S. Kooi, P. E. Pehrsson, L. J. Buckley, *J. Am. Chem. Soc.* **2003**, *125*, 4426.

- [95] A. Ortiz-Acevedo, H. Xie, V. Zorbas, W. M. Sampson, A. B. Dalton, R. H. Baughman, R. K. Draper, I. H. Musselman, G. R. Dieckmann, *J. Am. Chem. Soc.* **2005**, *127*, 9512.
- [96] A. Satake, Y. Miyajima, Y. Kobuke, *Chem. Mater.* **2005**, *17*, 716.
- [97] M. Zheng, A. Jagota, M. S. Strano, A. P. Santos, P. Barone, S. G. Chou, B. A. Diner, M. S. Dresselhaus, R. S. McLean, G. B. Onoa, G. G. Samsonidze, E. D. Semke, M. Usrey, D. J. Walls, *Science* **2003**, *302*, 1545.
- [98] K. T. Lau, C. Gu, D. Hui, *Composites Part B-Engineering* **2006**, *37*, 425.
- [99] P. M. Ajayan, O. Stephan, C. Colliex, D. Trauth, *Science* **1994**, *265*, 1212.
- [100] R. Haggemueller, H. H. Gommans, A. G. Rinzler, J. E. Fischer, K. I. Winey, *Chem. Phys. Lett.* **2000**, *330*, 219.
- [101] F. M. Du, J. E. Fischer, K. I. Winey, *J. Polym. Sci. B: Polym. Phys.* **2003**, *41*, 3333.
- [102] S. Barrau, P. Demont, A. Peigney, C. Laurent, C. Lacabanne, *Macromolecules* **2003**, *36*, 5187.
- [103] F. M. Du, J. E. Fischer, K. I. Winey, *Physical Review B* **2005**, *72*, 121404/1.
- [104] M. B. Bryning, M. F. Islam, J. M. Kikkawa, A. G. Yodh, *Adv. Mater.* **2005**, *17*, 1186.
- [105] J. K. W. Sandler, J. E. Kirk, I. A. Kinloch, M. S. P. Shaffer, A. H. Windle, *Polymer* **2003**, *44*, 5893.
- [106] S. Kirkpatrick, *Rev. Mod. Phys.* **1973**, *45*, 574.

- [107] J. Sandler, M. S. P. Shaffer, T. Prasse, W. Bauhofer, K. Schulte, A. H. Windle, *Polymer* **1999**, *40*, 5967.
- [108] J. Li, P. C. Ma, W. S. Chow, C. K. To, B. Z. Tang, J. K. Kim, *Adv. Funct. Mater.* **2007**, *17*, 3207.
- [109] S. Pegel, P. Potschke, G. Petzold, I. Alig, S. M. Dudkin, D. Lellinger, *Polymer* **2008**, *49*, 974.
- [110] A. Almasri, Z. Ounaies, Y. S. Kim, J. Grunlan, *Macromol. Mater. Eng.* **2008**, *293*, 123.
- [111] A. Mierczynska, M. Mayne-L'Hermite, G. Boiteux, J. K. Jeszka, *J. Appl. Polym. Sci.* **2007**, *105*, 158.
- [112] C. A. Mitchell, R. Krishnamoorti, *Macromolecules* **2007**, *40*, 1538.
- [113] P. V. Kodgire, A. R. Bhattacharyya, S. Bose, N. Gupta, A. R. Kulkarni, A. Misra, *Chem. Phys. Lett.* **2006**, *432*, 480.
- [114] A. W. Musumeci, G. G. Silva, J. W. Liu, W. N. Martens, E. R. Waclawik, *Polymer* **2007**, *48*, 1667.
- [115] Y. Xi, A. Yamanaka, Y. Z. Bin, M. Matsuo, *J. Appl. Polym. Sci.* **2007**, *105*, 2868.
- [116] B. Kim, J. Lee, I. Yu, *J. Appl. Phys.* **2003**, *94*, 6724.
- [117] J. R. Yu, K. B. Lu, E. Sourty, N. Grossiord, C. E. Konine, J. C. Loos, *Carbon* **2007**, *45*, 2897.
- [118] K. Jeon, L. Lumata, T. Tokumoto, E. Steven, J. Brooks, R. G. Alamo, *Polymer* **2007**, *48*, 4751.

- [119] F. M. Du, R. C. Scogna, W. Zhou, S. Brand, J. E. Fischer, K. I. Winey, *Macromolecules* **2004**, *37*, 9048.
- [120] Z. R. Li, H. R. Kandel, E. Dervishi, V. Saini, Y. Xu, A. R. Biris, D. Lupu, G. J. Salamo, A. S. Biris, *Langmuir* **2008**, *24*, 2655.
- [121] Y. I. Song, C. M. Yang, D. Y. Kim, H. Kanoh, K. Kaneko, *J. Coll. Inter. Sci.* **2008**, *318*, 365.
- [122] T. Oya, T. Ogino, *Carbon* **2008**, *46*, 169.
- [123] B. S. Shim, Z. Y. Tang, M. P. Morabito, A. Agarwal, H. P. Hong, N. A. Kotov, *Chem. Mater.* **2007**, *19*, 5467.
- [124] B. R. Sankapal, K. Setyowati, J. Chen, H. Liu, *Appl. Phys. Lett.* **2007**, *91*, 173103.
- [125] L. M. Clayton, B. Knudsen, M. Cinke, M. Meyyappan, J. P. Harmon, *J. Nanosci. Nanotechnol.* **2007**, *7*, 3572.
- [126] H. Nakamatsu, E. Itoh, K. Miyairi, *Mol. Cryst. Liq. Cryst.* **2007**, *472*, 485.
- [127] Y. Simsek, L. Ozyuzer, A. Seyhan, M. Tanoglu, K. Schulte, *J. Mater. Sci.* **2007**, *42*, 9689.
- [128] A. K. Kota, B. H. Cipriano, M. K. Duesterberg, A. L. Gershon, D. Powell, S. R. Raghavan, H. A. Bruck, *Macromolecules* **2007**, *40*, 7400.
- [129] S. C. Tjong, G. D. Liang, S. P. Bao, *Scripta Materialia* **2007**, *57*, 461.
- [130] J. B. Bai, A. Allaoui, *Composites Part a-Applied Science and Manufacturing* **2003**, *34*, 689.

- [131] J. C. Grunlan, A. R. Mehrabi, M. V. Bannon, J. L. Bahr, *Adv. Mater.* **2004**, *16*, 150.
- [132] O. Regev, P. N. B. ElKati, J. Loos, C. E. Koning, *Adv. Mater.* **2004**, *16*, 248.
- [133] J. G. Smith, D. M. Delozier, J. W. Connell, K. A. Watson, *Polymer* **2004**, *45*, 6133.
- [134] K. A. Watson, S. Ghose, D. M. Delozier, J. G. Smith, J. W. Connell, *Polymer* **2005**, *46*, 2076.
- [135] N. C. Das, S. Maiti, *J. Mater. Sci.* **2008**, *43*, 1920.
- [136] Y. Huang, N. Li, Y. F. Ma, D. Feng, F. F. Li, X. B. He, X. Lin, H. J. Gao, Y. S. Chen, *Carbon* **2007**, *45*, 1614.
- [137] P. Beecher, P. Servati, A. Rozhin, A. Colli, V. Scardaci, S. Pisana, T. Hasan, A. J. Flewitt, J. Robertson, G. W. Hsieh, F. M. Li, A. Nathan, A. C. Ferrari, W. I. Milne, *J. Appl. Phys.* **2007**, *102*, 043710.
- [138] K. Kordas, T. Mustonen, G. Toth, H. Jantunen, M. Lajunen, C. Soldano, S. Talapatra, S. Kar, R. Vajtai, P. M. Ajayan, *Small* **2006**, *2*, 1021.
- [139] X. Yu, R. Rajamani, K. A. Stelson, T. Cui, *Surf. Coat. Technol.* **2008**, *202*, 2002.
- [140] X. Yu, R. Rajamani, K. A. Stelson, T. Cui, *J. Nanosci. Nanotechnol.* **2006**, *6*, 1939.
- [141] R. Ramasubramaniam, J. Chen, H. Liu, *Appl. Phys. Lett.* **2003**, *83*, 2928.
- [142] K. Putz, R. Krishnamoorti, P. F. Green, *Polymer* **2007**, *48*, 3540.
- [143] S. H. Jin, Y. B. Park, K. H. Yoon, *Compos. Sci. Technol.* **2007**, *67*, 3434.

- [144] S. Kanagaraj, F. R. Varanda, T. V. Zhil'tsova, M. S. A. Oliveira, J. A. O. Simoes, *Compos. Sci. Technol.* **2007**, *67*, 3071.
- [145] J. Zhu, J. Kim, H. Peng, J. L. Margrave, V. N. Khabashesku, E. V. Barrera, *Nano Lett.* **2003**, *3*, 1107.
- [146] J. Zhu, H. Peng, F. Rodriguez-Macias, J. L. Margrave, V. N. Khabashesku, A. M. Imam, K. Lozano, E. V. Barrera, *Adv. Funct. Mater.* **2004**, *14*, 643.
- [147] L. Liu, H. D. Wagner, *Compos. Sci. Technol.* **2005**, *65*, 1861.
- [148] H. J. Choi, K. Zhang, J. Y. Lim, *J. Nanosci. Nanotechnol.* **2007**, *7*, 3400.
- [149] F. Liang, J. M. Beach, K. Kobashi, A. K. Sadana, Y. I. Vega-Cantu, J. M. Tour, W. E. Billups, *Chem. Mater.* **2006**, *18*, 4764.
- [150] A. M. Shanmugaraj, J. H. Bae, R. R. Nayak, S. H. Ryu, *J. Polym. Sci. A: Polym. Chem.* **2007**, *45*, 460.
- [151] Z. J. Jia, Z. Y. Wang, C. L. Xu, J. Liang, B. Q. Wei, D. H. Wu, S. W. Zhu, *Mater. Sci. Eng., A* **1999**, *271*, 395.
- [152] C. Velasco-Santos, A. L. Martinez-Hernandez, F. T. Fisher, R. Ruoff, V. M. Castano, *Chem. Mater.* **2003**, *15*, 4470.
- [153] L. W. Qu, L. M. Veca, Y. Lin, A. Kitaygorodskiy, B. L. Chen, A. M. McCall, J. W. Connell, Y. P. Sun, *Macromolecules* **2005**, *38*, 10328.
- [154] J. B. Gao, B. Zhao, M. E. Itkis, E. Bekyarova, H. Hu, V. Kranak, A. P. Yu, R. C. Haddon, *J. Am. Chem. Soc.* **2006**, *128*, 7492.
- [155] J. B. Gao, M. E. Itkis, A. P. Yu, E. Bekyarova, B. Zhao, R. C. Haddon, *J. Am. Chem. Soc.* **2005**, *127*, 3847.

- [156] M. S. P. Shaffer, A. H. Windle, *Adv. Mater.* **1999**, *11*, 937.
- [157] M. Cadek, J. N. Coleman, V. Barron, K. Hedicke, W. J. Blau, *Appl. Phys. Lett.* **2002**, *81*, 5123.
- [158] Z. Wang, P. Ciselli, T. Peijs, *Nanotechnology* **2007**, *18*, 455709.
- [159] R. Haggemueller, C. Guthy, J. R. Lukes, J. E. Fischer, K. I. Winey, *Macromolecules* **2007**, *40*, 2417.
- [160] B. Schartel, U. Braun, U. Knoll, M. Bartholmai, H. Goering, D. Neubert, P. Potschke, *Polym. Eng. Sci.* **2008**, *48*, 149.
- [161] S. M. Yuen, C. C. M. Ma, C. L. Chiang, J. A. Chang, S. W. Huang, S. C. Chen, C. Y. Chuang, C. C. Yang, M. H. Wei, *Composites Part a-Applied Science and Manufacturing* **2007**, *38*, 2527.
- [162] K. J. Loh, J. Kim, J. P. Lynch, N. W. S. Kam, N. A. Kotov, *Smart Materials & Structures* **2007**, *16*, 429.
- [163] H. H. Yu, T. Cao, L. D. Zhou, E. D. Gu, D. S. Yu, D. S. Jiang, *Sensors and Actuators B-Chemical* **2006**, *119*, 512.
- [164] Y. Wanna, N. Srisukhumbowornchai, A. Tuantranont, A. Wisitsoraat, N. Thavarungkul, P. Singjai, *J. Nanosci. Nanotechnol.* **2006**, *6*, 3893.
- [165] T. Zhang, M. B. Nix, B. Y. Yoo, M. A. Deshusses, N. V. Myung, *Electroanalysis* **2006**, *18*, 1153.
- [166] J. H. He, S. Singamaneni, C. H. Ho, Y. H. Lin, M. E. McConney, V. V. Tsukruk, *Nanotechnology* **2009**, *20*, 065502.
- [167] J. Li, Y. J. Lu, Q. Ye, M. Cinke, J. Han, M. Meyyappan, *Nano Lett.* **2003**, *3*, 929.

- [168] D. R. Kauffman, A. Star, *Angewandte Chemie-International Edition* **2008**, *47*, 6550.
- [169] W. F. Jiang, S. H. Xiao, C. Y. Feng, H. Y. Li, X. J. Li, *Sensors and Actuators B-Chemical* **2007**, *125*, 651.
- [170] P. G. Su, C. S. Wang, *Sensors and Actuators B-Chemical* **2007**, *124*, 303.
- [171] H. M. Li, F. O. Cheng, A. M. Duft, A. Adronov, *J. Am. Chem. Soc.* **2005**, *127*, 14518.
- [172] C. H. Tseng, C. C. Wang, C. Y. Chen, *Chem. Mater.* **2007**, *19*, 308.
- [173] C. A. Dyke, J. M. Tour, *Journal of Physical Chemistry A* **2004**, *108*, 11151.
- [174] M. L. Shofner, V. N. Khabashesku, E. V. Barrera, *Chem. Mater.* **2006**, *18*, 906.
- [175] A. A. Koval'chuk, V. G. Shevchenko, A. N. Shchegolikhin, P. M. Nedorezova, A. N. Klyamkina, A. M. Aladyshev, *Macromolecules* **2008**, *41*, 7536.
- [176] J. Amiran, V. Nicolosi, S. D. Bergin, U. Khan, P. E. Lyons, J. N. Coleman, *Journal of Physical Chemistry C* **2008**, *112*, 3519.
- [177] C. Bartholome, P. Miaudet, A. Derre, M. Maugey, O. Roubeau, C. Zakri, P. Poulin, *Compos. Sci. Technol.* **2008**, *68*, 2568.
- [178] M. Abdalla, D. Dean, P. Robinson, E. Nyairo, *Polymer* **2008**, *49*, 3310.
- [179] V. N. Khabashesku, W. E. Billups, J. L. Margrave, *Acc. Chem. Res.* **2002**, *35*, 1087.
- [180] B. Zhao, H. Hu, A. P. Yu, D. Perea, R. C. Haddon, *J. Am. Chem. Soc.* **2005**, *127*, 8197.

- [181] Z. Sun, V. Nicolosi, D. Rickard, S. D. Bergin, D. Aherne, J. N. Coleman, *Journal of Physical Chemistry C* **2008**, *112*, 10692.
- [182] L. Liu, J. C. Grunlan, *Adv. Funct. Mater.* **2007**, *17*, 2343.
- [183] J. H. Zou, L. W. Liu, H. Chen, S. I. Khondaker, R. D. McCullough, Q. Huo, L. Zhai, *Adv. Mater.* **2008**, *20*, 2055.
- [184] L. Liu, K. C. Etika, K. S. Liao, L. A. Hess, D. E. Bergbreiter, J. Grunlan, *Macromol. Rapid Commun.*, early view (DOI: 10.1002/marc.200800778).
- [185] H. Park, J. Zhao, J. P. Lu, *Nano Lett.* **2006**, *6*, 916.
- [186] N. Li, Y. Huang, F. Du, X. He, X. Lin, H. Gao, Y. Ma, F. Li, Y. Chen, P. C. Eklund, *Nano Lett.* **2006**, *6*, 1141.
- [187] A. Yu, H. Hui, E. Bekyarova, M. E. Itkis, J. Gao, B. Zhao, R. C. Haddon, *Compos. Sci. Technol.* **2006**, *66*, 1190.
- [188] F. H. Gojny, M. H. G. Wichmann, B. Fiedler, I. A. Kinloch, W. Bauhofer, A. H. Windle, K. Schulte, *Polymer* **2006**, *47*, 2036.
- [189] P. C. Ma, J. K. Kim, B. Z. Tang, *Compos. Sci. Technol.* **2007**, *67*, 2965.
- [190] F. Liang, J. M. Beach, P. K. Rai, W. Guo, R. H. Hauge, M. Pasquali, R. E. Smalley, W. E. Billups, *Chem. Mater.* **2006**, *18*, 1520.
- [191] K. S. Liao, A. Wan, J. D. Batteas, D. E. Bergbreiter, *Langmuir* **2008**, *24*, 4245.
- [192] P. E. Lyons, S. De, F. Blighe, V. Nicolosi, L. F. C. Pereira, M. S. Ferreira, J. N. Coleman, *J. Appl. Phys.* **2008**, *104*, 044302.
- [193] R. E. Grim, *Clay Mineralogy*; McGraw-Hill Book Company: New York, 1968.

- [194] R. E. Grim, *Applied Clay Mineralogy*; McGraw-Hill Book Company: New York, 1962.
- [195] T. J. Pinnavaia, *Science* **1983**, *220*, 365.
- [196] A. Okada, A. Usuki, *Macromol. Mater. Eng.* **2006**, *291*, 1449.
- [197] T. J. Pinnavaia, G. W. Beall, *Polymer-Clay Nanocomposites*; John Wiley & Sons: New York, 2000.
- [198] B. Chen, J. R. G. Evans, H. C. Greenwell, P. Boulet, P. V. Coveney, A. A. Bowden, A. Whiting, *Chem. Soc. Rev.* **2008**, *37*, 568.
- [199] P. C. LeBaron, Z. Wang, T. J. Pinnavaia, *Appl. Clay Sci.* **1999**, *15*, 11.
- [200] M. A. Osman, V. Mittal, M. Morbidelli, U. W. Suter, *Macromolecules* **2004**, *37*, 7250.
- [201] A. B. Morgan, *Polym. Adv. Technol.* **2006**, *17*, 206.
- [202] M. Si, M. Goldman, G. Rudomen, M. Y. Gelfer, J. C. Sokolov, M. H. Rafailovich, *Macromol. Mater. Eng.* **2006**, *291*, 602.
- [203] A. Usuki, Y. Kojima, M. Kawasumi, A. Okada, Y. Fukushima, T. Kurauchi, O. Kamigaito, *J. Mater. Res.* **1993**, *8*, 1179.
- [204] P. Maiti, M. Okamoto, *Macromol. Mater. Eng.* **2003**, *288*, 440.
- [205] C. S. Triantafillidis, P. C. LeBaron, T. J. Pinnavaia, *J. Solid State Chem.* **2002**, *167*, 354.
- [206] K. Yano, A. Usuki, A. Okada, T. Kurauchi, O. Kamigaito, *J. Polym. Sci. A: Polym. Chem.* **1993**, *31*, 2493.
- [207] S. Bourbigot, E. Devaux, X. Flambard, *Polym. Degrad. Stab.* **2002**, *75*, 397.

- [208] J. Zhu, M. Yudasaka, M. Zhang, S. Iijima, *J. Phys. Chem. B* **2004**, *108*, 11317.
- [209] J.-J. Lin, Y.-F. Lan, K.-L. Wei, Y.-N. Chan, *Polym. Mater. Sci. Eng.* **2007**, *97*, 42.
- [210] J. R. Yu, N. Grossiord, C. E. Koning, J. Loos, *Carbon* **2007**, *45*, 618.
- [211] H. Y. Ma, L. F. Tong, Z. B. Xu, Z. P. Fang, *Nanotechnology* **2007**, *18*, 375602.
- [212] D. Schaefer, J. M. Brown, D. P. Anderson, J. Zhao, K. Chokalingam, D. Tomlin, J. Ilavsky, *J. Appl. Crystallogr.* **2003**, *36*, 553.
- [213] J. L. Blackburn, C. Engtrakul, T. J. McDonald, A. C. Dillon, M. J. Heben, *J. Phys. Chem. B* **2006**, *110*, 25551.
- [214] H. Kawamoto, T. Uchida, K. Kojima, M. Tachibana, *J. Appl. Phys.* **2006**, *99*, 094309.
- [215] A. M. Rao, P. C. Eklund, S. Bandow, A. Thess, R. E. Smalley, *Nature* **1997**, *388*, 257.
- [216] S. D. M. Brown, A. Jorio, P. Corio, M. S. Dresselhaus, G. Dresselhaus, R. Saito, K. Kneipp, *Physical Review B* **2001**, *63*, 155414.
- [217] V. A. Karachevtsev, A. Y. Glamazda, U. Dettlaff-Weglikowska, V. S. Leontiev, P. V. Mateichenko, S. Roth, A. M. Rao, *Carbon* **2006**, *44*, 1292.
- [218] N. Bendiab, R. Almairac, M. Paillet, J. L. Sauvajol, *Chem. Phys. Lett.* **2003**, *372*, 210.
- [219] B. R. Priya, H. J. Byrne, *Journal of Physical Chemistry C* **2008**, *112*, 332.
- [220] A. Kumatani, P. A. Warburton, *Appl. Phys. Lett.* **2008**, *92*, 243123.

- [221] M. Kotaki, K. Wang, M. L. Toh, L. Chen, S. Y. Wong, C. He, *Macromolecules* **2006**, *39*, 908.
- [222] J. C. Grunlan, L. Liu, Y. S. Kim, *Nano Lett.* **2006**, *6*, 911.
- [223] H. Zhao, J. Gao, Y. Li, S. Shen, *J. Therm. Anal. Cal.* **2003**, *74*, 227.
- [224] S. Wang, Z. Liang, T. Liu, B. Wang, C. Zhang, *Nanotechnology* **2006**, *17*, 1551.
- [225] M. F. Yu, B. S. Files, S. Arepalli, R. S. Ruoff, *Phys. Rev. Lett.* **2000**, *84*, 5552.
- [226] A. Thess, R. Lee, P. Nikolaev, H. J. Dai, P. Petit, J. Robert, C. H. Xu, Y. H. Lee, S. G. Kim, A. G. Rinzler, D. T. Colbert, G. E. Scuseria, D. Tomanek, J. E. Fischer, R. E. Smalley, *Science* **1996**, *273*, 483.
- [227] D. Heer, *Mrs Bulletin* **2004**, *29*, 281.
- [228] A. Bianco, K. Kostarelos, C. D. Partidos, M. Prato, *Chemical Communications* **2005**, 571.
- [229] M. J. Biercuk, M. C. Llaguno, M. Radosavljevic, J. K. Hyun, A. T. Johnson, J. E. Fischer, *Appl. Phys. Lett.* **2002**, *80*, 2767.
- [230] J. C. Grunlan, L. Liu, O. Regev, *J. Coll. Inter. Sci.* **2008**, *317*, 346.
- [231] J. Choi, M. F. Rubner, *Macromolecules* **2005**, *38*, 116.
- [232] L. Liu, J. C. Grunlan, *Mater. Res. Soc. Proc.* **2006**, *922*, U06~02.
- [233] Y. F. Ma, W. Cheung, D. G. Wei, A. Bogozzi, P. L. Chiu, L. Wang, F. Pontoriero, R. Mendelsohn, H. X. He, *Acs Nano* **2008**, *2*, 1197.
- [234] H. T. Ham, Y. S. Choi, M. G. Chee, M. H. Cha, I. J. Chung, *Polym. Eng. Sci.* **2008**, *48*, 1.

- [235] J. Li, L. Hu, L. Wang, Y. Zhou, G. Gruner, T. J. Marks, *Nano Lett.* **2006**, *6*, 2472.
- [236] E. S. Gil, S. A. Hudson, *Progress in Polymer Science* **2004**, *29*, 1173.
- [237] G. D. Jaycox, *J. Polym. Sci. A: Polym. Chem.* **2006**, *44*, 207.
- [238] K. Matyjaszewski, J. H. Xia, *Chem. Rev.* **2001**, *101*, 2921.
- [239] C. J. Huang, F. C. Chang, *Macromolecules* **2008**, *41*, 7041.

VITA

Lei Liu was born in Beijing, P. R. China. He received his Bachelor of Engineering degree in Materials Science and Engineering from Beijing University of Aeronautics and Astronautics in 2001. After working for a year in Institute of Chemistry, Chinese Academy of Science, he joined the graduate program at Institute of Materials Research & Engineering (IMRE)/National University of Singapore (NUS) and received his Master of Science degree in 2004. He entered Materials Science and Engineering program at Texas A&M University in January 2005 and received his Ph.D. in May 2009. His research interests include synthesis/characterization of nanoparticles and electrically conductive polymer composites. His permanent address is: 619-4-13 Wukesong, No.79 Fuxing Road, Haidian District, Beijing, P. R. China. He may be reached at garfielder@hotmail.com.